THE
PHYSICAL REVIEW

A journal of experimental and theoretical physics established by E. L. Nichols in 1893

SECOND SERIES, VOL. 71, NO. 2 JANUARY 15, 1947

Slow Neutron Velocity Spectrometer Studies I. Cd, Ag, Sb, Ir, Mn*

L. J. RAINWATER, W. W. HAVENS, JR., C. S. WU, AND J. R. DUNNING
Columbia University, New York, New York

(Received October 19, 1946)

The Columbia Neutron Velocity Spectrometer has been completely redesigned and enlarged to permit 32 separate measurements to be made simultaneously with greatly improved resolution and precision. A detailed comparison between the experimentally measured cross section of Cd and the Breit-Wigner one-level formula gives excellent agreement for over a factor of 100 in energy and 1000 in cross section. The selected parameters are $\sigma_0=(7200\pm200)$, $E_0=(0.176\pm0.002)$ ev, and $\Gamma=(0.115\pm0.002)$ ev with a value of (5.3 ± 0.7) added as a "constant" term in the total cross section. (Energy is in ev and cross sections in units of $\times10^{-24}$ cm²/atom.) The silver resonance levels have been remeasured with essential agreement with the previous results. Three levels are well defined at (5.1 ± 0.1) ev, (16 ± 1) ev, and (45 ± 4) ev. Antimony has also been checked and the upper "level" has been partially resolved into two levels at (15 ± 1) ev and (21 ± 1.5) ev. The other level is at (5.8 ± 0.15) ev and there is no indication of higher energy levels. Manganese is found to have a strong level at (300 ± 40) ev and probably other unresolved higher energy levels. There is no indication of levels at lower energies where the cross section shows a normal $1/v$ type absorption with

$$\sigma=[(2.26\pm0.4)+(2.24\pm0.05)E^{\frac{1}{2}}].$$

The iridum curve shows high detail. This includes strong levels at (0.64 ± 0.015) ev, (1.27 ± 0.04) ev, (5.2 ± 0.2) ev, and (8.7 ± 0.3) ev. There is a low broad transmission dip for energies above about 20 ev, indicating several more levels may be present. A $1/v$-type absorption is observed in the thermal region with $\sigma=[(14\pm6)+(64\pm2)E^{-\frac{1}{2}}]$. Further analysis has been made for most of the resonances.

INTRODUCTION

Previous Measurements

IN two previous papers[1,2] a description has been given of a neutron spectrometer system developed for use with the Columbia University cyclotron. The factors involved in the use of such an instrument were discussed in detail and results given for the slow neutron cross sections *vs.* energy for Cd, B, Li, Ag, In, Sb, Hg, and Au. Since the completion of the measurements described in these references, the spectrometer system has been redesigned to permit much improved operation. These improvements, to be discussed in more detail below, consist mainly of the following: (a) The number of timing intervals to be simultaneously measured was increased to 16 for each of two measuring channels. This permits 32 separate measurements to be made simultaneously. The resulting increase in efficiency makes practical operation with greater resolution and statistical accuracy and also increases the rate at which the measurements may be made. (b) The basic circuits were completely redesigned to have fractional microsecond re-

* This document is based on work performed under Contract W-7405-Eng. 50 with the Manhattan Project at Columbia University. It will also appear in Book III, Division VIII, in the Manhattan Project Technical Series as part of the contribution of the Physics Department, Columbia University. Publication assisted by the Ernest Kempton Adams Fund for Physical Research of Columbia University, New York, New York.

[1] J. Rainwater and W. Havens, Phys. Rev. **70**, 136 (1946).

[2] W. Havens and J. Rainwater, Phys. Rev. **70**, 154 (1946).

sponse characteristics. This improves the resolution and precision of the system particularly for work at higher energies. (c) The timing is now accomplished automatically by setting 4 switches rather than by individual visual adjustment of all pulse widths. The resultant timings are as stable as the 100 Kc crystal oscillator which serves as the frequency standard. The use of successive "scale-of-2" and "chain" type scaling circuits permits precise control of all timing intervals. (d) The source detector path length has been increased to 6.2 meters and the BF_3 proportional counter length decreased to 10 cm to improve the resolution. A thinner source slab decreases the thermal delay correction to about 30 microseconds. (e) Much improved shielding with thick paraffin, boron, and Cd at the source position and around the collimating tubes and detector have greatly decreased the background intensity for high energy measurements (over 10 ev).

Since the new system has been in operation a large number of elements have been investigated and the earlier measurements[1,2] have been rechecked. This paper is the first of a series of papers in which the results of these measurements will be presented.

CHOICE OF ELEMENTS FOR STUDY

Cadmium

In the first reference results were given of measurements of the slow neutron cross section of cadmium as a function of energy. It was shown that there was good quantitative agreement between the experimentally measured cross sections *vs.* energy and those predicted by the Breit-Wigner one-level formula

$$\sigma(E)=\frac{\sigma_0\Gamma^2(E_0/E)^{\frac{1}{2}}}{\Gamma^2+4(E-E_0)^2}.$$

Values of $\sigma_0=(7800\pm800)\times10^{-24}$ cm²/atom, $E_0=(0.180\pm0.008)$ ev, and $\Gamma=(0.112\pm0.006)$ ev were obtained for the cross section at exact resonance, the energy at exact resonance, and the half-width of the level. Since the Breit-Wigner one-level formula is widely used in connection with slow neutron capture theory, and since the cadmium resonance is almost unique in its suitability for detailed comparison with the theory, it was considered to be of interest to repeat the cadmium measurements with better resolution and statistical accuracy and to extend the range of the measurements to higher energies to obtain a detailed comparison over the widest possible range of energies and cross sections. In the measurements to be described below comparison has been made for over 80 different values of the neutron energy between 0.0083 ev and 2.11 ev corresponding to a range of cross sections from 7200 to 6 ($\times10^{-24}$ cm²/atom). (The above values are not corrected for the fact that only one isotope of Cd is responsible for the resonance.)

Silver

In the earlier measurements for silver[2] precise results were obtained for the thermal cross sections including the "constant" term and the $1/v$ slope of the cross section in the thermal region. The main resonance at (5.1 ± 0.2) ev was also clearly shown and there was evidence of other levels at (13.7 ± 2) ev and (43 ± 5) ev. Since measurements are now easily made with better precision and resolution in the high energy region, these measurements were repeated. The new results (described below) are in substantial agreement with those of the earlier measurements.

Antimony

The previous measurements for antimony[2] showed that two levels were present near 6 ev and 19 ev with indication of a higher level or levels. The cross section in the thermal energy region was measured with some precision and the "$1/v$ factor slope" and the "constant" terms in the thermal cross section were determined. The high energy region has been reinvestigated with maximum resolution. The lower level at 5.8 ev remains single whereas the upper "level" splits into two almost equal levels at 15 and 21 ev. No evidence for resonances at still higher energies was found.

Manganese

Manganese is of considerable interest for slow neutron experiments because of its extensive use as a radioactive slow neutron detector. Previous attempts[3–5] to determine the energy of the Mn

[3] W. J. Horvath and E. O. Salant, Phys. Rev. **59**, 154 (1941).
[4] H. Feeny and F. Rasetti, Can. J. Research **23A**, 12 (1945).
[5] H. Goldsmith and F. Rasetti, Phys. Rev. **50**, 328 (1936).

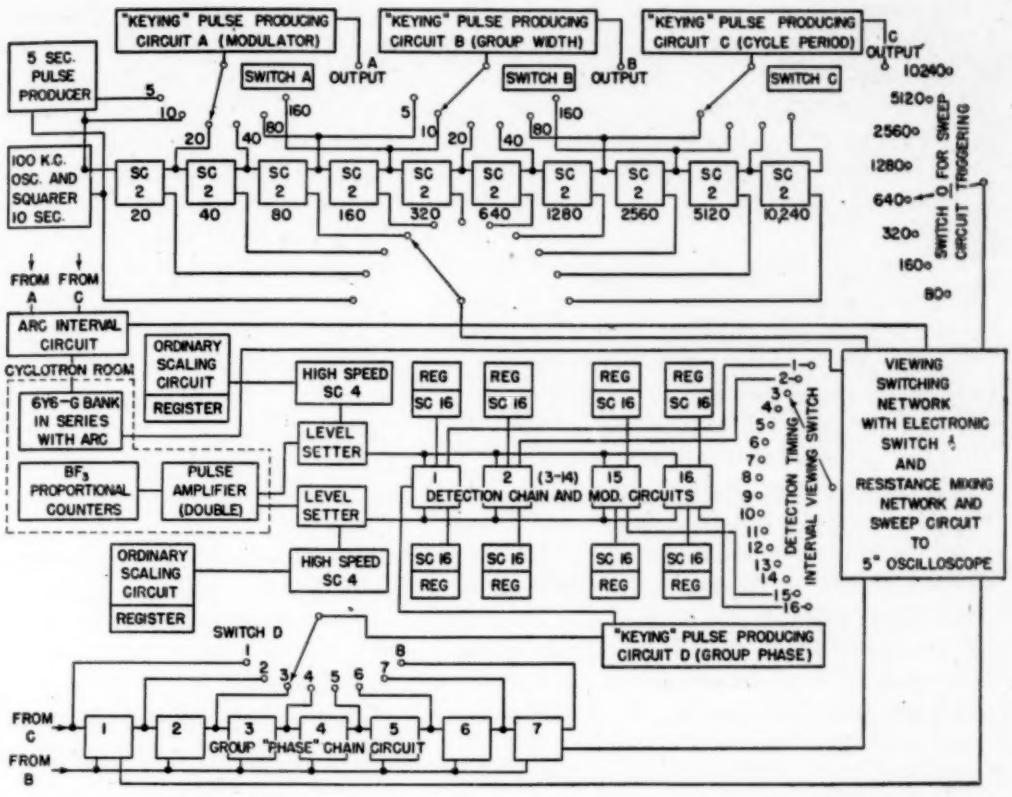

FIG. 1. Block diagram of the new spectrometer system.

resonances by "resonance detector" measurements have given widely different results varying from a resonant energy of less than a volt to about 20 ev. The present measurements show that the Mn cross section for energies below about 30 ev can be well matched by the usual $1/v$ slope plus a constant term as with boron and lithium. A strong resonance is found near 300 ev and the shape of the transmission curve on the high energy side of this resonance level suggests that another level (or levels) at still higher energies may be present.

Iridium

The results of the measurements for iridium are presented here since they display more detail than those for any other element yet investigated.

NEW SPECTROMETER SYSTEM

Timing Circuits

The block diagram of the new spectrometer system shown in Fig. 1 will serve as the basis for the following discussion. The fundamental timing is provided by a 100-Kc crystal controlled oscillator which is accurate to about 0.01 percent. The 10-μsec. wave is "squared up" by limiting amplification to give square wave pulses with about 0.1-μsec. rise time. This 10-μsec. period square wave is then fed to a special high speed scale of 1024 circuit which provides 20-, 40-, 80-, 160-, 320-, 640-, 1280-, 2560-, 5120-, and 10,240-μsec. period square waves. Special care has been taken to ensure a rapid switching action to ensure less than 0.1-μsec. time lag in the propagation of the switching pulse down the ten-stage chain of scale-of-2 circuits. By mixing normal and inverted 10-μsec. period pulses a 5-μsec. period pulse is obtained. Thus accurately synchronized timing pulses with periods ranging from 5 μsec. to 10,240 μsec. increasing by powers of 2 are available.

In normal operation time of flight measurements of less than 640 μsec. (at 6.2 meters) are obtained by using a 1280-μsec. period for the complete operation cycle and using thick Cd in the beam to remove all neutrons having times of flight greater than about 800 μsec. This prevents overlap from previous cycles.

For time of flight measurements of less than 1280 μsec. (6.2 meters) an operating cycle period of 5120 μsec. is used. Thin Hg filters are used to reduce the intensity of neutrons overlapping from the previous cycle to less than one percent of the main intensity without greatly decreasing the intensity of neutrons of the energies being studied.[2]

For time of flight measurements of 1280 to 5120 μsec. an operating cycle period of 5120 μsec. is also used but the Hg filter is omitted. The increased intensity in this region due to the thermal peak[1] gives the proper ratio of main intensity to overlap intensity. For timings greater than 5120 μsec. a period of 10,240 μsec. is used.

The choice of the length of the operating cycle repetition period is obtained by switch C in Fig. 1 which selects the square wave pulse of the desired period. A keying circuit then gives a single sharp pulse at the beginning of each cycle of the square wave. This keying pulse activates other circuits to determine the start of the operating cycle and the start of the cyclotron arc pulse (cyclotron "on time" pulse).

For the method of operation which has been adopted, the cyclotron arc pulse width is always made equal to the detection pulse width since this is most convenient and also gives the maximum intensity for a given over-all resolution width. The usual "on time" (to be denoted τ) is $\tau=5$, 10, or 20 μsec. when T (the operating cycle period) $=1280$ μsec. When $T=5120$ μsec. and t (the neutron time of flight selected by the detection interval) is less than 1280 μsec., the width $\tau=20$, 40, or 80 μsec. is usually chosen. For larger timings, t, the value of $\tau=20$, 40, 80, or 160 is chosen. The width of the cyclotron arc and the detection "on time," τ, is selected by switch A. The signal obtained is then converted to a single sharp "keying pulse" at the beginning of each cycle of the chosen square wave period to activate the other circuits.

In the new spectrometer system 16 detection intervals are measured simultaneously. These are automatically made adjacent (the spacing between adjacent intervals is equal to the width of each detection interval) and of equal width such that a *group* of 16 adjacent timing intervals is measured simultaneously. The factors involved in the operation may, at this point, best be illustrated by an example. Suppose that measurements with high resolution at the high energy end of the spectrum are being made; switch C is placed at 1280 μsec. (for T) and switch A is set at 5 μsec. (for τ). The arc pulse is turned on at the beginning of the cycle by the pulse from C and is turned off by the next pulse from A so that it is "on" from $t=0$ to $t=5$ μsec. This is accomplished by using one stage of a "chain" type scaling circuit to be described below.

The first detection interval (for the *first group*) now extends from $t=0$ to $t=5$ μsec., the second from $t=5$ to $t=10$ μsec., and so on with the 16th detection interval from $t=75$ to $t=80$ μsec. Each detection interval circuit is then inactive until the corresponding interval in the next operating cycle.

In order to extend the timing to values greater than 80 μsec., the whole group of detection intervals is shifted by 80 μsec. to give the *second group* of detection intervals. In practice this is done by simply setting switch D to the second position (the details of the operation will be explained below). The first detection interval now extends from $t=80$ to $t=85$ μsec. and the 16th from $t=155$ to $t=160$ μsec. For still larger timings switch D is set at its third position (*third group*) to obtain timings between 160 and 235 μsec.

The timing corresponding to each detection interval is expressed as a definite value equal to the time from the beginning of the cycle to the beginning of the detection interval. This also corresponds to the timing between the *center* of the arc pulse interval and the *center* of the given detection interval. This, when later corrected for the over-all time lag of the system (discussed below), specifies the corrected timing being measured. The superimposed resolution width then has the usual significance.

The complete timing interval is thus studied by measuring successive groups each containing 16 intervals. In the above example for high resolution the *first group* contains 16 detection intervals in the range of $t=0$ to $t=75$ μsec. corresponding to neutron energies of 50 electron volts and up. The *second group* contains 16 intervals from $t=80$ to $t=155$ μsec. corresponding to neutron energies between 10 ev and 50 ev. The *third group* measures from $t=160$ to $t=235$ μsec. corresponding to $E=4$ ev to 10 ev. The *fourth group* similarly ex-

tends from $t=240$ to $t=315$ μsec. or $E=2.5$ to 4 ev. There are provisions for measuring 8 *groups* and this has always proved adequate for all measurements. In fact groups 5, 6, 7, and 8 are only rarely used.

The choice of the detection *group width* is obtained by setting switch *B* to the proper position. This is normally chosen to be equal to 16τ as in the above example. It is possible to choose other values for special purposes, however, and this is frequently done.

The above description explains the operation of the spectrometer timing system from a schematic viewpoint to present a general picture of the operation. A more detailed description may now be given. In order to obtain the different *groups* of detection intervals a group chain circuit with 7 stages in series is used. Each stage consists of a trigger circuit which has two stable conditions which may be called "off" and "on." Each stage is normally "off" during the complete operating cycle until it is triggered "on" by a pulse from *C* (first stage) or by the previous stage in the process of going "off." It then remains "on" until the next pulse arrives from *B* which turns *it* "off" and the next stage "on." This condition of activation starts when the first stage goes "on" at the start of the operating cycle and moves one step along the chain for each pulse from *B* until the last stage goes "off" after which all stages remain "off" until the start of a new operating cycle. The switch *D* selects either the pulse from *C* or the extinguishing pulse from any of the 7 chain stages to give a choice of any of 8 successively spaced pulses for use to start the detection chain circuits at the appropriate time during the operating cycle.

The detection intervals are provided by a similar "chain" of 16 stages. The first stage is turned "on" by the pulse from *D* and the condition of activation is moved along the chain by pulses from *A* (which determine the width of each detection interval). When the last of the detection stages goes "off," all stages remain inactive until the next pulse from *D* during the next operating cycle.

Detection

The system is now operated with two parallel independent BF_3 proportional counter detectors with separate collimating systems. The new counters have cathodes 10 cm in length, about 5-cm diameter, and are filled to 50-cm pressure with purified BF_3 enriched in B^{10} content for greater efficiency. The proper operating voltage for these counters depends on the amplifier gain and may be varied over 500 volts by varying the amplifier gain. At present a potential of 3700 volts is used. The background rate is regularly measured during each "run" by inserting thick B_4C or Cd in the beam but it is usually completely negligible. Some trouble was experienced with H.V. "humidity" pulses for a while but this was remedied by continuously blowing dry air over the counters.

Amplifier, Pulse Discriminator, and Coincidence Circuits

The twin pulse amplifiers have been rebuilt to give greatly improved high frequency response. The outputs of the amplifiers are sent to the level selectors and switching circuits along coaxial lines terminated in their characteristic impedances. A special multivibrator type level selector circuit is used to give a short resolving time, a minimum time lag, and uniform output pulses. Pulses from the level selector are fed to one side of each of 16 coincidence circuits the other input of which is the particular detection interval pulse. The pulses from the coincidence circuits each go to a separate high speed scale-of-2 circuit and then to a standard scale-of-16 circuit (which is normally operated as a scale-of-4). The output of each of these 32 "scale-of-16" circuits then goes to one of 32 registers which indicate the "timed" counts. These are arranged in banks for easy reading.

The output of each level selector circuit also goes directly to a high speed scale-of-4 circuit and then to a standard scale-of-128 circuit and register to indicate the "total counts" in each "channel."

Arc Modulation

The arc modulation is accomplished by controlling the accelerating voltage to the cyclotron arc. A bank of 12 type 6Y6-*G* tubes in series with the arc accelerating voltage circuit controls the arc current which is of the order of 5 amperes instantaneous current. For high resolution work this gives instantaneous deuteron power of 5 to 15

kilowatts on the target. Since an internal probe is used with a normal energy setting of about 8 Mev, this corresponds to an instantaneous deuteron current of about 700 to 2000 microamperes at the Be target. A special viewing circuit has been devised to permit accurate viewing of the arc *current* pulse as opposed to the arc voltage pulse. This has proved useful in adjusting the arc filament heating as well as to monitor arc operation.

Circuit Monitoring

To view the circuit operation extensive viewing circuits have been provided and circuits to compare several wave forms simultaneously. This is accomplished by the use of mixing circuits and an electronic switch circuit of special design. All of the circuits used in the present system were designed especially for this use and have not been described in the literature. To obtain excellent fractional microsecond response speeds the basic scale-of-2 and chain circuits, for example, employ principally type 6AG7 tubes and use plate load impedances of the order of 140, 500, 1000, 2000, and 3000 ohms. Since good high frequency response requires low impedances and thus high plate currents from all tubes, it was necessary to construct regulated power supplies of large current capacities. Thus regulated voltages of 100 volts at 5 amperes, 250 volts at 2 amperes, and -50 volts (bias) at 400 milliamperes are used for the timing circuits.

GENERAL REMARKS ON THE EXPERIMENTAL RESULTS

Resolution Width and Over-All Delay Time

Since the cyclotron arc pulse width and the detection interval widths are equal, the resolution function would be triangular in shape and of width 2τ if only these factors were involved. For energies above about 0.2 ev the other possible sources of resolution broadening are caused by the counter length, by any extra time smear of the slow neutron pulse leaving the paraffin "source slab," and by effects due to the lack of perfect sharpness of the pulses from the BF_3 counter-amplifier-level selector system. In addition there will be an over-all delay time correction due to cumulative time lags in the system such as the time for the deuterons to be accelerated

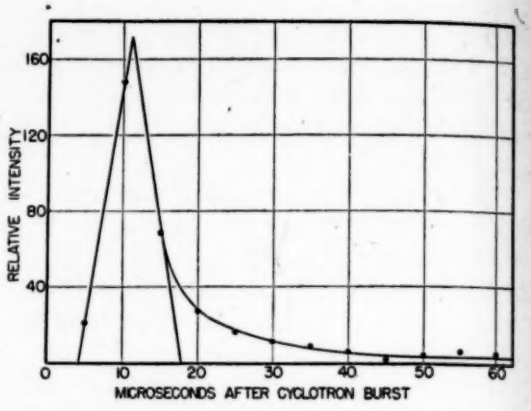

FIG. 2. Experimental resolution curve showing the over-all measured time delay in the system to be 11 μsec.

in the cyclotron (a low energy setting of the Be probe target decreases this effect), for the neutrons to be slowed in the paraffin slab, and the timing between the time when a neutron is captured in the BF_3 counter and the time corresponding to the center of the resultant pulse from the level selector circuit.

All of the above effects were important in the previous system and are described in the first two references. The net magnitude of these effects was experimentally determined with fair accuracy by placing the detector in a B_4C shield near the source. The intensity *vs.* timing was measured using 5 μsec. "on times" as shown in Fig. 2. This shows that the over-all time lag of the system is now about 11 μsec. The resolution function in this case is roughly triangular in shape and about 10 μsec. (2τ) wide. The "tail" shown on the right of the triangle (Fig. 2) is largely due to the effects of fast neutrons scattered around the cyclotron enclosure. Since the detector is normally outside the water barrier and better source shielding is employed, the magnitude of the "tail" in Fig. 2 is much greater than would be expected for normal operation.

The effect of the 10-cm counter length is to give an uncertainty of ± 5 cm in the total path length of 620 cm. This gives an extra broadening of the resolution width on a time of flight basis equal to 1.6 percent of the timing involved. This is usually much smaller than the value of τ selected. Although the resulting resolution function is no longer simply triangular in shape, it will be nearly so and has been taken to be of this form for simplicity.

As a result of the above reasoning it has been decided to omit the resolution function from all curves with the understanding that, almost always, the resolution function may be taken as triangular in shape with a width slightly greater than twice the spacing between adjacent points. It is unusual for the effective width to be as great as three times the spacing between adjacent points so the above rule will permit easy interpretation of the effect of the resolution width on the shape of the experimental curves.

Effect of the Thermal Lag from the Source

For energies below about 0.2 ev the lag in the emission of thermal neutrons from the source must be considered. This is caused by the diffusion time of the thermal neutrons in leaving the source. The present paraffin source slab is slightly thinner than the one previously used so the calculated delay time is now about 30 μsec. and this value has been used. This means that 4.5 μsec./meter must be deducted from the timings and added to the resolution width for timings greater than about 200 μsec./meter. For intermediate timings a graded correction factor is used. For the resolution normally used in the thermal region the width of the resolution triangle is less than three times the spacing between adjacent points.

Convention Regarding Cross Section and Energy

To simplify the notation it will be understood that cross sections are always expressed in units of $\times 10^{-24}$ cm^2/atom, and the symbol E will refer to the neutron energy in electron volts. The units will usually not be explicitly stated.

Significance of Measured Cross Sections at Resonance

Except in the case of Cd where a detailed analysis of the resonance has been made, it is usual for resonances to occur at several ev energy or higher. For these resonances the transmission curve shows a dip at resonance such that the area under the transmission curve is related to $\sigma_0\Gamma^2$, the strength of the level.[2] When the resolution width is large compared to the level half-width there is thus little relation between the value of σ_0 (the true cross section at exact resonance) and $[-(1/n)\log T_{\min}]$, the cross section calculated directly from the experimental transmission curve. It is possible to say that σ_0 is greater than $[-(1/n)\log T_{\min}]$ but in many cases the ratio of the two values may be of the order of 10 to 1000 and a comparison may be more misleading than helpful. From experience it has been found that curves plotting the measured cross section of a sample in the region of a resonance *vs.* neutron energy (or $\log E$) while of some interest are easily misinterpreted and such questions as the reality of a resonance dip and significance of the magnitude of the dip can better be judged when a curve showing measured transmission *vs.* time of flight is used. To permit easy determination of the neutron energy a neutron energy scale is also given. Also, since the value of the measured cross section away from a resonance is significant, a cross-section scale is usually indicated at the right of each curve. An additional advantage of this method for measurements in the thermal region is the fact that the $(1/v)$ capture term in the thermal region shows as a straight line when the transmission on a logarithmic scale is plotted as a function of the timing.

The Assignment of Resonance Levels to Particular Isotopes

While it is true that each observed resonance in a sample should be assigned to a particular isotope of the element, there is usually insufficient information available to make this assignment. As a result the policy has been adopted of stating the values of σ and σ_0 as if only one isotope were present (in terms of the element as a single material). In cases where the proper isotope assignment can be made, the true cross section per atom may be obtained by dividing the uncorrected value by the fractional concentration of the responsible isotope in the natural element. In special cases where this can be done the values will be given in the usual manner first and then special mention will be made of the corrected values.

Calculation of $\sigma_0\Gamma^2$, the "Strength" of the Level

If σ_0 is the cross section at exact resonance for a sample and n is the number of absorbing atoms

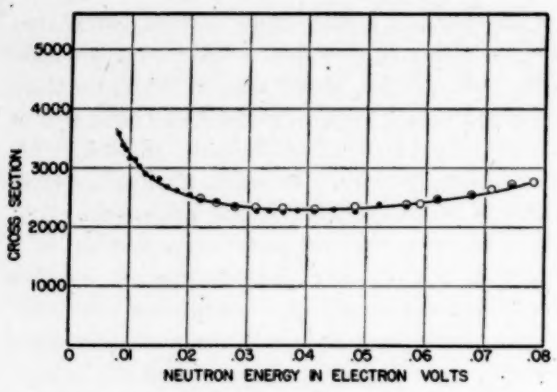

FIG. 3. The slow neutron cross section of cadmium in the energy interval 0–0.08 ev.

● Experimental points for the 43.8 mg/cm² sample
○ Experimental points for the 219 mg/cm² sample

The solid line is a theoretical curve using the Breit-Wigner one-level formula with $E_0=0.176$ ev, $\Gamma=0.115$ ev, and $\sigma_0=7200$.

per square centimeter, then $T=e^{-n\sigma_0}$ is the true transmission for exact resonance. If $n\sigma_0$ is large compared with unity it has been shown[2] that the area *above* the transmission *vs.* time-of-flight curve is a function of $n\sigma_0\Gamma^2$ and, for dips with small area, is proportional to $(n\sigma_0\Gamma^2)^{\frac{1}{2}}$. The theory has been developed to permit $\sigma_0\Gamma^2$ to be determined for such a resonance dip and it has been applied to the cases of In, Ag, Au, and Sb[2] where it probably applies.

From the results of measurements using a number of other elements, however, it has been found that many of the resonance dips are quite small even when rather thick samples are used. After these results were examined there was some question as to whether it was proper to assume that $n\sigma_0\gg1$ for all of these levels. If $n\sigma_0\ll1$ and the level dip area is obtained by a comparatively large level width Γ, the area *above the transmission curve* will be proportional to $n\sigma_0\Gamma$ rather than to $(n\sigma_0\Gamma^2)^{\frac{1}{2}}$ while intermediate conditions will apply when $n\sigma_0$ is neither large nor small. This uncertainty in many cases has tended to discourage the calculation of $\sigma_0\Gamma^2$ by the usual method. In that case the information presented about a level would be limited to a statement of the position of the level plus what rough evidence can be obtained concerning the relative strength of the level from the appearance of the transmission curve.

After some consideration it has been decided that a statement of the calculated value of $\sigma_0\Gamma^2$ should be given but with the understanding that the assumption $n\sigma_0\gg1$ is involved. Since this assumption may sometimes be incorrect it should be understood that the values given are valid only to the extent that this condition is satisfied. Values of $\sigma_0\Gamma^2$ will always be expressed in units of $\times10^{-24}$ (ev)² cm²/atom, although for simplicity the units will not be explicitly stated.

There is also the possibility that some of the observed resonance dips may be caused by many unresolved levels. In this case the interpretation will be of limited significance. In particular if $\sigma_0\gg1$ for each level and Γ much less than the spacing between levels, the area is proportional to the sum of the $(n\sigma_0\Gamma^2)^{\frac{1}{2}}$ terms while if $\sigma_0\ll1$ for each level and Γ much less than the spacing between levels, the area is proportional to the sum of the $n\sigma_0\Gamma$ terms. In particular the "broad" resonances may always be caused by two or more unresolved sharp levels.

RESULTS

Cadmium

The samples used for the cadmium transmission measurements were cut from sheets rolled to 0.010″ and 0.022″ thicknesses. A spectrographic analysis of the cadmium showed less than 0.05 percent of Pb and Tl; less than 0.005 percent of Al, Ag, and Cu; traces of Ca, Cr, Fe, Sn. For all

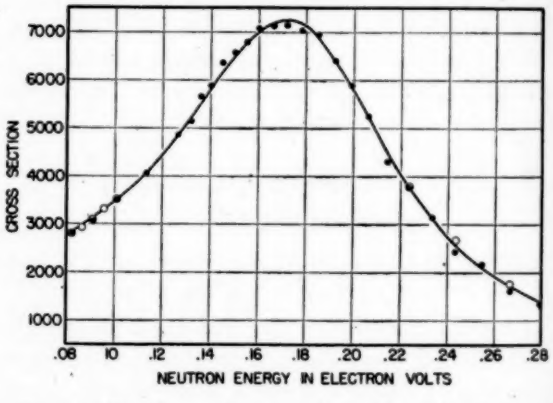

FIG. 4. The slow neutron cross section of cadmium in the energy interval from 0.08 ev to 0.28 ev.

● Experimental points for the 43.8 mg/cm² sample
○ Experimental points for the 219 mg/cm² sample

The solid line is a theoretical curve using the Breit-Wigner one-level formula with $E_0=0.176$ ev, $\Gamma=0.115$ ev, and $\sigma_0=7200$.

the other metals the prominent lines were not apparent, therefore the impurity was probably less than 0.05 percent for arc insensitive elements or less than 10^{-5} percent for arc sensitive elements.

The results of the measurements of the slow neutron cross section *vs.* energy for cadmium are shown in Figs. 3–5. In order to obtain a detailed comparison of the experimental results and the Breit-Wigner one-level formula, it was necessary to use four different sample thicknesses since changes in the total cross section of a factor greater than 1000 were studied. The samples were rolled Cd foil with thicknesses of 43.8 mg/cm², 219 mg/cm², 4.47 g/cm², and 11.03 g/cm². The thick sample was also used to investigate the possibility of other resonances at higher energies as shown in Fig. 6.

The agreement between the theoretical curve and the experimental results in Figs. 3–5 are seen

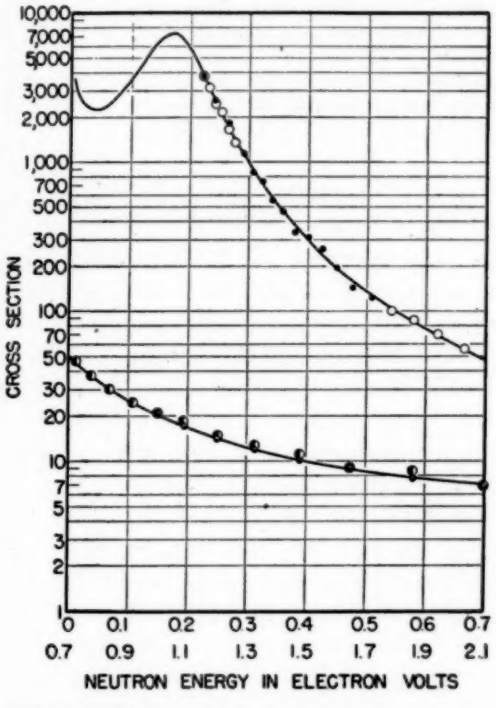

FIG. 5. The slow neutron cross section of cadmium in the energy interval from 0.2 ev to 2.1 ev.

● Experimental points for 43.8 mg/cm² sample
○ Experimental points for 219 mg/cm² sample
◐ Experimental points for 4.47 g/cm² sample
◒ Experimental points for 11.03 g/cm² sample

The solid line is a theoretical curve using the Breit-Wigner one-level formula with $E_0=0.176$ ev, $\Gamma=0.115$ ev, and $\sigma_0=7200$. A "constant term" of 5.3 has been added to the theoretical curve to account for the scattering cross section.

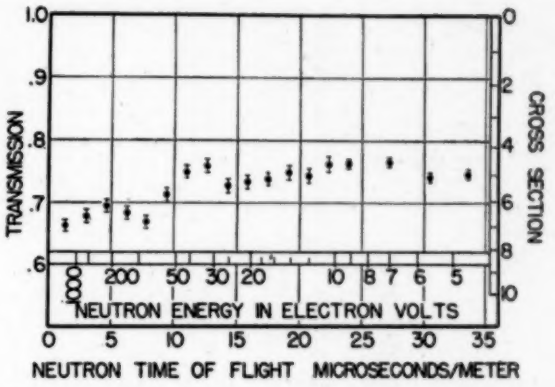

FIG. 6. The slow neutron transmission of 11.03 g/cm² cadmium. This curve indicates that the Cd cross section remains approximately constant in the high energy region, although weak levels may be present above 10 ev.

to be within the experimental accuracy of the measurements over the entire region investigated. The statistical uncertainties of the points have not been indicated as their magnitude is often equal in size to the circles used to indicate the experimental points. Individual transmission measurements have a statistical accuracy of the order of (1–3) percent. The degree to which the points fall on a smooth curve illustrates the statistical accuracy involved. Since the best "experimental" curve through the points coincides with the theoretical curve over an extremely wide range of energy and cross section, it is concluded that the Breit-Wigner one-level formula applies for the cadmium resonance over the region investigated.

The sensitivity of the agreement to the choice of the parameters $E_0=0.176$ ev, $\Gamma=0.115$ ev, $\sigma_0=7200$ is such that, if σ_0 is held constant a change of ± 0.001 ev in E_0 or Γ produces a noticeably poorer agreement between the curve and the experimental points. If σ_0 is changed by ± 200 and Γ is adjusted for best fit, the agreement cannot be made to extend over the entire region represented by Fig. 3. The cross section values indicated by the curve in Fig. 5 are not the Breit-Wigner values directly but have been increased by an amount equal to the scattering cross section (constant term) which was chosen to be 5.30. As shown in Fig. 6, the cross section does not reach and remain constant at this value for still higher energies but fluctuates somewhat possibly due partly to experimental uncertainties and perhaps also due to the presence of other

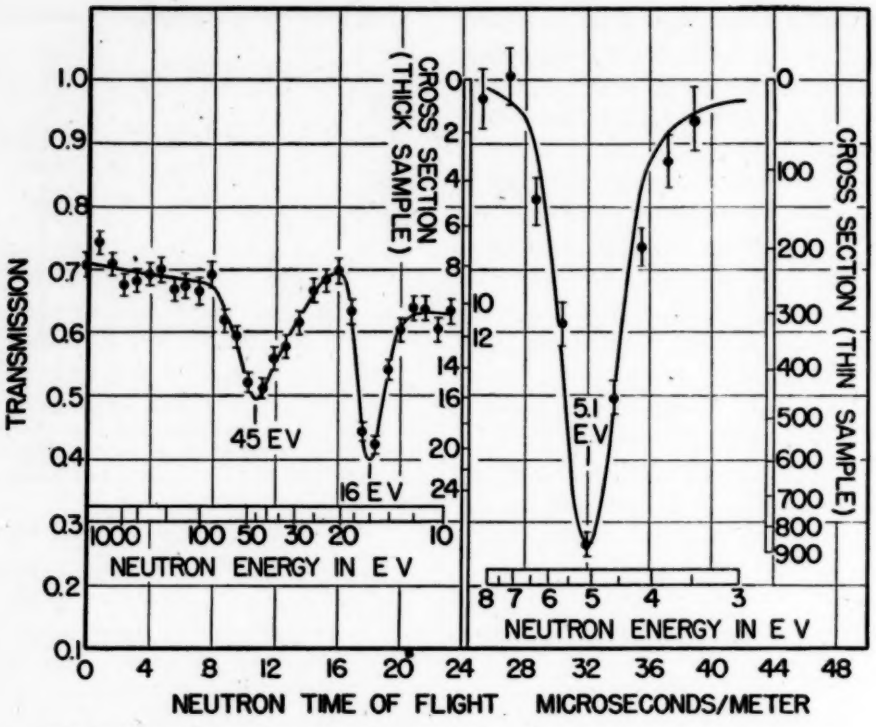

FIG. 7. The slow neutron transmission of silver. The curve on the left shows the transmission of a 7.84 g/cm² sample in the high energy region showing the resonances at 45 ev and 18 ev. The curve on the right shows the transmission of a 0.276 g/cm² sample in the vicinity of the level at 5.1 ev.

weak levels at higher energies. Thus, for example, one or more weak levels may be present near 100 ev. These levels will have a negligible effect on the total cross section in the region covered by Figs. 3–5 so the value $\sigma_{const}=(5.30\pm0.7)$ is justified below 2 ev. If the cross section in the resonance region also contains a much smaller resonance term for the scattering cross section, this will be included in the main parameters given above. In conclusion, when all possible sources of error are considered, the results for the cadmium parameters have been chosen as

$$E_0=(0.176\pm0.002)\text{ ev},$$
$$\Gamma=(0.115\pm0.002)\text{ ev},$$
$$\sigma_0=(7200\pm200)\text{ cm}^2,$$
$$\sigma_{scatt}=(5.30\pm0.7)\text{ cm}^2.$$

The resonance has now been shown[6] to be attributed to Cd^{113}, so the isotopic value of σ_0 will be 58,500.

[6] B. J. Mayer, B. Peters, and E. H. Schmidt, Phys. Rev. 69, 666 (1946).

Silver

The samples used for the transmission measurements were of metallic silver. A spectrographic analysis of the silver showed less than 0.05 percent of Cu, Pb; less than 0.005 percent of Mg, Mn, Fe, Tl, and Bi. For all the other metals the prominent lines were not apparent, therefore the impurity was probably less than 0.05 percent for arc insensitive materials or less than 10^{-5} percent for arc sensitive materials.

Since the slow neutron transmission of silver has already been investigated using the earlier form of the spectrometer system,[2] the purpose of the present measurements was to investigate the higher energy region with better resolution. The results of these measurements are shown in Fig. 7. The solid curve shown for the 5.1-ev resonance is a calculated curve based on the parameters given in the previous paper.[2] The agreement is seen to be within the experimental accuracy.

The results of the measurements using the thick sample clearly show the presence of a broad

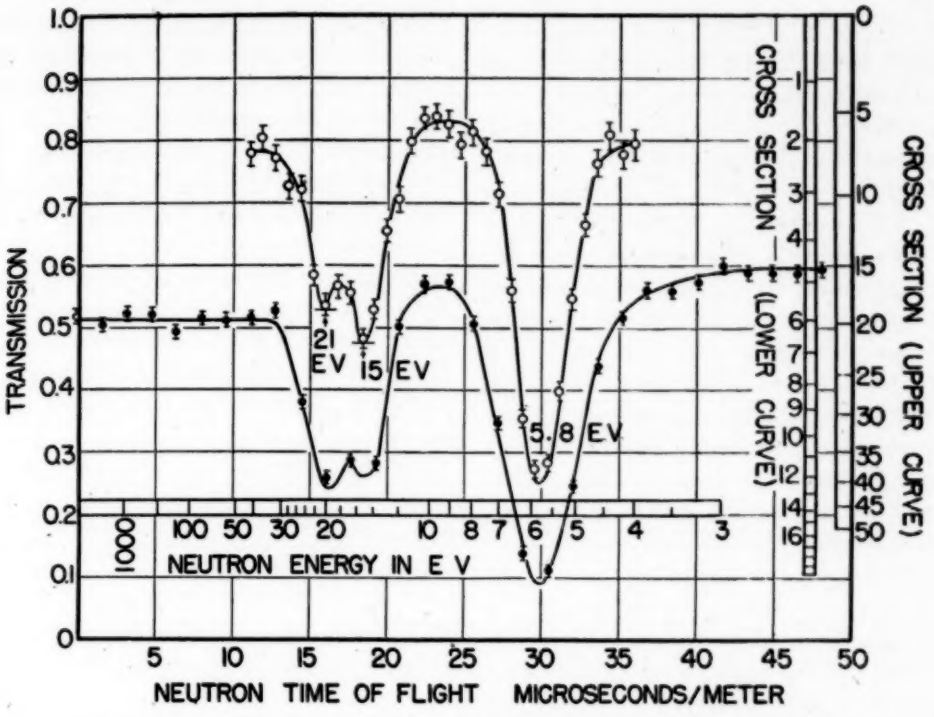

FIG. 8. The slow neutron transmission of antimony. The upper curve shows the transmission of a 6.84-g/cm² sample of antimony with 1.8 μsec./meter resolution width. The lower curve shows the transmission of a 22.4-g/cm² sample of antimony with a 3.6 μsec./meter resolution width. The use of a thinner sample and higher resolution permits a partial resolution of the levels at 15 and 21 ev.

level at (45±4) ev and a level at (16±1) ev in good agreement with the previous results of 13.7 ev and 43 ev. There are three well-established activities with half-lives of 2.3 min., 22 sec., and 225 days induced in silver by $(n-\gamma)$ reactions.[7,8]

As mentioned above, the measured values of the cross section σ_{max} at exact resonance has no simple relation to the true value of σ_0 for the level since σ_0 is usually very much larger than σ_{max}. The cross section scales are shown only for orientation purposes and are significant only on either side of the resonance dips where the transmission is a slowly varying function of the energy. Thus $\sigma=(8 \text{ to } 9)$ for $E=(80 \text{ to } 1000)$ ev as seen in Fig. 7.

In the previous studies[2] the cross section in the thermal region was found to be given by $\sigma_{thermal}=[(6.6\pm0.5)+(9.05\pm0.10)E^{-\frac{1}{2}}]$. The value of $\sigma_0\Gamma^2$ for the main resonance at 5.1 ev agrees well with the previous value of (300±50). Approximate calculations indicate that $\sigma_0\Gamma^2=24$ and 700 for the levels at 16 ev and 45 ev, respectively. These values are perhaps significant to within a factor of two. Because of the width of the level at 45 ev (as indicated by the fact that the observed width of the dip is several times the resolution width for a small amplitude of dip in the transmission curve), there is reason to suspect that $\sigma_0\Gamma^2 \ll 1$ rather than $\gg 1$ as assumed. In this case an approximate calculation indicates that $\sigma_0\Gamma=200$ roughly. Also, if the resonance is assumed to be almost resolved in Fig. 7, direct observation indicates that $\sigma_0 \sim 6$ to 10 and $\Gamma \sim 25$ ev which gives about a factor of 7 difference for the two assumptions of $n\sigma_0 \gg 1$ or $\ll 1$. If several narrow unresolved levels are responsible the above discussion is meaningless. Since silver has only two almost equally abundant stable isotopes, the true values of $\sigma_0\Gamma^2$ will be about double the uncorrected values given above for the normal element.

[7] E. Amaldi, O. D'Agostino, E. Fermi, B. Pontecorve, F. Rasetti, and E. Segrè, Proc. Roy. Soc., London **A149**, 522 (1935).

[8] J. J. Livingood and G. Seaborg, Phys. Rev. **54**, 88 (1938); K. Alexeeva, Comptes rendus, U.S.S.R. **18**, 533 (1938); A. C. G. Mitchell, Phys. Rev. **53**, 269 (1938).

Antimony

The samples used for the transmission measurements on antimony were cast disks of the metal. A spectrographic analysis of the antimony showed less than 0.05 percent of Ca, Ag, and Si; less than 0.005 percent of Mg, Ni, Cu, and Ge; traces of Co, Pb, and As. For all other metals the prominent lines were not apparent therefore the impurity was probably less than 0.05 percent for arc insensitive materials or less than 10^{-5} percent for arc sensitive materials.

Antimony has also been studied previously using the "old" system.[2] The measurements have been repeated using the "new" system to determine more precisely the position of the resonances and as a comparison of measurements using the two systems. The new results are shown in Fig. 8. The measurements were first made using the 22.4 g/cm² sample as shown in the lower curve. The two main resonances are observed as before but the upper level now appears to be composed of two unresolved levels near 15 and 20 ev, respectively. The first level is at (5.8 ± 0.15) ev. There is no indication of still higher levels which were previously suspected to exist.[2]

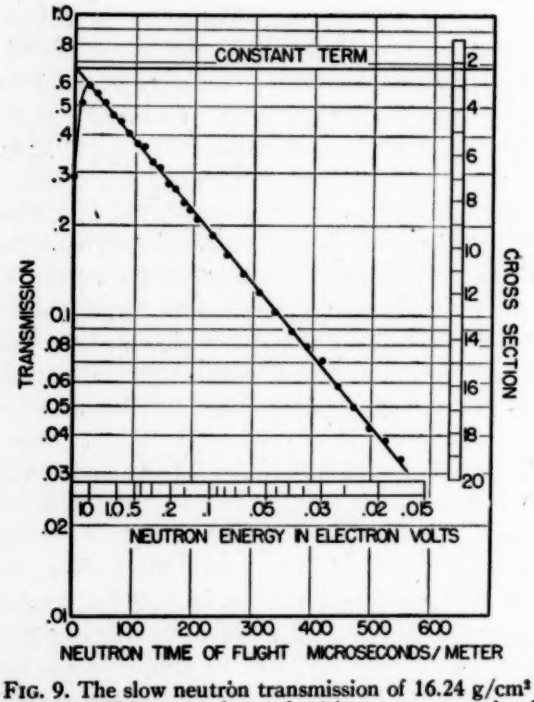

FIG. 9. The slow neutron transmission of 16.24 g/cm² of manganese. This curve shows the $1/v$ type cross section for manganese in the thermal region with $\sigma=(2.26+2.24E^{-\frac{1}{2}})$ and also shows indications of resonances at higher energies.

In order to investigate the nature of the upper "double" resonance, the measurements were repeated using a 6.84 g/cm² sample and double the resolution. The results are shown in the upper curve which more nearly resolves the two peaks. They are seen to be at (15 ± 1) and (21 ± 1.5) ev. The samples used are the same as were used for the earlier measurements.[2] As previously remarked, the value of σ_{max}, the "*measured*" cross section at resonance, is not even approximately equal to the σ_0 the true cross section at resonance. There are two well-established activities of 2.8 d. and 60 d. known to be induced in antimony by $(n-\gamma)$ reactions.[7,9]

In the previous studies[2] the cross section in the thermal region was found to be given by $\sigma_{thermal}=[(4.2\pm0.5)+(0.64\pm0.04)E^{-\frac{1}{2}}]$. On the basis of Fig. 8 approximate calculations have been made to determine the values of $\sigma_0\Gamma^2$ for each of the three levels assuming that the values are approximately equal for the levels at 15 ev

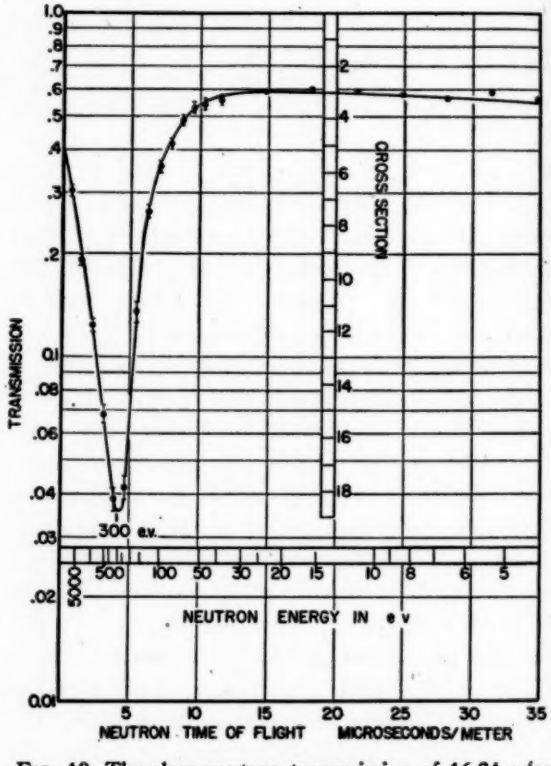

FIG. 10. The slow neutron transmission of 16.24 g/cm. of manganese. This curve shows the transmission of manganese in the higher energy region. The position of the resonance level is approximately 300 ev.

[9] J. J. Livingood and G. Seaborg, Phys. Rev. 55, 414 (1939).

and 21 ev. The results which are perhaps significant to within a factor of two, are $\sigma_0\Gamma^2=12$, 35, and 35 for the levels at 5.8 ev, 15 ev, and 21 ev. Antimony also has only two stable isotopes of almost equal abundance so the above values of $\sigma_0\Gamma^2$ will be twice as large on an isotopic basis.

It is interesting to note that the cross section above 40 ev is quite constant but *not* equal to the value predicted from the intercept of the thermal $1/v$ curve.

Manganese

The results of the measurements using a 16.24 g/cm² sample of pure electrolytic manganese are shown in Figs. 9 and 10. It is seen that the cross section below about 30 ev is well matched by the simple $1/v$ line $\sigma=[2.26+2.24E^{-\frac{1}{2}}]$. Figure 10 shows that there are no observable resonance levels below the main resonance at (300 ± 40) ev. The level is of particular interest since it represents a strong level which has been measured with good resolution in the region of several hundred volts and also since this value is of the order of ten or more times as large as previously reported values for the manganese resonance.[3-5]

Previous determinations of the energy of the manganese resonance have been made using Mn detectors and the boron absorption method to determine the energy. The values reported were 15 ev[3,4] and 37 ev[5] and it is of interest to observe the degree to which such measurements can be in error. The reason for the low values is easily understood by reference to Figs. 9 and 10. Since the Mn resonance occurs so high it was necessary to use a comparatively thick Mn detector for the measurements to obtain sufficient sensitivity whereas an extremely thin sample is required to obtain correct results. When a thin detector is used it is assumed that the absorption can be considered as the sum of that near exact resonance and that in the "$1/v$ region" for energies considerably lower than the resonance energy. In particular it is usually assumed that essentially all of the $1/v$ absorption is for neutrons having energies below about 0.5 ev which are removed by thick Cd. Whereas this latter condition applies for resonances at a few ev like those of In, Rh, Ag, and Au; the $1/v$ region in Figs. 9 and 10 is seen to contain a large "area of absorption" (since actual *transmission* of the sample is shown)

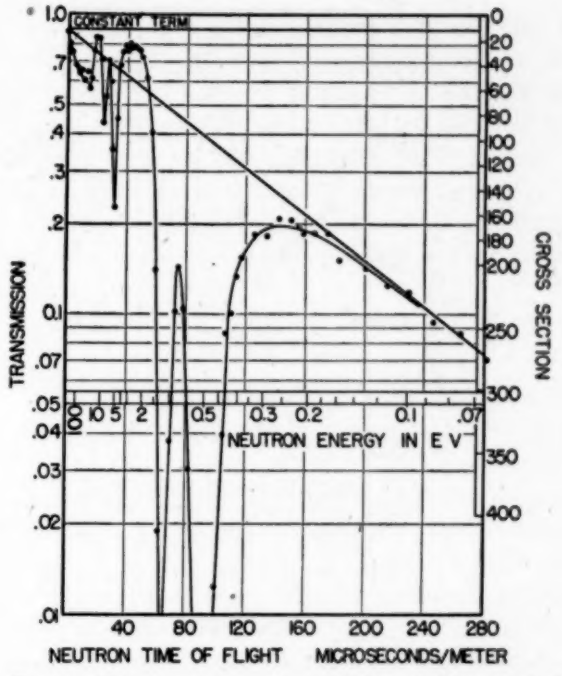

FIG. 11. The slow neutron transmission of 3.08 g/cm² of iridium. The curve illustrates the fact that the iridium cross section approaches the $1/v$ line in the thermal region with $\sigma=(14+64.5E^{-\frac{1}{2}})$ and also shows the several resonance levels in this energy region.

above 0.5 ev. In particular it is probable that over half of the total absorption, which was attributed entirely to the resonance region, was due to absorption in the $1/v$ region. This easily accounts for the low resonance energies observed.

In Fig. 9 the statistical uncertainty of the points has not been indicated since it is of the order of magnitude of the size of the circles used to represent the experimental points. This is also true of the unmarked points in Fig. 10. It will be observed that there is no indication of a resonance below 0.4 ev as was indicated by other investigators (the above discussion is intended as a general criticism of the boron absorption method for determining the energy of resonant levels rather than as a particular criticism of the papers mentioned). When several levels are responsible for a given activity the boron method will also be misleading. For this reason references to the results of the boron absorption method will be omitted for most elements.

The results may be summarized as follows:

$\sigma=[(2.2\pm0.4)+(2.24\pm0.05)E^{-\frac{1}{2}}]$ below 30 ev; there is a strong resonance with $E_0=[300\pm40]$ ev.

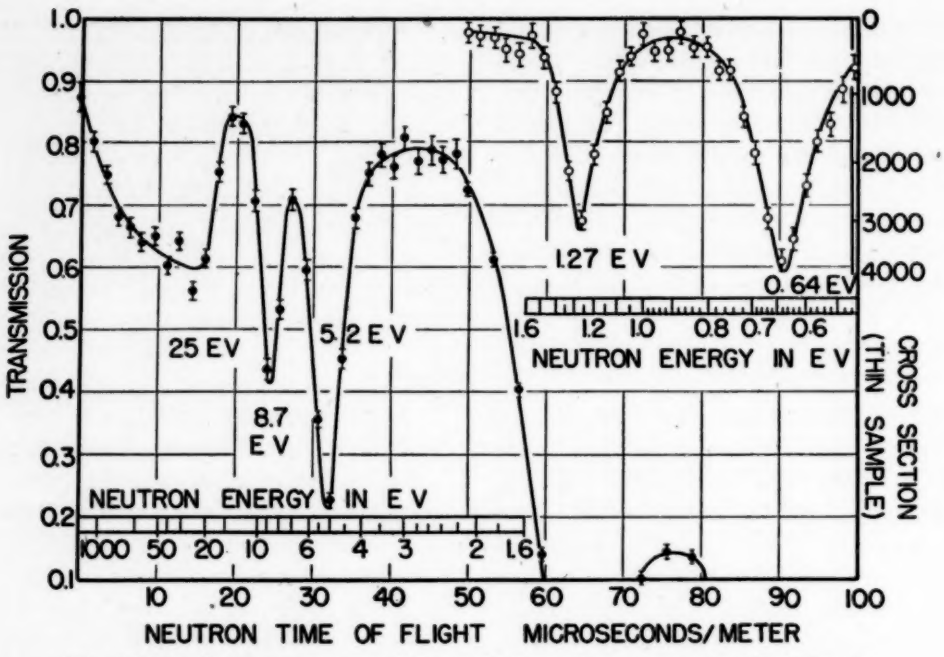

FIG. 12. The slow neutron transmission of iridium. The curve on the left shows the transmission of a 3.08 g/cm² sample in the high energy region and shows the levels at 8.7 ev, 5.2 ev, and indications of levels at 25 ev and above. The curve on the right shows the transmission of an 0.0424 g/cm² sample which emphasizes the levels at 1.27 and 0.64 ev.

The rise in transmission is slow on the high energy side of resonance indicating that higher (strong) unresolved levels may be present. A value of $\sigma_0\Gamma^2$ has not been calculated due to the shape of the curve on the high energy side of the resonance. Since manganese has only one isotope there is no uncertainty in the assignment of the resonance level to this isotope.

Iridium

The results of the iridium transmission measurements are shown in Figs. 11 and 12. The 3.08 g/cm² sample was made from C.P. metallic powder and heated to 800°C in a nitrogen atmosphere. The 0.0424 g/cm² sample consisted of the metallic powder mixed in sulphur to obtain uniformity. A spectrographic analysis of the iridium showed that there was less than 0.5 percent of Si; less than 0.05 percent of Ca and Ni; less than 0.005 percent of Mg and Pb; traces of Be, Fe, Rh, Pt, Cu, and Ag. For all other metals the prominent lines were not apparent therefore the impurity was probably less than 0.05 percent for arc insensitive materials and less than 10^{-5} percent for arc sensitive materials.

Figure 11 shows part of the data in the thermal region which shows the $1/v$ slope. Measurements were made up to 480 microseconds/meter and the best straight line for the $1/v$ slope. $\sigma=(14+64.5E^{-\frac{1}{2}})$ is shown in Fig. 11. The overall features of the transmission curve are shown in Fig. 11 including the resonances near 0.64, 1.27, 5.2, 8.7, and 25 ev.

Iridium has two stable isotopes and there are three known activities of 15 min., 19 hr., and 60 d. induced in Ir by $(n-\gamma)$ reactions.[7,10]

The resonance region is expanded in Fig. 12 and the results of the measurements at the first two levels using the thin sample are shown. The thin sample was used to obtain more accurate values for the energies of these resonances and to obtain higher values for the lower limits of the σ_0 values at exact resonance. It is seen that measured values of σ_{max} of about 4000 and 3000 were obtained so the σ_0 values for the resonances are probably equal to or greater than 5000.

[10] E. McMillan, M. Kamen, and S. Ruben, Phys. Rev. 52, 375 (1937); M. L. Pool, J. M. Cork, and R. L. Thornton, Phys. Rev. 52, 239 (1937); V. Fomin and F. G. Hontesmans, Physik. Zeits. Sowjetunion 9, 273 (1936); R. Jaeckel, Zeits. f. Physik 110, 330 (1938).

The results for iridium may be summarized:

1. $\sigma_{\text{thermal}} = [(14\pm6)+(64\pm2)E^{-\frac{1}{2}}]$.
2. For the first resonance:
   $E_0(0.64\pm0.015)$ ev,
   $\sigma_0\Gamma^2 = (5 \text{ to } 20)\times10^{-24}$ (ev)^2 cm^2/atom,
   $\sigma_0 \geqslant 4500$ (probably). $\Gamma \leqslant 0.07$ ev (probably).
3. For the second resonance:
   $E_0 = (1.27\pm0.04)$ ev,
   $\sigma_0\Gamma^2 = (5 \text{ to } 20)$,
   $\sigma_0 \geqslant 4000$ and $\Gamma \leqslant 0.07$ ev (probably).
4. $\sigma = (25\pm4)$ for 2.2 ev $\leqslant E \leqslant$ 3.5 ev.
5. For the third resonance
   $E_0 = (5.2\pm0.2)$ ev,
   $\sigma_0\Gamma^2 = 55$ roughly.
6. For the fourth resonance:
   $E_0 = (8.7\pm0.3)$ ev,
   $\sigma_0\Gamma^2 = 50$ roughly.
7. $\sigma = (18\pm3)$ near $E = 14$ ev.
8. For the "fifth" resonance
   $E_0 = (25\pm5)$ ev.

9. The shape of the transmission curve for $E > 25$ ev indicates that probably more levels are present at higher energies so $\sigma_0\Gamma^2$ has not been calculated for this "level."

10. Iridium has the isotopes Ir^{191} and Ir^{193} of 38.5 percent and 61.5 percent abundance, respectively. The above values of σ_0 and $\sigma_0\Gamma^2$ for the resonances are uncorrected values for the natural element. Depending on which isotope is responsible for a given level, the values should be increased by a factor somewhat greater or somewhat less than two to give the true values for the responsible isotope.

Conclusion

Since the measurements were made which have been described in two previous papers[1,2] slow neutron transmission *vs.* time of flight measurements have been made for a large number of elements and the slow neutron spectrometer system has been considerably improved. In this first of the new series of papers describing these measurements, the results for Cd, Ag, Sb, Mn, and Ir, have been presented and other results will be presented soon in subsequent papers. This work represents, in all, several thousand hours of cyclotron running time. We wish to thank those who have made this work possible and assisted in the measurements.

PHYSICAL REVIEW VOLUME 71, NUMBER 2 JANUARY 15, 1947

Angular Momentum of Photons

José A. Balseiro
Córdoba Observatory, Córdoba, Argentina
(Received August 12, 1946)

The theory of elementary particles permits one to attribute well-defined angular momentum expressions to a given radiation field. A few simple examples are discussed, which involve systems of two photons, and of one atom and one photon, and which permit one to account for the conservation of total angular momentum. Conservation of total angular momentum, including radiation, is, however, of little practical importance, because spatial orientation of a given system requires, in general, the use of external magnetic fields, which perturb the angular momentum balance.

1. INTRODUCTION

ACCORDING to the field theory of elementary particles, angular momentum expressions can be attributed to a given particle field, which, in general, can be divided into an orbital angular momentum and a spin part.[1] In the particular case of electromagnetic radiation, however, no gauge invariant separation between spin and orbital momentum is possible.[2]

[1] F. J. Belinfante, Physica 6, 887 (1939); W. Pauli, Rev. Mod. Phys. 13, 203 (1941).
[2] L. Rosenfeld, Mém. Acad. Roy. Belg. (Cl. Sc.) 18, 562 (1942).

TABLE I. Quantum states.

	$M=2$	1	0	−1	−2
$L=0$		$\frac{1}{\sqrt{3}}\Gamma 00(\nu_1\nu_2)+\frac{1}{\sqrt{3}}\Gamma 1\,-1(\nu_1\nu_2)+\frac{1}{\sqrt{3}}\Gamma -11(\nu_1\nu_2)$			
$L=1$	$-\frac{1}{\sqrt{2}}\Gamma 10(\nu_1\nu_2)+\frac{1}{\sqrt{2}}(\Gamma 01\nu_1\nu_2)$	$\frac{1}{\sqrt{2}}\Gamma 1\,-1(\nu_1\nu_2)-\frac{1}{\sqrt{2}}\Gamma -11(\nu_1\nu_2)$		$-\frac{1}{\sqrt{2}}\Gamma -10(\nu_1\nu_2)+\frac{1}{\sqrt{2}}\Gamma 0\,-1(\nu_1\nu_2)$	
$L=2$	$\Gamma 11(\nu_1\nu_2)$ $\frac{1}{\sqrt{2}}\Gamma 10(\nu_1\nu_2)+\frac{1}{\sqrt{2}}\Gamma 01(\nu_1\nu_2)$	$\left(\frac{2}{3}\right)^{\frac{1}{2}}\Gamma 00(\nu_1\nu_2)-\frac{1}{6^{\frac{1}{2}}}\Gamma 1\,-1(\nu_1\nu_2)-\frac{1}{6^{\frac{1}{2}}}\Gamma -11(\nu_1\nu_2)$	$\frac{1}{\sqrt{2}}\Gamma -10(\nu_1\nu_2)+\frac{1}{\sqrt{2}}\Gamma 0\,-1(\nu_1\nu_2)$	$\Gamma -1\,-1(\nu_1\nu_2)$	

The angular momentum operator of an electromagnetic field is given by

$$\mathbf{J}=\frac{1}{8\pi c}\int \mathbf{r}\times[\mathbf{E}^{\dagger}\times\mathbf{H}-\mathbf{H}^{\dagger}\times E]d\tau, \qquad (1)$$

$$\mathbf{E}=\sum_{s,k} a_s(k)\mathbf{E}_s(k), \quad \mathbf{H}=\sum_{s,k} a_s(k)\mathbf{H}_s(k),$$

where $a_s^{\dagger}(k)$ and $a_s(k)$ represent, respectively, emission and absorption operators, $\mathbf{k}$ the wave vector, $\mathbf{E}_s$ and $\mathbf{H}_s$ field vectors belonging to an orthogonal set of solutions of Maxwell's equations, normalized to represent single photons.

Equation (1) permits one to attribute to the angular momentum of a radiation field a matrix representation, which, in the case of a single photon present, reduces to

$$\mathbf{J}_{ik}=\frac{1}{8\pi c}\int \mathbf{r}\times[\mathbf{E}_i^{*}\times\mathbf{H}_k-\mathbf{H}_k\times\mathbf{E}_i^{*}]d\tau. \qquad (2)$$

Diagonal terms of (2) were already known in classical theory and led M. Abraham to attribute to a circular polarized dipole wave $J_z=J_y=0$; $J_x=\pm W/2\pi\nu$.

2. ANGULAR MOMENTUM MATRICES

It is well known that the use of a set of spherical solutions of Maxwell's equations is adequate to our problem. We shall use the solutions given by Born,[3] distinguishing between electric (E) and magnetic (M) waves, normalized by

$$(lm|W(kk')|l'm')=\frac{1}{8\pi}\int[\mathbf{E}^{*l'm'}(k')\cdot\mathbf{E}^{lm}(k) +\mathbf{H}^{*l'm'}(k')\cdot\mathbf{H}^{lm}(k)]d\tau =h\nu\delta_{kk'}\delta_{ll'}\delta_{mm'}. \qquad (3)$$

[3] M. Born, *Optik* (Julius Springer, Berlin, 1933), p. 278.

In the case of a single photon present in the field, the angular momentum matrices become, both for (E) and (M) waves,

$$(lm|J_z|l'm')=\hbar m\delta_{ll'}\delta_{mm'},$$
$$(lm|J_x\pm iJ_y|l'm')=\hbar[(l\pm m)(l\mp m+1)]^{\frac{1}{2}}\times\delta_{ll'}\delta_{m\mp 1m'}, \qquad (4)$$

while the transition elements $(E)\leftrightarrow(M)$ vanish.

In the case of an arbitrarily large number of photons, only those matrix elements do not vanish, for which no transitions between states of different frequency ν and different angular momentum l occur, and in which, within the mentioned limitations, the total number of photons is conserved and no more than one photon shifted from one state, i, to another, f.

J_z turns out to be a diagonal matrix

$$(n_1\cdots|J_z|n_1\cdots)=\hbar\sum n_i m_i, \qquad (5)$$

while

$$(n_1\cdots n_i\cdots n_f\cdots|J_x\pm iJ_y|n_1\cdots n_i-1\cdots n_f+1) =\hbar[n_i(n_f+1)(l\pm m_i)(l\mp m_i+1)]^{\frac{1}{2}} \qquad (6)$$

with $m_f=m_i\pm 1$.

W. Heitler has proved that the matrices (5) and (6) satisfy the well-known commutation relations between angular momenta.[4]

3. COMPOSITION OF ANGULAR MOMENTUM OF TWO PHOTONS

The matrices (5) and (6) permit us, immediately, to compose angular momenta of two photons, which may have different frequencies, $\nu_1\neq\nu_2$, but which may both belong to dipole waves of angular momentum quantum numbers m_1, m_2. In particular, we shall denote the field eigenfunctions of this configuration by $\Gamma_{m_1m_2}(\nu_1\nu_2)$.

[4] W. Heitler, Proc. Camb. Phil. Soc. **32**, 112 (1936).

TABLE II. Angular intensity distribution.

	$M=2$	1	0	−1	−2
$L=0$			$K=\frac{C}{r^2}(\nu_1+\nu_2)$		
$L=1$		$K(1+\frac{1}{2}\sin^2\theta)$	$K(1+\cos^2\theta)$	$K(1+\cos^2\theta)$	
$L=2$	$K(1+\cos^2\theta)$	$K(1+\frac{1}{2}\sin^2\theta)$	$K(\frac{2}{3}+\sin^2\theta)$	$K(1+\frac{1}{2}\sin^2\theta)$	$K(1+\sin^2\theta)$

Transforming the total angular momentum to principal axes, we obtain nine different states belonging to the total angular momentum quantum numbers $L=0, 1, 2$; $-L\leqq M\leqq +L$, corresponding to the following linear combinations which are analogous to the eigenfunctions of two material particles, obeying Bose-Einstein statistics. As in the case of material particles, the solutions belonging to $L=1$ vanish, if we put $\nu_1=\nu_2$.

The linear combinations of Table I permit us immediately to determine the angular intensity distribution of the two photon fields (Table II) which is identical with that one would obtain in classical theory by superposing the corresponding dipole waves and averaging over the relative phases. This last remark permits us to account immediately for the polarization state of the field in any direction.

It is a characteristic feature of the radiation field, that no coordinates can be attributed to a photon. The localization of a photon cannot be made, therefore, unless we refer explicitly to the type of position measurement we have in mind, and it will depend, in general, on the particular method adopted for position determination. Measuring, e.g., the position of our two photons by the coordinates of two atoms in which they produce photo-effects, we can easily study the relative angular distribution of our two photons, which shows interference phenomena similar to those we find for the relative angular distribution of two material particles, obeying Bose-Einstein statistics.[5]

4. RELATIONS WITH THE ZEEMAN EFFECT

Applying our considerations to a system consisting of a photon and a (Schrödinger) electron, we can easily transform the total angular momentum to principal axes. The linear combinations which appear, for a p electron and a dipole photon, are the same as those contained in Table I if, now, the Γ's are understood to be eigenfunctions of the system: electron-photon. As a matter of fact, conservation of total angular momentum should hold if an emission process takes place in free space, without the influence of an external field. Orientating the initial states of an atom by a magnetic field, in order to have a well-defined initial angular momentum, and removing the magnetic field afterwards in order not to perturb the subsequent emission process, the total angular momentum of photon and electron after emission has to be equal to that of the initial state. It can be shown that the linear combinations resulting from these considerations are identical with the ones which one obtains from the Zeeman transition probabilities in a vanishing magnetic field. In a finite magnetic field, however, we can determine individually the angular momentum both of the electron and the photon in the final state while the total angular momentum is not transferred to principal axes, influenced by the external field. In principle, the conservation of total angular momentum should hold for a weak magnetic field, i.e., not one sufficiently strong for the decoupling of the angular momenta of photon and electron. The coupling energy between the two mentioned momenta can be computed by a second-order perturbation calculation and turns out to be equivalent to an extremely weak magnetic field (of the order of 10^{-18} gauss in the case of dipole radiation).

It is a pleasure to express my indebtedness to Professor G. Beck for having suggested this investigation and for many helpful discussions and advice.

[5] A more detailed account of this point will be given in a paper to be published in the *Revista de la Unión Matemática Argentina*.

Production of Mesotrons up to 30,000 Feet at a Magnetic Latitude of 22° North

P. S. GILL*
Forman Christian College, Lahore, India
(Received October 23, 1946)

The production of mesotrons by non-ionizing radiation in a lead thickness of 2 cm was measured in an airplane at a magnetic latitude of 22° North. In general the results are in agreement with those obtained by Schein, Jesse, and Wollan. In addition it was found that mesotrons passing through 8 cm of lead exhibit in the intensity *vs.* altitude curve a marked hump in the neighborhood of a pressure of 530 millibars.

IN 1939, Schein and Wilson[1] studied the production of mesotrons in lead by non-ionizing particles at higher altitudes. They reached a height of 25,000 feet in an airplane at Chicago (54°N) and found that at these altitudes mesotrons were produced by non-ionizing radiation. Schein, Jesse, and Wollan[2] extended these measurements to considerably higher altitudes by means of balloons. In 1945 the author studied the production of mesotrons in 2-cm lead up to an elevation of 30,000 feet at the latitude of Lahore (22° magnetic North). The equipment used was similar to that used by Schein and Wilson[1] and is shown diagramatically in Fig. 1. The apparatus consisted of four Geiger-Müller tubes placed one above the other in a vertical line. Slabs of lead 2 cm thick were placed between the upper two tubes and between the lower two tubes, while a block of lead 6 cm thick was inserted between the second and the third tubes. The upper G-M tubes constituted a cosmic-ray telescope with a lead absorber 8 cm in thickness. The lower three G-M tubes constituted the second telescope with a lead absorber of 10-cm thickness. The third tube from the top was shielded from the sides with one-cm lead in order to reduce effects of soft side showers. The cone of both telescopes was 22° 38′ in the vertical and 65° 48′ in the lateral plane. The efficiency of the two coincidence sets was exactly the same. The apparatus was placed in the nose of a R.A.F. Mosquito aircraft and was supported by double gimbles so that it remained vertical in spite of the tilting of the plane.

The results of the flight made on December 4, 1945 are shown in the curves of Fig. 2. Curve *A* represents the coincidences from the upper telescope and curve *B* those of the lower one. For both curves the number of triple coincidences per minute is plotted against the pressure in millibars. The minimum pressure reached during this flight was 300 millibars above sea level. Records were made throughout the flight beginning at the

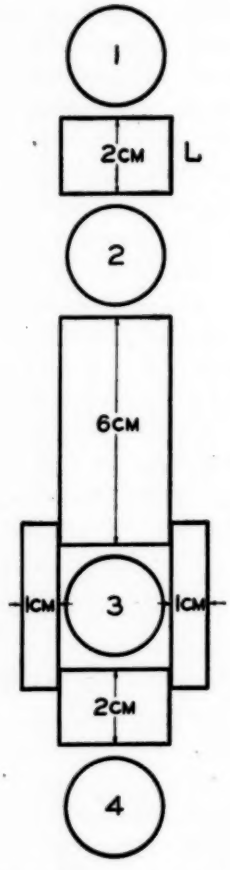

FIG. 1. Arrangement of counters.

* At present at the University of Chicago, Chicago, Illinois.
[1] M. Schein and V. C. Wilson, Rev. Mod. Phys. 11, 292 (1939).
[2] M. Schein, W. P. Jesse, and E. O. Wollan, Phys. Rev. 57, 847 (1940).

ground at an altitude of 600 feet above sea level. At the ground level very little difference between the counting rates of the two telescopes should be observed. Ordinarily the lower telescope should give a slightly lower number of coincidences per unit time than the upper one because of (a) the absorption of mesotrons in the additional 2-cm lead block and (b) the scattering of these particles in the same block of lead. Curves *A* and *B* show that up to a height of 17,000 feet the average number of coincidences from the lower set of G-M tubes is somewhat less than from the upper set as is expected because of the two above-mentioned effects. Above this height the lower telescope begins to show a very marked increase in the number of coincidences per unit time over the upper one. The average difference between the counting rates of the two sets between the elevations of 17,000 feet and 30,000 feet is about 33 percent. This large difference is in accordance with the findings of Schein, Jesse, and Wollan[2] from their balloon data. As already pointed out by them, the production of mesotrons in a 2-cm lead block does take place abundantly at higher elevations and in this small thickness of lead such a large difference definitely indicates that the mesotron producing radiation is strongly absorbable in lead and hence should most probably consist of photons.

The accuracy of each point given in the curves is approximately 8 percent. This follows from the fact that the duration of flight at a particular height was between 25 and 35 minutes. These data seem to confirm in general the results obtained by Schein, Jesse, and Wollan.[2] However, because of the fact that considerably more data were collected in these experiments, the curves of Fig. 2 give much more detailed information at intermediate altitudes where the production of mesotrons by photons just sets in. Schein, Jesse, and Wollan[2] sent their equipment up by using balloons which usually ascend to much higher altitudes and therefore pass through these regions of the atmosphere in a very short time. As a result their data in these altitudes were not sufficiently accurate to show all the details of the curves obtained here.

The curves shown in Fig. 2 reveal some interesting information not only regarding the production of mesotrons by photons but also regarding the intensity *vs.* altitude curve (*A*) for mesotrons passing through 8 cm of lead. As seen from the figure, Curve *A* shows a distinct hump at a pressure around 530 millibars. The nature and magnitude of this hump presumably depends on the geometry of the cosmic-ray telescope and the lead thickness interposed. This point needs further investigation. It is, however, quite clear that the mesotron intensity *vs.* altitude curve is not a smoothly increasing curve as is generally assumed but shows a break in the neighborhood of 500 millibars pressure. This might mean that either a group of softer mesotrons produced at higher layers of the atmosphere are not able to penetrate more than one-half of the atmosphere or that some non-ionizing radiation responsible for the production of softer mesotrons is abundantly present in the upper atmosphere only. It is interesting to note that at practically the same pressure (530 millibars) where the hump in curve *A* occurs, curve *B* crosses curve *A*. Since the lower telescope registers in addition to the mesotrons passing through 10 cm of lead those produced by non-ionizing radiation in 2 cm of lead, no pronounced hump was found to be present in curve *B* at 530 millibars. The rapidly increasing production of mesotrons with altitude in 2 cm of lead smoothes out curve *B* sufficiently that no definite inflection could be detected

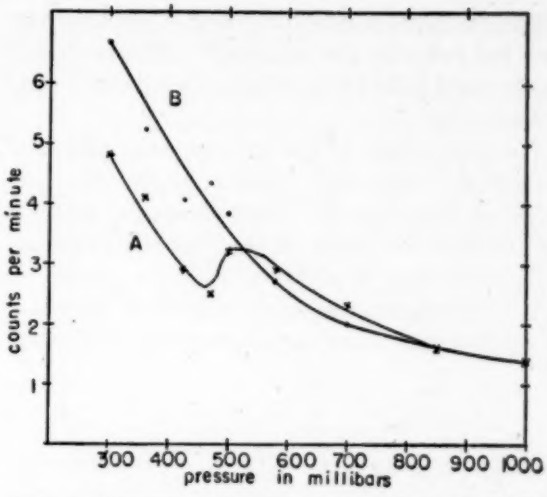

FIG. 2. Mesotron intensity as a function of altitude. Curve *A* (crosses) represents coincidences for upper telescope and curve *B* (solid dots) represents coincidences for lower telescope.

within the experimental precision. This, however, does not rule out the possibility of its existence which could only be established by more precise measurements.

The comparison of the present data with that of Schein, Jesse, and Wollan[2] shows that the curves *A* and *B* at 22° North magnetic latitude are consistently lower at the higher elevations, thus exhibiting a definite latitude effect on mesotrons passing through 8 cm of lead. This is in agreement with recent measurements of Bhabha and his collaborators[3] who also found a latitude effect of the same order of magnitude on the mesotron component.

The author acknowledges with thanks the valuable suggestions and criticism given by Professor Marcel Schein. The author also wishes to express his thanks to the R.A.F. for putting at his disposal one of their Mosquito aircraft in which the flights were made.

[3] H. J. Bhabha, S. V. Chandrashekhar Aiya, H. E. Hoteko, and R. C. Saxena, Phys. Rev. **68**, 147 (1945).

PHYSICAL REVIEW VOLUME 71, NUMBER 2 JANUARY 15, 1947

X-Ray Absorption Structure of $GeCl_4$ and $AsCl_3$*

S. T. STEPHENSON
State College of Washington, Pullman, Washington
(Received October 31, 1946)

The fine structure on the short wave-length side of the *K* x-ray absorption edges of Ge and As in $GeCl_4$ and $AsCl_3$ has been measured with a double crystal spectrometer having resolution sufficient to resolve all structure predicted by theory. The results are compared with the theory and with previous measurements made with spectrographs of lower resolving power. Structure is obtained closer to the edge than that resolved heretofore, which structure is not altogether in agreement with the theory.

INTRODUCTION

THE fine structure to be found on the short wave-length side of the x-ray absorption edge of a molecular gas was explained by Kronig[1] in terms of the scattering of the ejected electron by neighboring atoms in the molecule. The probability of the ejection of the electron, and consequently the absorption coefficient, is found to be dependent upon the energy with which the electron leaves the parent atom. Kronig's general arguments have been summarized by Snyder and Shaw[2] and applied to the Br_2 molecule which had been shown to have a pronounced structure.[3–5] The theory was in agreement with the experimental structure near the edge in so far as position was concerned but not as regards the intensity. Structure which was predicted for positions further from the edge was not observed.

Perhaps the most detailed theoretical calculation of the fine structure for a gaseous molecule is that made for the germanium edge in $GeCl_4$ by Hartree, Kronig, and Petersen.[6] $GeCl_4$ has been studied experimentally by Coster and Klamer[7] and by Drynski and Smoluchowski.[8] Agreement between theory and experiment was acceptable at an energy separation of 50 volts and more from the main edge. Unfortunately, the experiments were carried out using a photographic spectrograph of low resolving power; consequently, the several pronounced structures nearer to the edge than 50 volts which were predicted by theory could not be checked experimentally. $AsCl_3$ was also considered by Hartree,

* This work was carried out as part of Contract N6ori-167, Task Order II with the U. S. Navy Office of Naval Research.

[1] R. de L. Kronig, Zeits. f. Physik **75**, 468 (1932).
[2] T. M. Snyder and C. H. Shaw, Phys. Rev. **57**, 882 (1940).
[3] S. T. Stephenson, Phys. Rev. **50**, 790 (1936).
[4] B. Cioffari, Phys. Rev. **51**, 630 (1937).
[5] C. H. Shaw, Phys. Rev. **57**, 877 (1940).
[6] D. R. Hartree, R. de L. Kronig, and H. Petersen, Physica **1**, 895 (1934).
[7] D. Coster and G. H. Klamer, Physica **1**, 889 (1934).
[8] T. Drynski and R. Smoluchowski, Physica **6**, 929 (1939).

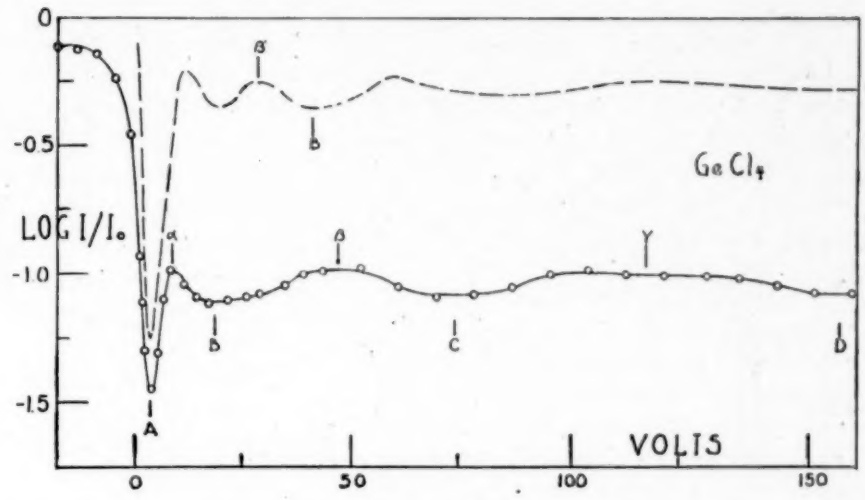

FIG. 1. K x-ray absorption edge of Ge in $GeCl_4$. The circles on the solid line are experimental points. The broken line represents theory drawn to an arbitrary and displaced $\log I/I_0$ scale.

Kronig, and Petersen and was measured by Coster and Klamer. It is the purpose of this paper to present experimental results on $GeCl_4$ and $AsCl_3$ as obtained with a double crystal spectrometer having resolving power adequate to check all predictions of the theory. A better understanding of the relatively simple case of absorption structure for molecules is perhaps necessary before one can expect quantitative agreement between theory and experiment on absorption structure for the more complicated case of the solid state.

EXPERIMENTAL

The double crystal spectrometer is of the type described by Ross[9] constructed from a good Societé Genevoise optical spectrometer. The circular scale on the table for crystal B could be read to a second of arc by means of microscopes with micrometer eyepieces. The ways on which crystal A was mounted were part of a comparator. The crystals were split from one piece of optical quality calcite and were the same pair used previously.[3] Since that time they have been etched with HCl.[10] As finally used the crystals gave a $(1, -1)$ curve at ca. 1116 x.u. of 13 seconds full width at half-maximum. X-ray intensities were measured with a Geiger-Mueller counter of the type sold commercially by the Cyclotron Specialties Company. Counting rates ranged from as high as ten counts per second on the low absorption side to as low as four counts per second on the high absorption side including a natural count of 2.3 counts per second. The x-ray background and natural count together were about 2.9 counts per second with crystal B turned some 10° away from the position for reflection. From four to ten thousand counts were registered for each point in a run. A total of six runs were made for $GeCl_4$ and four runs for $AsCl_3$. In order to make certain that the incident intensity was constant throughout the region covered by a run, blank runs were made without any absorber in the beam.

The $GeCl_4$ and $AsCl_3$ were sealed in glass absorption cells 10 cm long and 3 cm in diameter with thin windows blown on each end. The cells were placed in a small electric furnace. The furnace windows were of double walled Cellophane and the furnace windings were placed near the windows in such a fashion that no condensation of vapor was noted on the thin glass walls of the cell. The temperature in the furnace was taken with a thermocouple and kept nearly constant with a Variac control. The temperature of the vapor was about 45°C for $GeCl_4$ and 75°C for $AsCl_3$. The absorption cells were placed between crystals A and B. In order to make sure that variations in the thin windows were not contributing to the structure the cells were moved slightly between runs or moved end for end.

The source of x-rays was a commercial General Electric CA-6 x-ray tube, with molybdenum target and beryllium window, run at 23,000 volts and 35 milliamperes. The voltage

[9] P. A. Ross, Rev. Sci. Inst. **3**, 253 (1932).
[10] K. V. Manning, Rev. Sci. Inst. **5**, 316 (1934).

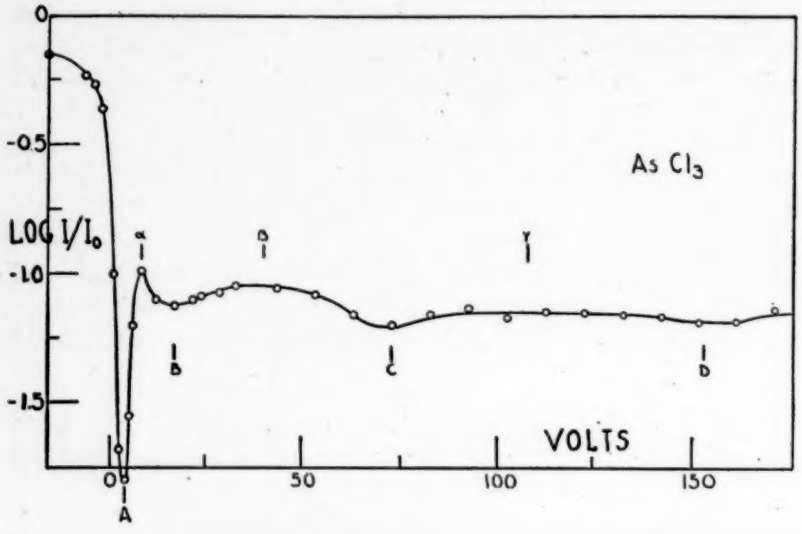

FIG. 2. K x-ray absorption edge of As in $AsCl_3$. The circles on the solid line are experimental points.

was read on a microammeter in series with a resistor of 10^9 ohms. The power supply was a conventional full wave rectifier with 0.2 mf capacity for smoothing. The control was by means of a Variac supplied through a commercial voltage stabilizer so that voltage variations were less than one percent.

RESULTS

Figure 1 shows the averaged data obtained on the six runs for $GeCl_4$. The temperature of the furnace and the position of the absorbing tube were changed between runs; most of the scattering of points results from the difficulty in correcting for the former together with small variations caused by the latter. Similarly Fig. 2 presents data for four runs over $AsCl_3$. The scale of $\log I/I_0$ is arbitrary as follows: I was readily obtained by subtraction of the natural count and x-ray background from the recorded intensity. I_0, however, could not be obtained directly because of the absorption in the chlorine. A blank run with absorption tube and furnace windows alone would not yield I_0 because the chlorine, of course, goes with the germanium or arsenic. It was finally decided to choose I_0 so that the ratio of the average $\log I/I_0$ on the high absorption side of the edge to that on the low absorption side was about eight,[11] a value of the jump ratio characteristic of elements near Ge and As in the periodic table.

[11] J. B. Platt, Phys. Rev. 69, 337 (1946).

The distances (in volts) from the center (point of inflection) of the main edge of the structure observed are given in Table I together with the predictions of theory and previous experimental results.

The uncorrected edge widths, defined as the distance between points where the $\log I/I_0$ curve reaches $\frac{1}{4}$ and $\frac{3}{4}$ of the asymptotic values, are 2 volts in each case.

DISCUSSION

It is immediately apparent from an inspection of the figures and table that the double crystal spectrometer reveals several pronounced features of the fine structure which were not observed in earlier photographic studies. The first absorption minimum recorded heretofore nearly coincides with the feature β in the present work. The agreement with previous experimental results at distances of 45 volts and more from the edge is satisfactory when one considers that the structure is very broad in this region and can hardly be placed to closer than 10 volts. Structure beyond D is very weak and hardly exceeds experimental error. Also experimental error is larger beyond D because of slight tungsten filament evaporation which causes $WL\gamma_1$, to appear about 176 volts from the Ge edge and $WL\gamma_4$ about 195 volts from the As edge.

To aid in comparison of the experimental data with the theoretical predictions of Hartree, Kronig, and Petersen the theoretical curve (with an arbitrary and displaced $\log I/I_0$ scale) is

redrawn from their paper and appears in Fig. 1. Strictly speaking the theoretical curve is for the ratio of the absorption coefficient for Ge in $GeCl_4$ to the absorption coefficient for an isolated Ge atom. However, the absorption edge for an isolated Ge atom probably departs from a symmetrical curve only within a very few (about 5) volts of the short wave-length side of the edge and there only slightly because of the narrow atomic optical levels and the broad K state (compare krypton and bromine[5]). Consequently the features of the theoretical curve should be directly comparable with the experimental results except as regards some uncertainty concerning the magnitude of the first absorption maximum A. There is acceptable agreement between theory and experiment, 50 volts and more from the edge, as has been pointed out previously. The predicted structure within 50 volts could not be resolved in the earlier studies. The present experimental results are not in agreement with certain predictions of the theory in this range. In particular, the resolution is quite adequate to detect β^1 and B^1 but these features were not observed; instead these features are lumped together in a broad β. The agreement for A and α is perhaps as close as could be expected. According to theory the pronounced structure at A is caused by the behavior of δ_l, the phase constant expressing the phase shift of the electron wave of angular momentum l scattered by a Cl atom, for an l of 1. Theory predicts a value of π at zero energy instead of 2π and a deep sharp structure. The experiments do, in fact, show A to be the most pronounced feature of the fine structure; β^1 and B^1 have their theoretical origin chiefly in the behavior of δ_l for an l of 2 and it is here that the chief disagreement with experiment is noted.

TABLE I. Energy positions in volts of fine structure maxima and minima as measured from the point of inflection of the main edge.

Structure	Present work	Theory[a]	Previous experiment Ref.[b]	Ref.[c]	Present work	Previous experiment[b]
	$GeCl_4$				$AsCl_3$	
A	3.4	2.8			3.8	
α	8.5	10.5			7.5	
B	18	19		16	17	
β^1		27				
B^1		40				
β	46	59	50	48	39	48
C	74	85	86	79	72	73
γ	117	117	120	110	107	104
D	157	155	160	160	153	138
δ		196	203	208		181
E			257	258		224

[a] Reference 6.
[b] Reference 7.
[c] Reference 8.

The experimental results for $AsCl_3$ are quite similar to those for $GeCl_4$ except that the structures are a little closer to the edge. Hartree, Kronig, and Petersen[6] point out that the structure for $AsCl_3$ should be positioned the same as that for $GeCl_4$ if a factor involving the ratio of the squares of the nuclear separations is applied. Experiment indicates, therefore, that the distance from Ge to Cl atoms is somewhat less than from As to Cl atoms. It is further expected[6] that the fluctuations in absorption coefficient should be less for $AsCl_3$, with 3 chlorine atoms to scatter the ejected electron waves, than for $GeCl_4$ with 4 scattering chlorine atoms. It is not considered that the experimental data are sufficiently precise to test this point definitely although the structure seems weaker beyond B for $AsCl_3$. However, A appears more pronounced for $AsCl_3$ than $GeCl_4$ and this is regarded as a true effect larger than experimental variations.

Ionization by Meteoric Bombardment

J. A. PIERCE*
Cruft Laboratory, Harvard University, Cambridge, Massachusetts
(Received October 28, 1946)

The meteor shower of October 9–10, 1946, produced intense ionization in the upper atmosphere. This phenomenon provides the first opportunity to calculate directly the energy required to produce an ionospheric layer. The necessary power is found to be a few watts per square kilometer, a value comfortably exceeded by the blackbody radiation of the sun in the region of 1000A.

IONIZATION BY METEORIC BOMBARDMENT

THE ionization of the upper atmosphere by meteoric bombardment has been observed and occasionally reported since 1930.[1–4] In general, the effects noted are those associated with the reflection of radiofrequency energy from clouds of free electrons, although increased absorption is occasionally produced by the obtrusion of a large, low meteor into the path of a radio wave in the ionosphere.[5] The maintenance of an increased general level of ionization at the altitude of the *E* layer during a meteor shower[6,7] and bursts of reflected energy at distances beyond ground-wave range have been attributed to meteors.[5,8] Finally, the Doppler beat between a steady, weak ground wave, or other ray, and a reflection from a moving meteoric cloud of ionization has been reported in India[9] and in the United States.[10]

The mechanism of these phenomena appears to be roughly as follows: Meteoroids enter the atmosphere at relative velocities of from 10 to 70 km/sec. Since the corresponding energies of impact range from 10 to several hundred electron volts, most of the atoms or molecules subjected to collision are at least singly ionized.[11,12] Thus a single meteor frees a large number of electrons along a line many kilometers in length. The free electrons diffuse radially with respect to the path of the meteor and are subject to recombination and attachment, all of these processes being at rates determined by the density and constitution of the atmosphere. The growth of the electron cloud may be aided by ionization produced at some distance from the path by ultraviolet light radiated by the atoms in collision with the meteor. Thus, with the passage of time, the cloud of ionization grows in girth and decreases in density until it becomes so diffuse that it is imperceptible.

If an electromagnetic wave is to be reflected from such a cloud of free electrons, two conditions must be fulfilled. The density of ionization must exceed the critical value for the radiofrequency under consideration and this minimum value must be maintained throughout a volume whose dimensions are at least of the order of the wave-length. These criteria are complementary for a meteor of more than some minimum energy, because the critical ionic density varies inversely with the square of the wave-length. Thus, in the absence of recombination and attachment, if a cloud of ionization meets the requirements of volume and density for some short wave-length, it will, as diffusion proceeds, eventually provide conditions satisfactory for the reflection of energy of any greater wave-length. Because recombination reduces the number of free electrons as time passes, reflection of a longer radio wave-

* These experiments were prepared and carried out by the following people under the direction of the author: E. H. Cooper, D. Davidson, G. H. Musselman, A. M. Pannesi, W. G. Perry, A. J. Poté, G. C. Trembly, A. T. Waterman, J. C. Williams, R. H. Woodward. Except that the list of names is inconveniently long they would have been included as co-authors.

[1] A. M. Skellett, Phys. Rev. **37**, 1668 (1931).
[2] A. M. Skellett, Proc. I.R.E. **20**, 1933 (1932).
[3] A. M. Skellett, Proc. I.R.E. **23**, 132 (1935).
[4] J. A. Pierce, Phys. Rev. **59**, 625 (1941).
[5] J. A. Pierce, Proc. I.R.E. **26**, 892 (1938).
[6] S. K. Mitra, P. Syam, and B. N. Ghose, Nature **133**, 533 (1934).
[7] J. N. Bhar, Nature **139**, 470 (1937).
[8] Testimony on f-m transmission before the FCC.
[9] Chamanlal and K. Venkatamaran, Electrotechnics (Bangalore) **14**, 28 (1941).
[10] O. G. Villard, Jr., QST **30**, 59 (1946).
[11] A. Lindeman and G. B. Dobson, Proc. Roy. Soc. **102**, 411 (1923).
[12] H. B. Maris, Terr. Mag. Atmos. Elec. **34**, 309 (1929).

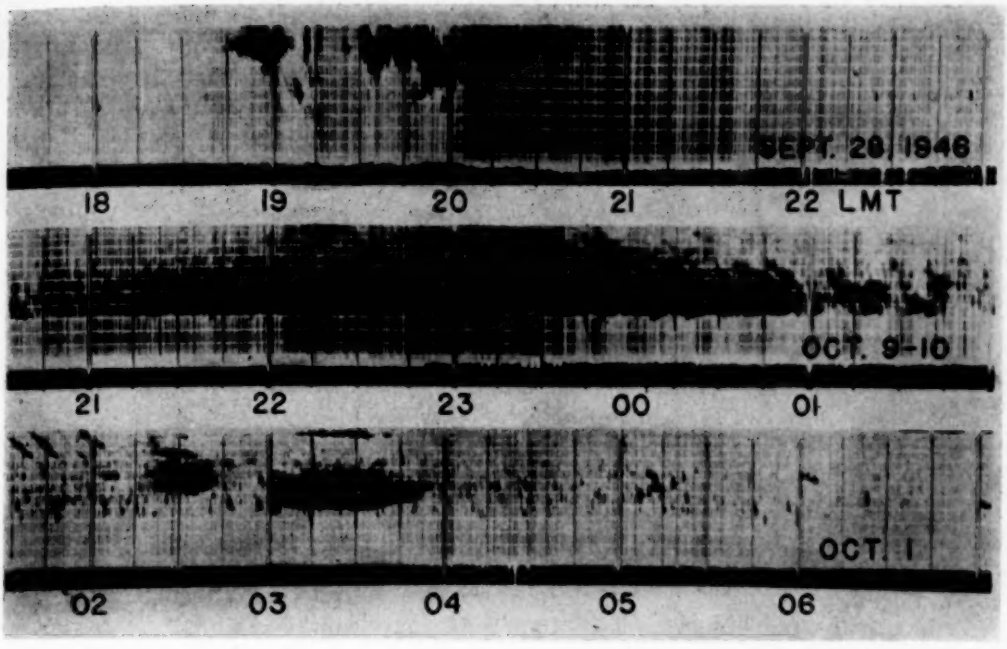

FIG. 1. Pulse reflection patterns of 3.5 Mc. The top record shows reflection from aurora borealis; the center pattern records the meteor shower of October 9–10, 1946; and at the bottom are shown two clouds of sporadic *E* region ionization and a number of individual meteoric reflections.

length actually requires the initial expenditure of more meteoric energy per unit length of path.

A sufficiently small meteor, therefore, will produce ionization in the upper atmosphere, but will fail to fulfill one of the two basic conditions. We cannot expect to observe the reflection of electromagnetic energy from that single cloud of ions, although the cumulative effect of many such meteors may well be perceptible. The stellar magnitude corresponding to this radio threshold has not yet been established. There is no evidence that single meteors fainter than about the fifth magnitude have been detected by radio methods, and the third magnitude is a more usual limit. This level, however, is apparently a temporary one caused by the limited sensitivity of current observing methods; that is, the energy reflected by an ionic cloud with dimensions of the order of a wave-length cannot be detected at present.

During the meteor shower of October 9–10, 1946, which occurred when the earth passed close to the orbit of the Giacobini-Zinner comet, observations were made by three related methods.

1. Pulse ranging by the standard fixed-frequency ionosphere-sounding technique at 3.5 Mc.

2. Detection of the Doppler beat with an unmodulated carrier at 12.9 Mc.

3. Observation of bursts of reception of a distant f-m station at 42.8 Mc.

For about four hours during the maximum of the shower it is fair to say that a remarkably dense but inhomogeneous *E* layer was maintained entirely by meteoric bombardment. This effect is shown in the center record of Fig. 1, which exhibits three examples of reflection patterns obtained by the pulse-sounding method. In this figure the abscissae are indicated in hours of local mean time, and the ordinate scale for each pattern includes 220 kilometers of virtual height, or range. The horizontal white lines are at intervals of 100 microseconds, or 15 kilometers. The cloud of ionization in the center record has a minimum virtual height of 90 ± 2 km. The Harvard Observatory reports that the maximum of the visual shower occurred at 10:50 P.M. E.S.T., or at 2305½ L.M.T. The maximum density in the record of Fig. 1 is found at this same time, plus or minus five minutes. Throughout most of the shower period it is impossible to resolve the reflection patterns from individual meteors, but comparison of the blackened area with the aver-

age extent of a meteoric trace indicates that this layer could not have been formed by less than 4000 meteors.

Comparable records showing the patterns reflected from aurora borealis and sporadic E region ionization are included at the top and bottom of Fig. 1. The aurora is easily distinguishable. The sporadic E pattern differs from that of the meteor shower chiefly in the sharp, relatively smooth, lower boundary of the patches of reflection. Meteoric activity is near its diurnal minimum at the time of the auroral record and near maximum at the time of the lower record of Fig. 1. The echoes due to meteors appear as small black areas lasting a minute or less in most cases. The normal number of meteors may be judged from the top and bottom records for the periods when the auroral or sporadic E reflections did not mask them.

The experiments for the observation of the Doppler effect were not entirely satisfactory, partly because of the very magnitude of the meteoric ionization. A continuous wave transmitter was operated at 12.9 Mc with a power of about 1.2 kw. At a distance of 22 miles the ground wave was judged to be of a suitable amplitude for production of the beats. On the night of the shower, however, a strong but very rapidly fluctuating comparison signal was obtained by reflection from the meteoric ionized layer. The equivalent modulation of the comparison signal by the reflection from each single meteor was small and because of the low power only occasional beats were heard above the noise level. At about 2330 L.M.T. the signal from a high power teleprinter transmitter at 150 miles was found to exhibit the beats well. For the remainder of the night this signal was monitored and about 3500 Doppler whistles were recorded, the maximum rates being 83 in five minutes and 735 in an hour. At sunrise on October 10 the rate had dropped to a third of that at midnight.

The whistles heard in this experiment almost invariably fell in pitch from a value (say 1000 c.p.s.) commensurate with the "radial" velocity of the shower meteors. The rate of decrease, however, was rapid and the pitch fell, in most cases, to the lower limit of audibility at what seemed to be a fairly uniform rate. The duration of the whistles ranged from $\frac{1}{2}$ to 3 seconds, with the more rapid ones predominating. This behavior is in sharp contrast to the observed deceleration of meteors, which typically lose only about five percent of their initial velocity before coming nearly to the end of their courses.[13] It is only necessary to note the remarkable uniformity of a number of these whistles to realize that the Doppler beat is produced by what might be called the "ionic bow wave" of the meteor and that the pitch is a function of both the velocity of the meteor and the rate of diffusion of the free electrons. Presumably the pitch falls from the first because the growth of the cloud of ions is most rapid at its initial height; and the beat goes to zero when recombination prevents the further expansion of the boundary containing the requisite density of ionization. The tone is not often heard to rise as the boundary retires, presumably because the velocity of retreat is too low for the pitch to be audible.

A cloudy sky prevented the visual observation of meteors on October 9 at Cambridge. During the evening of the 10th, however, the experiment was repeated and some dozen visual correlations were obtained, the visual meteors being indicated to the radio observers by the click of a telegraph sounder. In two instances the whistle was loud enough to be heard clearly by the visual observers outdoors some 40 feet from the receiver. In these cases the correlation was startling, the whistle being noted within the first quarter of the meteor's course. The tone then fell in pitch throughout the period of the meteor's visibility. If the whistles persisted longer than the light from the meteors, the delay was not more than, say, $\frac{1}{4}$ second.

The Doppler whistle is thus a peculiarly interesting subject for quantitative analysis. The recordings so far obtained are too much contaminated by noise for successful measurement of the beat frequencies, but this approach is certainly possible and should yield direct information on rates of diffusion in the upper atmosphere.

Bursts of signal from a 42.8 Mc f-m station at 180 miles were observed and recorded on the evenings of October 8 and 9. The control data on the 8th were entirely satisfactory; a clear burst of reception of—usually—$\frac{1}{2}$- to 1-second duration

[13] F. L. Whipple, Rev. Mod. Phys. **15**, 246 (1943).

being heard, on the average, once every two to three minutes. On the 9th, however, the magnitude of the shower prevented the accumulation of any quantitative information. The signal was continuously audible although completely unsteady in character. Occasional strong bursts could be identified, but the major phenomena were those associated with multiple-path transmission.

This same effect was noted, near the maximum of the meteor shower, on the signal of a broadcast transmitter operating at 1.2 Mc at a distance of 16 miles. Multiple phase interference phenomena so distorted the signal that speech could hardly be understood, an effect which was reminiscent of a high frequency signal during a magnetic storm. The field strength fluctuated violently and rapidly, as did that of every sky-wave signal heard during the shower.

The normal records similar to those of Fig. 1 exhibit an average of about 100 meteor traces per day. Occasional reflections are observed at ranges up to 200 km; the average lateral radius within which reflections are observed may be taken as 100 km.

The corresponding rate for the whole surface of the earth is therefore

$$100\frac{\text{meteors}}{\text{day}}\times\frac{4\pi(6470\text{ km})^2}{\pi(100\text{ km})^2}$$

$$=1.7\times10^6\frac{\text{meteors}}{\text{day}}. \quad (1)$$

According to Watson[14] this is approximately the average number of third-magnitude meteors. We may therefore consider that the sensitivity of the recording equipment is adequate, on the average, to exhibit a trace corresponding to a third-magnitude visual meteor.

While the meteoric ionized layer during this shower was not similar to the normal homogeneous daytime E layer, the magnitude of the ionic density seems to have been comparable. A considerable number of nuclei were of a density far beyond the normal, and although the layer was unquestionably full of "holes," it is reasonable to assume that a normal E layer could have been produced by the same energy if uniformly distributed. This assumption gives us an opportunity to calculate, within one or two orders of magnitude, the energy required to maintain an ionospheric layer at a height of 100 km. This computation is of value because a direct measurement of this energy has not heretofore been possible.

We have said that not less than 4000 meteors must have fallen within the range of the pulse-sounding equipment within a period of four hours; or rather, that 4000 meteors of third magnitude and larger would have been required to produce the record of Fig. 1. For the moment let us disregard smaller meteors. If the total number was 4000, and if Watson's conclusions about the magnitude-frequency relation[14] are adopted, there must have been about 2400 of the third magnitude, 1000 second, and so on to four of -4 magnitude and one or two of -5. The total range includes nine magnitudes and is limited in the negative magnitude region by the decreasing probability that any larger meteors fell during the shower.

Opik[15] gives 6.3×10^{11} ergs as the average energy of a third-magnitude meteor. Therefore, since Watson has indicated that the total energy per magnitude may be taken as constant,[14] the total energy of our 4000 meteors is:

$$E_T=2.4\times10^3\text{ 3rd mag. meteors}$$
$$\times6.3\times10^{11}\text{ ergs/3rd mag. meteor}$$
$$\times9\text{ magnitudes}=1.4\times10^{16}\text{ ergs}. \quad (2)$$

This energy was released into the atmosphere in four hours within an area which may be deduced (from the ranges observed on the pulse record) as equivalent to a circle of 100-km radius. The rate of flow of energy was therefore

$$E_M=\frac{1.4\times10^{16}\text{ ergs}}{\pi\cdot10^{14}\text{ cm}^2\cdot1.44\times10^4\text{ sec.}}$$
$$=3\times10^{-3}\text{ ergs/cm}^2\text{ sec.}=3\text{ watts/km}^2. \quad (3)$$

The rate of production of free electrons may be calculated on the assumptions that approximately all[12] of the energy went into ionization, that the

[14] F. G. Watson, *Between the Planets* (Blakiston, Philadelphia, 1941).

[15] Opik, "Atomic Collisions and Radiation of Meteors," Tartu Observatory, Harvard Reprint No. 180 (1933).

energy was expended in a uniform layer 30 km thick, and that 15 electron volts are required per ion:

$$N_1 = \frac{3\times10^{-3}\ \text{erg/cm}^2\ \text{sec.}}{3\times10^{6}\ \text{cm}\cdot 1.59\times10^{-12}\ \text{ergs/ev}\cdot 15\ \text{ev/ion}}$$

$$= 42\ \text{ions/cm}^3\ \text{sec.} \quad (4)$$

On a simple recombination hypothesis the density of ionization, N, which will be sustained by a production of N_1 new ions/cm^3 sec. is

$$N = (N_1/\alpha)^{\frac{1}{2}}, \quad (5)$$

where α is the recombination coefficient.

Various observations on the E layer indicate that the equivalent recombination coefficient is of the order of 10^{-9}. Therefore

$$N = \left(\frac{42\ \text{ions/cm}^3\ \text{sec.}}{10^{-9}\ \text{cm}^3\text{/ion sec.}}\right)^{\frac{1}{2}} = 2\times10^{5}\ \text{ions/cm}^3. \quad (6)$$

This is in fact the order of the maximum density of ionization in the normal E layer at the subsolar point.

The energy flow found in Eq. (3) may now be compared with that which would be obtained from the suitable part of the solar spectrum, considering the sun to radiate as a blackbody at 6000°K.

The ultraviolet absorption spectrum of atomic oxygen, into which O_2 is dissociated in the upper reaches of the atmosphere, is so broad that it is unlikely that any solar ultraviolet light of wavelengths less than 913A penetrates to the height of the E layer. On the other hand, light of wavelengths greater than 1014A could not directly ionize molecular oxygen, which appears abundantly at and below that height. It seems reasonable, therefore, to believe that the E layer is produced by ionization of O_2 by ultraviolet light in a band about 100A wide at 1000A.

From integration of Planck's formula the energy radiated in this band from a body at 6000°K is 8.7×10^{3} ergs/cm^2 sec. The total energy flux at the distance of the earth is, therefore,

$$E_L = \frac{8.7\times10^{3}\ \text{ergs/cm}^2\ \text{sec.}\cdot 6.1\times10^{22}\ \text{cm}^2}{2.8\times10^{27}\ \text{cm}^2},$$

$$= 1.9\times10^{-1}\ \text{erg/cm}^2\ \text{sec.} \quad (7)$$

This quantity is the rate of flow of energy in this wave-length range into the atmosphere at the subsolar point and is about 60 times the energy flow during the shower for the meteors from the third to the −5th magnitude.

Within the limits of these calculations, this result is not greatly affected by the inclusion of the energy from meteors fainter than the third magnitude. Our range already includes nine magnitudes; doubling this number would only double the energy. If we included meteors down to the thirtieth magnitude the energy flow in Eq. (3) would be increased only to 1.2×10^{-2} erg/cm^2 sec., or 1/15 of the rate derived in Eq. (7). Extremely small meteors would, of course, expend their energy at greater altitudes and would contribute to the thickness but not to the maximum ionic density of the layer.

It thus appears that the solar ultraviolet energy in the range between 900A and 1000A is ample to produce the ionization observed in the E layer. The energy required to maintain the F layer is presumably of lower magnitude because the effective recombination rates at the height of the F region are much less. There is, therefore, no need to search for a mechanism which would provide a phenomenally intense source of ionizing radiation in order to account for the existence of the ionosphere.

Molecular Dissociation by Electron Bombardment: A Study of $SiCl_4$*

R. H. Vought†
Randal Morgan Laboratory of Physics, University of Pennsylvania, Philadelphia, Pennsylvania
(Received October 26, 1946)

The first part of this paper deals with molecular dissociation in general, with reference to the determination of appearance potentials of molecular fragments. Appearance potentials are generally determined from plots of ion current *versus* electron energy by either of two methods: determination of the energy at which ion current is first detected; or location of the intercept with the energy axis of the extrapolation of the straight line portion of the ionization efficiency curve. It is pointed out that the first procedure has a rather indefinite relation to the physical quantities involved and that the value obtained by the second method corresponds quite closely to the energy necessary to produce a transition through the center of the Franck-Condon region. The last section of the paper contains an analysis of data obtained in a study of the dissociation of silicon tetrachloride. Both positive and negative ions are formed in processes resulting in most of the possible configurations. The data are correlated with values of dissociation energies from external data, and estimates are made of the ionization energies of the radicals involved. Ionization energies of $SiCl_4$ and $SiCl_2$ are measured directly and are found to be 11.6 ± 0.2 volts and 11.8 ± 0.3 volts, respectively.

INTRODUCTION

THE use of a mass spectrometer to determine the energy necessary to produce a particular type of molecular dissociation is quite common.[1] This energy, generally called the appearance potential of the ions observed, is composed of three quantities: the dissociation energy necessary to disrupt the molecule into various fragments; an ionization energy (or electron affinity) necessary to produce an ion from one of the dissociated fragments; and excess energy resulting from the dissociation process which may be manifest either as excitation energy of the fragments or as kinetic energy of relative motion of the dissociation products.

This latter quantity is not of great interest *per se* but it is desirable to know it in order that the dissociation energies and ionization energies may be determined. It has only been determined for a few simple processes[2] and is generally found to be quite small, around one volt or less, for energies which are just sufficient to produce the dissociation. The procedure is to measure directly, by stopping potentials, the kinetic energy of dissociation as a function of bombarding energy, the difference between these two quantities giving the difference of potential energy of the molecule in its initial and final states. The recently developed use of retarding fields on analyzed ion beams[3] will make it possible to perform these measurements for any dissociation process, the advantage of this method over that of Lozier being that each type of ion may be studied separately and identified by its e/m value. This should also provide information about the shapes of surfaces representing the potential energy of various configurations of the molecule.

Of the other two quantities, a knowledge of one permits a limit to be placed on the other, the uncertainty being caused by the unknown excess energy. For silicon tetrachloride neither the dissociation energies nor the ionization energies are known accurately beforehand. However, most molecular configurations are involved in production of both positive and negative ions

* A preliminary report of this work was given at the June, 1946 meeting of the American Physical Society at Chicago. Cf. Phys. Rev. **70**, 109A (1946).

This paper is a summary of a thesis submitted to the Faculty of the Graduate School of the University of Pennsylvania in partial fulfillment of the requirements for the degree of Doctor of Philosophy.

This work was done under contract NObs 34144 between the Navy Department, Bureau of Ships and the Trustees of the University of Pennsylvania.

† Now located at the Research Laboratory, General Electric Company, Schenectady, New York.

[1] A list of the most recent references for substances that have been studied is given by J. A. Hipple, J. App. Phys. **13**, 551 (1942).

[2] J. T. Tate and W. W. Lozier, Phys. Rev. **39**, 254 (1932); W. W. Lozier, Phys. Rev. **46**, 268 (1934).

[3] J. A. Hipple, R. E. Fox, and E. U. Condon, Phys. Rev. **69**, 347 (1946).

so that two checks are obtained on each dissociation energy, and the processes resulting in negative chlorine ions involve the electron affinity of chlorine which is fairly well known.

APPEARANCE POTENTIAL DETERMINATION

There is always some question as to just how curves of ion current *versus* electron energy should be interpreted for determining appearance potentials. The energy at which ion current is "first detected" is one definition of appearance potential often used, while the other method is to extrapolate the straight line portion of the ionization efficiency curve back to zero current and take the intercept with the voltage axis as the appearance potential. The principle objection raised to the first method is that the electrons in the ionizing beam have a definite spread in energy caused by the high temperature of the source and perhaps also caused by the fact that the source is not an equipotential surface. This difficulty can be overcome by calibrating all measurements against some standard whose ionization energy is well known, provided the true ionization efficiency curves of the standard and unknown processes do not differ appreciably near their origins. The objection to the second method is that it assumes that the ionization efficiency is a linear function of the energy at the onset of the curve.[4] The discussion to follow shows that in dissociation processes releasing kinetic energy the two methods would be expected to give significantly different values. This effect is independent of any of the objections to either method of analysis mentioned above, and would result in a "tail" at the base of the ionization efficiency curve for any ion that acquires kinetic energy in the dissociation process. Neither method is correct or wrong, but each has a different meaning in terms of the physical ideas used in explaining molecular dissociation.

In Fig. 1a are shown schematic sections of the potential energy curves for the hydrogen molecule. The lower curve is for the normal state while the line across the top is a straight line approximation of the curve for the repulsive state of the molecular ion, the numbers indicating the potential energy in electron volts. Superimposed on the lower curve is the expectation function of the lowest vibrational state, while the dashed vertical lines represent the limits of nuclear oscillations if the molecule be considered a classical harmonic oscillator; that is, they define the Franck-Condon region. This curve may be interpreted as indicating the relative number of molecules in a gas having a given nuclear separation. Thus a beam of electrons of say 28 volts would be able to excite to the repulsive H_2^+ state only that fraction of the molecules represented by the area under the expectation function to the right of the Franck-Condon limit. As the energy is increased a larger fraction of the molecules will become susceptible for excitation until at about 34 volts, essentially all of the molecules may be excited to the upper state. Hence, if it be assumed, as is customary, that the probability of the transition is proportional to the excess energy above the minimum required energy, it is evident that the ion current would increase more rapidly than linearly in the energy range from 26 to 34 volts

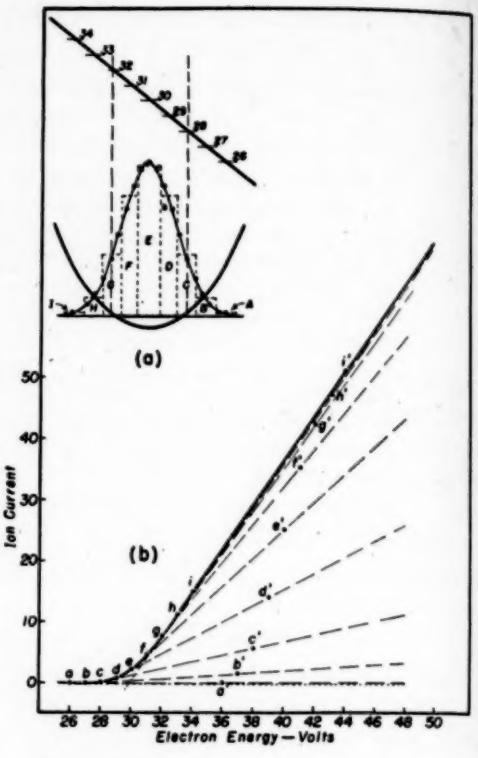

FIG. 1. Construction to explain shape of appearance potential curve. (See text.)

[4] D. P. Stevenson and J. A. Hipple, Phys. Rev. 62, 237 (1942).

since more molecules are constantly being made available for excitation. Because the probability of finding a nuclear separation outside of the limits given by the Franck-Condon region is very small, the curvature of the ionization efficiency curve will be noticeable only in the range from 28 to 32 volts.

The shape of the ionization efficiency curve may be approximated graphically for this simplified case and is shown in Fig. 1b. The area under the expectation curve is divided into sections A, B, C, $\cdots$, representing those fractions of molecules which can undergo transitions when supplied with energies of 26, 27, 28, $\cdots$ volts. The contributions to the ion current from each of these sections is then given by the dashed lines aa', bb', cc', $\cdots$, of Fig. 1b. These are drawn on the assumption that the transition probability increases linearly with surplus energy above the minimum energy required for the process by making the ion currents at energies of $26+10$, $27+10$, $\cdots$ proportional to the areas A, B, $\cdots$ and connecting the points a and a', b and b' $\cdots$ with straight lines. The curve thus obtained, $abc\cdots ii'$, represents the ion current as a function of bombarding electron energy.

When the straight line portion of the curve is now extrapolated back to zero current, the intercept on the energy axis is 30 volts. This is just the energy necessary to produce a transition between the two states if the molecule has the equilibrium nuclear separation; that is, the transition is through the center of the Franck-Condon region. The energy range over which a distinct curvature is evident will also give a rough idea of the energies at which the upper potential energy curve crosses the Franck-Condon region.

Several factors will determine the exact shape of the ionization efficiency curve. In the case above, the expectation function for the lowest vibration state was used, but any expectation function which is symmetrical about the equilibrium position could have been used and the extrapolated appearance potential would have been the same. A symmetrical energy distribution of ionizing electrons would spread the curve slightly but would still give a straight line extrapolation corresponding to a transition through the center of the Franck-Condon region. Since the actual distribution is Maxwellian, which gives more electrons with energy greater than the most probable energy, the appearance potential determined by this method would be slightly lower than for a symmetrical distribution.

The factor that affects the ionization efficiency curve most strongly, and about which least is known, is the potential energy curve for the state to which the transition occurs. The majority of known curves have minima at larger nuclear separations than for the normal state, and in the Franck-Condon region they are slightly concave towards smaller separations. The result of this slight concavity would be to give a higher extrapolated appearance potential than is obtained with a straight line approximation. However, this effect is very slight if the concavity is not great and is partly compensated by the opposite effect resulting from a Maxwellian distribution of the electrons.

In cases of molecular dissociation and ionization, then, the two methods of determining appearance potentials have quite different physical interpretations. The electron energy at which current is "first detected" in Fig. 1a would evidently cause excitation of molecules with nuclear separations greater than the classical limit; just what point it corresponds to will depend on the distribution in energy of the ionizing electrons, the sensitivity of the amplifier, the probability of the process being studied and the angle at which the upper potential energy curve intersects the Franck-Condon region. The straight line extrapolation method, however, gives the energy necessary to produce a transition through the center of the Franck-Condon region subject to the conditions outlined above. Neither method, in general, gives the true dissociation energy, or dissociation plus ionization energy, so that an independent study of the kinetic energy of dissociation products as a function of bombarding energy would be necessary to determine this quantity. This report will use the straight line extrapolation method. Although the above arguments were given for a simple diatomic molecule, it is evident that similar considerations would hold in the more complicated dissociation processes in polyatomic molecules.

Production of negative ions by resonance capture of an electron gives appearance potential

curves with much sharper breaks than for positive ions, so that the effect of a spread of the electron energies would be quite different in the two cases. In fact, some resonance curves for negative ions have a width that is quite comparable with the energy distribution of the electrons which is quite broad in the experiments to be described because of the high temperature of the tungsten filament and the fact that it is not an equipotential surface. In these cases an error nearly as large as half the width of the energy distribution could conceivably occur by using the method of first detected current. To determine the value analogous to that obtained with the extrapolation method, the appearance potential is taken as the energy at the maximum of the resonance peak.

EXPERIMENTAL

The mass spectrometer used for this work was a Nier type 60° instrument which has been described in some detail in a previous paper.[5] Principle changes from Nier's published design are the use of a permanent magnet for the deflecting field, and the use of an electromagnet on the ion source. The electromagnet was placed on the ion source to increase the ion current and resolving power but it is also necessary in appearance potential measurements to keep the energy of the ionizing electrons at a known value. Since the electrons are subjected to the ion draw-out potential of about 3 volts after passing into the ionizing region their energy on collision could be appreciably different from the measured value. However a magnetic field of a hundred gauss is sufficient to keep the energy constant within a few percent for initial energies as low as 1 volt. The electron energy scale was calibrated by introducing argon into the instrument with the gas to be studied.

The silicon tetrachloride used for the analyses was kindly supplied by C. M. Olson, Pigments Department, E. I. du Pont de Nemours and Company. It had not been subjected to the pyralysis treatment used to "crack" out impurities of carbon tetrachloride but a previous

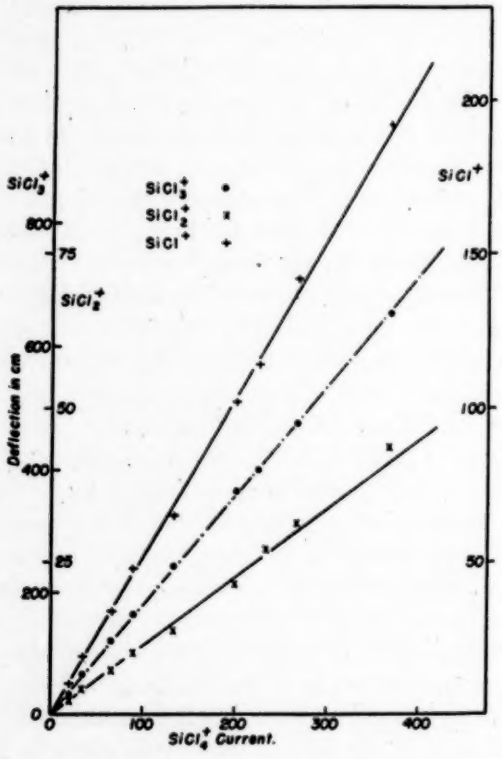

FIG. 2. Ion current for fragment ions *vs.* ion current for parent ion at different pressures.

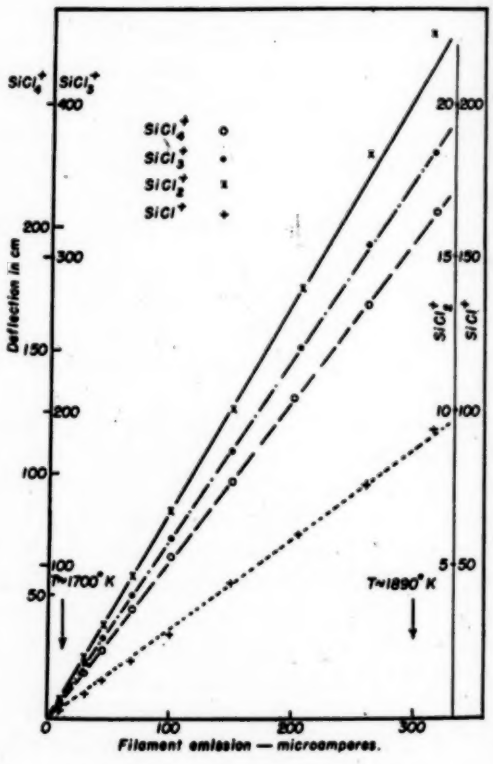

FIG. 3. Ion current *vs.* ionizing current.

[5] J. E. Taylor, Rev. Sci. Inst. **15**, 1 (1944).

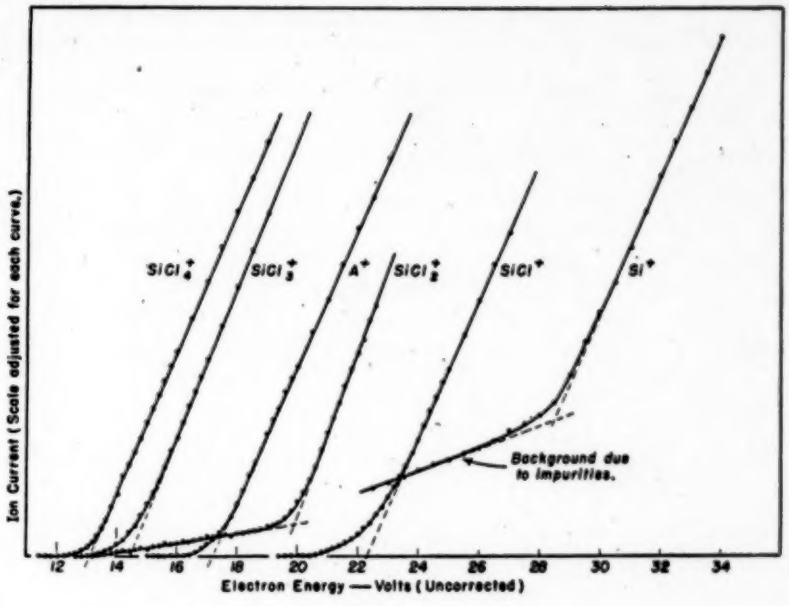

FIG. 4. Appearance potential curves for singly-charged positive ions in $SiCl_4$.

investigation showed that such impurities were present to less than 0.1 percent.[6] Before admitting the gas to the system for analysis the pressure in the ion source was about 10^{-6} mm of Hg, the impurities being water and some carbon monoxide and nitrogen. While taking measurements the pressure in the ion source was kept between 10^{-4} and 10^{-5} mm of Hg. Once $SiCl_4$ had been admitted to the system a disturbing background of HCl appeared, probably caused by the reaction $SiCl_4+2H_2O \rightarrow 4HCl+SiO_2$. This could not be pumped out and the Cl^+ ions from dissociation of HCl make the appearance potential curve for Cl^+ from $SiCl_4$ invalid.

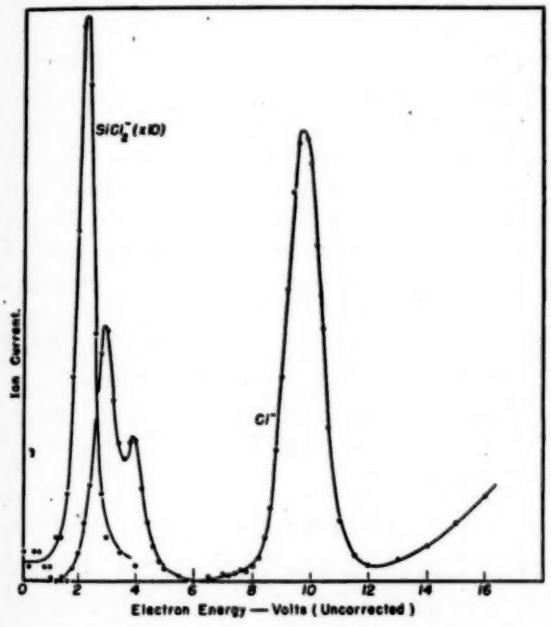

FIG. 5. Appearance potential curves for negative ions in $SiCl_4$.

The mass spectrometer used does not employ differential pumping on the ion source, so measurements of ion current as a function of pressure and filament temperature were made to distinguish processes due to electron bombardment of $SiCl_4$ from possible secondary processes. Figure 2 shows various ion currents plotted against $SiCl_4^+$ current. (This current is a more accurate pressure indicator than the ionization gauge.) The filament temperature and ionizing current could not be varied independently so in Fig. 3 are shown the ion currents plotted as a function of total filament emission, the filament temperature varying by about 190°C in this range. It is seen that with the exception of $SiCl_2^+$ the currents are linear functions of the variables and hence caused by primary processes. The fact that the $SiCl_2^+$ current increases more rapidly at high pressure, and especially at high temperature, indicates that $SiCl_2$ due to thermal decomposition is probably present. This is also indi-

[6] R. H. Vought, Report No. 588 for OSRD Contract OEMsr-388, Division 14, NDRC, October 5, 1945.

TABLE I. Ions formed in $SiCl_4$.

Ion	Relative intensity at 75 v	Appearance potential (volts)	Suggested process $SiCl_4 \rightarrow$:	Minimum energy required (volts)	Excess energy or ionization potential deduced (volts)
$SiCl_4^+$	56	11.6±0.2	$SiCl_4^+$	$I(SiCl_4)$	$I(SiCl_4)=11.6$
$SiCl_3^+$	100	12.9±0.2	$SiCl_3^+ + Cl$ $SiCl_3^+ + Cl^-$	$4.4+I(SiCl_3)$ $0.6+I(SiCl_3)$	$I(SiCl_3) \leqslant 8.5$ $I(SiCl_3) \leqslant 12.3$
$SiCl_2^+$	4.1	11.8±0.3 18.4±0.3	$SiCl_2 \rightarrow SiCl_2^*$ $SiCl_2^+ + Cl_2$ $SiCl_2^+ + 2Cl$	$I(SiCl_2)$ 15.2 17.7	$I(SiCl_2)=11.8$ $T+E=3.2$ $T+E=0.7$
$SiCl^+$	13	20.5±0.3	$SiCl^+ + Cl_2 + Cl$ $SiCl^+ + 3Cl$	$8.1+I(SiCl)$ $10.6+I(SiCl)$	$I(SiCl) \leqslant 12.4$ $I(SiCl) \leqslant 9.9$
Cl^+	5.5				
Si^+	14	27 ± 1	$Si^+ + 2Cl_2$ $Si^+ + Cl_2 + 2Cl$ $Si^+ + 4Cl$	18.0 20.4 22.9	$T+E=9.0$ $T+E=6.6$ $T+E=4.1$
$SiCl_2^-$	0.25	0.8±0.3	$SiCl_2^- + Cl_2$ $SiCl_2^- + 2Cl$ $SiCl_2 \rightarrow SiCl_2^-$	5.9 3.4	$EA(SiCl_2) \geqslant 5.1$ $EA(SiCl_2) \geqslant 2.6$
Cl^-	4.0	1.4±0.3 2.4±0.3 8.2±0.3	$Cl^- + SiCl_3$ $Cl^- + SiCl_2 + Cl$ $Cl^- + SiCl + Cl_2$ $Cl^- + SiCl + 2Cl$	0.6 2.1 4.3 6.8	$T+E=0.8$ $T+E=0.3$ $T+E=3.9$ $T+E=1.4$
$SiCl_3^{++}$	4.9	33.8±0.5			
$SiCl_2^{++}$	0.65	37.3±0.5			
$SiCl^{++}$	1.2	42 ± 1			

cated by the fact that while pumping out the system a background current of $SiCl_2^+$ ions greater than that owing to $SiCl_3^+$ ions was observed, whereas the ratio while admitting gas was 25 to 1 with the $SiCl_3^+$ current larger.

RESULTS

The ion currents due to the various ions observed in silicon tetrachloride are shown in Figs. 4 and 5. The appearance potentials from these curves and the relative abundances of each type of ion are recorded in Table I. This also includes the results of some energy calculations to be discussed later. The relative intensity of each ion was determined from a measurement of the current due to one isotope and then dividing by the fraction of the total number of ions of this type having this mass, as determined from the relative abundances of the isotopes of silicon and chlorine. Corrections were made for Cl^+ and Si^+ currents due to impurities and for Cl^- and $SiCl_2^-$ currents due to the poor negative ion collecting efficiency of the mass spectrometer. The efficiency was known to be low from a comparison of measurements made on carbon tetrachloride with the results of Baker and Tate.[7] It was also found that above 15 volts the ionization efficiency curves for negative ions had shapes characteristic of the instrument rather than of the gas, so that appearance potential measurements of negative ions from ion pair production were invalid. The only explanation suggested for this low efficiency is improper geometry of the slit system, as evidenced by extreme sensitivity of ion current to position of the ion source electromagnet.

DISCUSSION

The notation to be used is: $A(X^+)$—appearance potential of X^+; $D(XY)$—heat of dissociation of XY; $I(X)$—ionization energy of X; $EA(X)$—electron affinity of X; $T+E$—excess energy in

[7] R. F. Baker and J. T. Tate, Phys. Rev. **53**, 683A (1938).

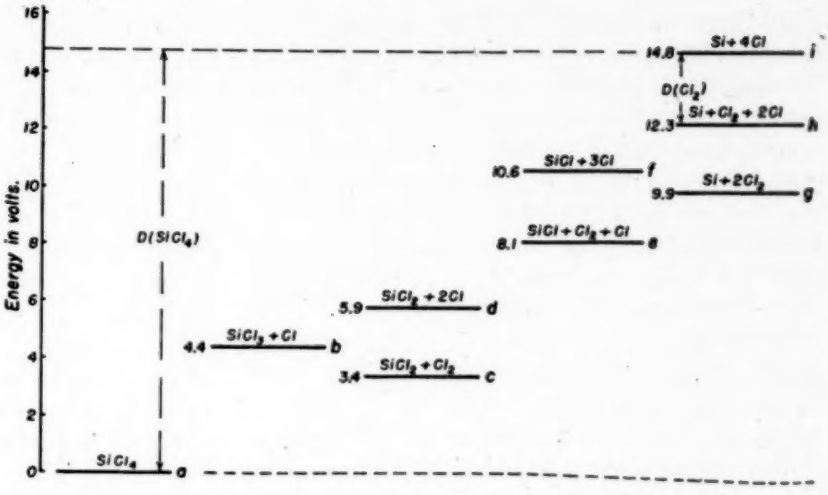

FIG. 6. Energies of the possible configurations of one silicon and four chlorine atoms relative to that of the parent molecule, $SiCl_4$.

a dissociation process, where T represents kinetic energy of relative motion and E is the excitation energy of the dissociation products.

For relating the observed quantities to other properties of the gas the following estimates of heats of dissociation of $SiCl_4$ can be made. From the usual Born cycle the heat of dissociation of $SiCl_4$ is

$$D(SiCl_4)=Q(SiCl_4)+2D(Cl_2)+L(Si),$$

where $Q(SiCl_4)$ is the heat of formation of $SiCl_4$ and $L(Si)$ is the heat of sublimation of silicon. Using values from Bichowsky and Rossini[8] $D(SiCl_4)=142.5+2\times56.9+85=341$ kilocalories per mole, or 14.8 electron volts. This determines the separation of levels a and i, Fig. 6. Evidently, level h is below i by $D(Cl_2)=2.47$ volts, and g, e, and c are below h, f and d by the same amount. $D(SiCl)$ was determined[9] as 4.2 volts from the vibrational constants for transitions to the six lowest levels of the ground electronic state from the data of Jevons.[10] Parti and Samuel[11] estimate $D(SiCl_2)$ as $\frac{3}{2}D(SiCl_4)$. This relation holds for the tin chlorides and gave consistent results when applied to other halogen compounds of this type. $D(SiCl_3)$ may be estimated from the $Si^{IV}-Cl$ bond energy. Asundi, Karim, and Samuel[12] point out that this is not simply $\frac{1}{4}D(SiCl_4)$ since the electronic configuration of silicon in the $SiCl_4$ molecule is sp^3 rather than s^2p^2 of the normal atom. Using their estimate of this excitation energy the strength of the $Si^{IV}-Cl$ bond is determined as $\frac{1}{4}(14.8+2.7)=4.4$ volts.

Since the electron affinity of chlorine is known to be 3.8 volts,[13] calculations on processes involving this ion will give closer checks on heats of dissociation than can be obtained with processes involving positive ions such as $SiCl_3^+$ for which ionization energies are not known. The first two resonance appearance potentials for Cl^- must evidently correspond to dissociation to levels b and d, Fig. 6. The excess energy in each process is the difference between the appearance potential and the algebraic sum of the dissociation energy and electron affinity. Thus we have $T+E=1.4-(4.4-3.8)=0.8$ volt for the process giving $SiCl_3+Cl^-$, and $T+E=2.4-(5.9-3.8)=0.3$ volt for the process $SiCl_4\rightarrow SiCl_2+Cl+Cl^-$. The energies required to produce Cl^- by transitions to e, f and h are 4.3, 6.8 and 8.5 volts, respectively. The 8.2 volts for the third appearance potential for Cl^- is not sufficient for the latter transition and would leave an unlikely large amount of excess energy for the former, so that the process is probably $SiCl_4\rightarrow SiCl+2Cl+Cl^-$ requiring 6.8 volts and leaving 1.4 volts excess energy. This may still be some-

[8] F. R. Bichowsky and F. D. Rossini, *Thermochemistry of Chemical Substances* (Reinhold Publishing Corporation, New York, 1936).

[9] G. Herzberg, *Molecular Spectra and Molecular Structure* (Prentice-Hall, Inc., New York, 1939).

[10] W. Jevons, Proc. Roy. Soc. London **48**, 563 (1936).

[11] Y. P. Parti and R. Samuel, Proc. Phys. Soc. London **49**, 568 (1937).

[12] R. K. Asundi, M. Karim, and R. Samuel, Proc. Phys. Soc. London **50**, 581 (1938).

[13] H. S. W. Massey, *Negative Ions* (Cambridge University Press, London, 1938).

what large and might indicate that the long extrapolation used to get $D(SiCl)$ is inaccurate. However, the width of this resonance peak is seen to be about a volt greater than the maximum possible spread in energy of the electrons,* indicating that the potential energy surface for the system $SiCl-Cl-Cl-Cl^-$ intersects the Franck-Condon region over a range of at least a volt and it may well be above the asymptote for infinite separation by about a volt.

If the $SiCl_2^-$ ions appearing at 0.8 volt are produced from $SiCl_4$ the electron affinity must be at least equal to the energy required for a transition to levels c or d, minus $A(SiCl_2^-)$. Thus $EA(SiCl_2) \geq 2.6$ or 5.1 volts. Either value seems large never to have been reported and is larger than would be expected for such a molecule. Because of the non-linearity of $SiCl_2^+$ current with temperature and pressure, and because of the type of appearance potential curve found for $SiCl_2^+$ ions, free $SiCl_2$ molecules were probably present in the ion source and the ions observed here could be produced by simple capture of an electron. If this is the case nothing can be said of the electron affinity of $SiCl_2$ except that it exists.

Of the processes leading to formation of positive ions the simplest is ionization of the parent molecule and this requires no discussion. The process resulting in $SiCl_3^+$ ions is not so easily identified since it could be accompanied by either a free or negatively ionized chlorine atom. The energies required would differ by $EA(Cl)$, and the ionization energy for $SiCl_3$ deduced from the two cases is ≤ 8.5 volts or ≤ 12.3 volts. Using the interpretation presented in the first part of this paper, the foot of the ionization efficiency curve for $SiCl_3^+$ indicates that about one volt of kinetic energy is released on dissociation, so that the first possibility would give too low a value for $I(SiCl_3)$. For this reason, and because Cl^- ions from ion pair production are also observed at about 13 volts, the process is probably $SiCl_4 \rightarrow SiCl_3^+ + Cl^-$. Using the comparison with Baker and Tate's work on carbon tetrachloride[7] to determine the negative ion collecting efficiency of this mass spectrometer, the corrected value for Cl^- current is still much smaller than the $SiCl_3^+$ current, so that $SiCl_3^+ + Cl$ should also be produced at 3.8 volts higher energy than the 12.9 volts attributed to the process $SiCl_4 \rightarrow SiCl_3^+ + Cl^-$. However no break in the ionization efficiency curve is observed. It is possible that the estimate of efficiency is wrong and that equal numbers of $SiCl_3^+$ and Cl^- ions are produced. The uncertainty here must be attributed to the poor negative ion collecting efficiency.

Two appearance potentials are found for $SiCl_2^+$. From the previous evidence for the existence of free $SiCl_2$ in the ion source the 11.8-volt value is attributed to the ionization potential of $SiCl_2$. The second value at 18.4 volts may then be assigned to the process $SiCl_4 \rightarrow SiCl_2^+ + 2Cl$, which should require 17.7 volts energy. This leaves the reasonable value of 0.7 volt for excess energy.* That the curve for $SiCl_2^+$ ions shown in Fig. 4 is actually owing to $SiCl_2^+$ and not an impurity was demonstrated by taking measurements on the isotopes $Si^{28}Cl^{35}Cl^{37}$ and $Si^{28}Cl^{35}Cl^{35}$. Identical curves were obtained in both cases.

If the 20.5-volt appearance potential for $SiCl^+$ be attributed to production of $SiCl^+ + 3Cl$, a limit on the value of $I(SiCl)$ is determined as $I(SiCl) \leq 20.5 - 10.6 = 9.9$ volts. From the appearance potential curve it is seen that there is probably some kinetic energy released by the process so this may make the value seem low. However, it is not unreasonably low, since SiCl is a highly polymeric substance[14] and this tendency to bond formation indicates that a relatively free electron is present. The alternative explanation that the products are $SiCl^+ + Cl_2 + Cl$, would be the only case observed in which two chlorine atoms came off as a molecule rather than as free atoms.

The production of Si^+ ions at 27 volts is probably due to the process $SiCl_4 \rightarrow Si^+ + 4Cl$, which requires an energy of $D(SiCl_4) + I(Si)$. $I(Si)$ being 8.14 volts,[8] this value is 22.9 volts. Since 4 volts is a large energy to attribute to kinetic energy, the possibility that the ion is

* The narrow peak observed for $SiCl_2^-$ ions shows that this spread is about 1.5 volts.

* The attempt to explain the 11.8-volt value, as caused by the process $SiCl_4 \rightarrow SiCl_2^+ + Cl + Cl^-$, requires that $I(SiCl_3) \leq 9.7$ volts. It is then impossible to explain the 18.4-volt value, since dissociation to $SiCl_2^+ + 2Cl$ would leave about 3 volts excess energy but still not enough for the 3.5 volt excited state of $SiCl_2$.

[14] R. Schwarz and U. Gregor, Zeits. f. anorg. allgem. Chemie **241**, 395 (1939).

TABLE II. Comparison of $SiCl_4$ with CCl_4.

Dissociation products	Appearance potential (volts)	Relative intensity at 75 v
CCl_4^+	11 ±1.0	0.02
$CCl_3^+ + Cl^-$	12.2±0.2	100
$SiCl_4^+$	11.6±0.2	56
$SiCl_3^+ + Cl^-$	12.9±0.2	4–100

produced by transitions to levels h or g, which would result in 2.5 or 5 volts more kinetic energy, is ruled out. Furthermore it indicates that $D(SiCl_4)$ is at least 14.8 volts, rather than the lower value obtained by Asundi, Karim, and Samuel,[12] using the lower value of the heat of sublimation of silicon.[15]

It is noticed that all processes except that producing $SiCl^+$ are identified with reasonable certainty as caused by dissociation into the greatest number of products. Thus the third Cl^- peak was explained as due to production of $SiCl+2Cl+Cl^-$, rather than $SiCl+Cl_2+Cl^-$. Similarly the second appearance potential for $SiCl_2^+$ involves the extra chlorine atoms in the free state rather than as a molecule, and the Si^+ ions are accompanied by four free chlorines rather than chlorine molecules. Even in the doubtful case of $SiCl^+$ the evidence favors the process resulting in $SiCl^+ + 3Cl$ rather than $SiCl^+ + Cl_2 + Cl$. This effect was noticed by Smith[16] working with methane, although with silicon tetrachloride it is rather to be expected, since the Cl−Cl distance in silicon tetrachloride is so great (3.27A) that the attractive force between the two atoms is very small. (The Cl−Cl distance in Cl_2 is only 2A.)

A striking contrast between the dissociation processes in carbon tetrachloride and silicon tetrachloride is the relative probability of processes of the type $MCl_4 \rightarrow MCl_4^+$ and $MCl_4 \rightarrow MCl_3^+ + Cl^-$. The appearance potentials and relative probabilities at 75 v electron energy are shown in Table II.* Presumably the large error in $A(CCl_4^+)$ is caused by the small ion current. The range in intensities for $SiCl_3^+ + Cl^-$ is because of the uncertainty in ion collecting efficiency of the mass spectrometer used for $SiCl_4$. It is seen that ion pair production is relatively much more probable in carbon tetrachloride. This is not unexpected from the fact that carbon tetrachloride has simple valence binding, while the binding in silicon tetrachloride is partially double-bond and partially ionic in character[17] and hence should be stronger. A further consequence of the double bond character of silicon tetrachloride binding is that some of the relatively unstable d orbitals of silicon must be used to accommodate the extra electron pair in the double bond, whereas only the s and p orbitals are used in carbon. This should make removal of an electron from silicon tetrachloride easier than from carbon tetrachloride. Although these qualitative arguments agree with the observed ion intensities at 75 volts, the energies at which each process is observed do not. Using the probable values from Table II, the energy difference for the two processes in carbon tetrachloride is 1.2 volts while in silicon tetrachloride it is 1.3 volts. Hence the probability that a process occur must depend more strongly on factors other than the minimum energy required.

ACKNOWLEDGMENTS

The author would like to thank Dr. W. E. Stephens for his supervision of this work and for discussions of problems that arose at various times. It is also a pleasure to express appreciation to Dr. D. W. Wilson for the use of the mass spectrometer that was constructed for the Medical School, and to Dr. J. G. Miller of the Chemistry Department for several interesting discussions of the results. Acknowledgment is also due the Navy Department, Bureau of Ships, for support of this work, and for permission to publish.

[15] *International Critical Tables.*
[16] L. G. Smith, Phys. Rev. 51, 263 (1937).
* Data for CCl_4 are from reference 7.

[17] L. C. Pauling, *The Nature of the Chemical Bond* (Cornell University Press, Ithaca, New York, 1940).

Mutual Magnetic Interactions of Electrons

H. H. MARVIN
Brace Laboratory of Physics, University of Nebraska, Lincoln, Nebraska
(Received August 23, 1946)

The formulae for the matrix components of the mutual spin-orbit and spin-spin interactions of two electrons are derived from Heisenberg's formula for the Hamiltonian function. The matrices of all two-electron configurations of s, p, and d electrons are computed. Numerical tables of certain functions of interaction integrals are given, which are useful in such calculations.

THE relative positions of the multiplets in atomic spectra are given correctly, and the energy levels are placed in their proper order in most cases, by a theoretical consideration of the mutual electrostatic interactions and the individual spin-orbit interactions of the orbital electrons. The numerical agreement with the empirical values of the energy levels is poor in many instances. The calculated values should be improved appreciably when the mutual magnetic interactions of the electrons are taken into account.

Operators for these interactions, developed both from the model of the spinning electron and from Dirac's relativistic theory, are well known. Calculations from these operators are extraordinarily difficult. Matrices of the mutual magnetic interactions have been computed for only a few of the simplest configurations. Adequate tests have been made only on the triplets of a few sl configurations.[1] Inglis has derived a general formula for these triplets in LS coupling.

The purpose of the present paper is to develop a general method for the calculation of matrices for mutual spin-orbit and spin-spin interactions from the Hamiltonian function of the spinning electron model.[2] The Hamiltonian operator for these interactions of two electrons is

$$\begin{aligned} H_m = &-Cr_{12}^{-3}[(\mathbf{r}_1-\mathbf{r}_2)\times(\mathbf{p}_1-2\mathbf{p}_2)\cdot\mathbf{S}_1 \\ &+(\mathbf{r}_2-\mathbf{r}_1)\times(\mathbf{p}_2-2\mathbf{p}_1)\cdot\mathbf{S}_2] \\ &-2C[3r_{12}^{-5}\mathbf{S}_1\cdot(\mathbf{r}_2-\mathbf{r}_1)\mathbf{S}_2\cdot(\mathbf{r}_2-\mathbf{r}_1) \\ &-r_{12}^{-3}\mathbf{S}_1\cdot\mathbf{S}_2], \quad (1) \end{aligned}$$

where $C=e^2/2\mu^2c^2$. The spin and linear momentum operators are $\mathbf{S}_1$, $\mathbf{S}_2$, $\mathbf{p}_1$, and $\mathbf{p}_2$. The radius vectors from the nucleus to the electrons are $\mathbf{r}_1$ and $\mathbf{r}_2$, and the distance between the electrons is denoted by r_{12}.

The electron eigenfunctions and the antisymmetric eigenfunctions of two-electron states are constructed as specified in TAS.[3] The most general interaction integral is one in which there are four sets, a, b, c, d, of electron parameters. The matrix component connecting two antisymmetric states is

$$\begin{aligned} (A\,|\,H_m\,|\,B) = &\tfrac{1}{2}(ab\,|\,H_m\,|\,cd)-\tfrac{1}{2}(ba\,|\,H_m\,|\,cd) \\ &+\tfrac{1}{2}(ba\,|\,H_m\,|\,dc)-\tfrac{1}{2}(ab\,|\,H_m\,|\,dc), \quad (2) \end{aligned}$$

in which an exchange of letters indicates permutation of the electron parameters with respect to the coordinates.

As the first step in separating the variables, differentiate the relation

$$\begin{aligned} r_{12}^{-1} &= (r_1^2-2r_1r_2\cos\omega+r_2^2)^{-\frac{1}{2}} \\ &= \sum_{k=0}^{\infty}[r_<^k/r_>^{k+1}]P_k(\cos\omega) \end{aligned}$$

(Eq. (8^{6}3), TAS) twice with respect to $\cos\omega$, and after each step substitute for the derivative of P_k from the familiar formula

$$P_k' = (2k-1)P_{k-1}+(2k-5)P_{k-3}+\cdots.$$

From the resulting equations one obtains

$$\begin{aligned} r_{12}^{-3} &= \sum_{k=0}^{\infty}\xi(k)T(k), \\ r_{12}^{-5} &= \sum_{k=0}^{\infty}\eta(k)T(k)/3r_1r_2, \end{aligned} \quad (3)$$

[1] G. Breit, Phys. Rev. **36**, 383 (1930); **39**, 616 (1932); G. Araki, Proc. Math. Phys. Soc. Japan **19**, 128 (1937); D. R. Inglis, Phys. Rev. **61**, 297 (1942).
[2] W. Heisenberg, Zeits. f. Physik **39**, 499 (1926).
[3] E. U. Condon and G. H. Shortley, *Theory of Atomic Spectra* (Cambridge University Press, New York, 1935).

in which

$$\xi(k)=r_<^k/r_>^{k+3}+r_<^{k+2}/r_>^{k+5}+\cdots,$$
$$\eta(k)=(2k+3)\xi(k+1)+(2k+7)\xi(k+3)+\cdots, \quad (4)$$
$$T(k)=(2k+1)P_k(\cos\omega),$$

where $r_<$ is the lesser and $r_>$ the greater of r_1 and r_2, and ω is the angle between the radius vectors.

Introduce the unit radius vector $\mathbf{u}$, defined by

$$\mathbf{r}=r\mathbf{u}, \quad (5)$$

as an aid in separating the variables in the scalar and vector products. The orbital angular momentum operator for an electron is

$$\mathbf{r}\times\mathbf{p}=\mathbf{L}. \quad (6)$$

Also,

$$\mathbf{r}\cdot\mathbf{p}=-i\hbar r\partial/\partial r,$$

since the components of $\mathbf{p}$ are $-i\hbar\partial/\partial x$, etc. By substituting these relations in

$$\mathbf{r}\times(\mathbf{r}\times\mathbf{p})=\mathbf{r}\mathbf{r}\cdot\mathbf{p}-\mathbf{r}\cdot\mathbf{r}\mathbf{p},$$

and solving for $\mathbf{p}$, it follows that

$$\mathbf{r}'\times\mathbf{p}=(\mathbf{u}\times\mathbf{L})\times\mathbf{u}'r'/r+i\hbar\mathbf{u}\times\mathbf{u}'r'\partial/\partial r, \quad (7)$$

where $\mathbf{r}'$ is the radius vector to another electron.

The variables in Eq. (1) can be separated with the aid of Eqs. (3), (5)–(7). Each integral in Eq. (2) can be expressed as the product of a double integral over the radial coordinates and a factor that depends on the six angle and spin coordinates. Subsequent calculations are simplified by making a transformation which reduces H_m from ten additive terms to six. The operator is separated into two parts that are similar except for the order of the coordinate subscripts, the subscripts in one part are exchanged, and the parts are reassembled. $(A|H_m|B)$ is invariant in this transformation, the net effect of which is an exchange of certain related pairs of integrals between the first and third components in Eq. (2), and likewise between the second and fourth components, with interchange of coordinate subscripts and of electron parameters. The components are no longer equal in pairs. The evaluation of $(ab|H_m|cd)$ is the next step, after which the other components can be written by performing the indicated permutations of electron parameters. The transformed Hamiltonian operator is the unsymmetrical form

$$\begin{aligned}H_m=&-C\sum_{k=0}^{\infty}\xi(k)T(k)\\&\times\{2\mathbf{L}_1-(\mathbf{u}_1\times\mathbf{L}_1)\times\mathbf{u}_2(r_>/r_<+r_</r_>)\\&-i\hbar\mathbf{u}_1\times\mathbf{u}_2(r_>\partial/\partial r_<+r_<\partial/\partial r_>)\}\\&\cdot(\mathbf{S}_1+2\mathbf{S}_2)\\&-2C\sum_{k=0}^{\infty}T(k)\{\eta(k)[\mathbf{u}_1\cdot\mathbf{S}_1\mathbf{u}_1\cdot\mathbf{S}_2(r_>/r_<\\&+r_</r_>)-\mathbf{u}_1\cdot\mathbf{S}_1\mathbf{u}_2\cdot\mathbf{S}_2-\mathbf{u}_2\cdot\mathbf{S}_1\mathbf{u}_1\cdot\mathbf{S}_2]\\&-\xi(k)\mathbf{S}_1\cdot\mathbf{S}_2\}. \quad (8)\end{aligned}$$

The first and second parts of Eq. (8) are, respectively, the mutual spin-orbit operator H_m^{I} and the spin-spin operator H_m^{II}.

The radial integrals in Eq. (2) between the states ab and cd are all related to two elementary integrals

$$\left.\begin{aligned}&\frac{Ch^2}{4}\int_0^\infty\int_0^\infty\frac{r_<^k}{r_>^{k+3}}R_1(a)R_2(b)R_1(c)R_2(d)dr_1dr_2\\&\qquad={}^3R^k(n^al^a n^bl^b,\ n^cl^c n^dl^d),\\&\frac{Ch^2}{4}\int_0^\infty\int_0^\infty\frac{R_1(a)}{r_1}\frac{R_2(b)}{r_2}\frac{r_<^k}{r_>^{k+3}}\\&\times\left(r_>\frac{\partial}{\partial r_<}+r_<\frac{\partial}{\partial r_>}\right)\left[\frac{R_1(c)}{r_1}\frac{R_2(d)}{r_2}\right]r_1^2r_2^2dr_1dr_2\\&\qquad={}^3D^k(n^al^a n^bl^b,\ n^cl^c n^dl^d),\end{aligned}\right\}(9)$$

which will be denoted by

$${}^3R^k(ab,\,cd) \quad \text{and} \quad {}^3D^k(ab,\,cd)$$

hereafter. It follows from Eqs. (4) that the radial integrals that contain the operators $\xi(k)$,

$$\xi(k)(r_>/r_<+r_</r_>),\quad \xi(k)(r_>\partial/\partial r_<+r_<\partial/\partial r_>),$$
$$\eta(k),\quad \text{and}\quad \eta(k)(r_>/r_<+r_</r_>)$$

are, respectively,

$$\left.\begin{aligned}\xi^k(ab,\,cd)&={}^3R^k(ab,\,cd)+{}^3R^{k+2}(ab,\,cd)+\cdots,\\\rho^k(ab,\,cd)&=\xi^{k-1}(ab,\,cd)+\xi^{k+1}(ab,\,cd),\\\Delta^k(ab,\,cd)&={}^3D^k(ab,\,cd)\\&\quad+{}^3D^{k+2}(ab,\,cd)+\cdots,\\\eta^k(ab,\,cd)&=(2k+3)\xi^{k+1}(ab,\,cd)\\&\quad+(2k+7)\xi^{k+3}(ab,\,cd)+\cdots,\\\sigma^k(ab,\,cd)&=\eta^{k-1}(ab,\,cd)\\&\quad+\eta^{k+1}(ab,\,cd)+2\xi^k(ab,\,cd).\end{aligned}\right\}(10)$$

The mutual spin-orbit integral between states ab and cd can be expressed now, from the first summation in Eq. (8), in the form

$$(ab|H_m{}^I|cd)=-\frac{4}{\hbar^2}\sum_{k=0}^{\infty}[(ab|Q_1{}^k|cd)\xi^k(ab,cd)+(ab|Q_2{}^k|cd)\rho^k(ab,cd)+(ab|Q_3{}^k|cd)\Delta^k(ab,cd)], \quad (11)$$

where

$$\left.\begin{aligned} Q_1{}^k&=T(k)2\mathbf{L}_1\cdot(\mathbf{S}_1+2\mathbf{S}_2),\\ Q_2{}^k&=-T(k)(\mathbf{u}_1\times\mathbf{L}_1)\times\mathbf{u}_2\cdot(\mathbf{S}_1+2\mathbf{S}_2),\\ Q_3{}^k&=-T(k)i\hbar\mathbf{u}_1\times\mathbf{u}_2\cdot(\mathbf{S}_1+2\mathbf{S}_2).\end{aligned}\right\}(12)$$

The spin-spin integral is, from the second summation in Eq. (8),

$$(ab|H_m{}^{II}|cd)=\frac{8}{\hbar^2}\sum_{k=0}^{\infty}[(ab|Q_4{}^k|cd)\sigma^k(ab,cd)+(ab|Q_5{}^k|cd)\eta^k(ab,cd)+(ab|Q_6{}^k|cd)\xi^k(ab,cd)], \quad (13)$$

where

$$\left.\begin{aligned} Q_4{}^k&=-T(k)\mathbf{u}_1\cdot\mathbf{S}_1\mathbf{u}_1\cdot\mathbf{S}_2,\\ Q_5{}^k&=T(k)(\mathbf{u}_1\cdot\mathbf{S}_1\mathbf{u}_2\cdot\mathbf{S}_2+\mathbf{u}_2\cdot\mathbf{S}_1\mathbf{u}_1\cdot\mathbf{S}_2),\\ Q_6{}^k&=T(k)\mathbf{S}_1\cdot\mathbf{S}_2.\end{aligned}\right\}(14)$$

The non-vanishing matrix components of $\mathbf{L}$ and $\mathbf{S}$ are

$$\left.\begin{aligned} (lm_l\pm1m_s|\mathbf{L}|lm_lm_s)&=\tfrac{1}{2}\hbar[(l\mp m_l)\times(l\pm m_l+1)]^{\frac{1}{2}}(\mathbf{i}\mp i\mathbf{j}),\\ (lm_lm_s|\mathbf{L}|lm_lm_s)&=\hbar m_l\mathbf{k},\\ (lm_lm_s\pm1|\mathbf{S}|lm_lm_s)&=\tfrac{1}{2}\hbar(\mathbf{i}\mp i\mathbf{j}),\\ (lm_lm_s|\mathbf{S}|lm_lm_s)&=\hbar m_s\mathbf{k},\end{aligned}\right\}(15)$$

by Eqs. (3[3]7) and (9[3]11), TAS. A comparison of Eqs. (4[3]21) and (9[3]11), TAS, shows that the non-vanishing matrix components of the unit radius vector are

$$\left.\begin{aligned} (l+1m_l\pm1m_s|\mathbf{u}|lm_lm_s)&=\mp\tfrac{1}{2}A(l+1m_l\pm1,lm_l)(\mathbf{i}\mp i\mathbf{j}),\\ (l+1m_lm_s|\mathbf{u}|lm_lm_s)&=A(l+1m_l,lm_l)\mathbf{k},\\ (l-1m_l\pm1m_s|\mathbf{u}|lm_lm_s)&=\pm\tfrac{1}{2}A(l-1m_l\pm1,lm_l)(\mathbf{i}\mp i\mathbf{j}),\\ (l-1m_lm_s|\mathbf{u}|lm_lm_s)&=A(l-1m_l,lm_l)\mathbf{k},\end{aligned}\right\}(16)$$

where

$$A(l+1m_l\pm1,lm_l)=\left[\frac{(l\pm m_l+1)(l\pm m_l+2)}{(2l+1)(2l+3)}\right]^{\frac{1}{2}},$$

$$A(l+1m_l,lm_l)=\left[\frac{(l-m_l+1)(l+m_l+1)}{(2l+1)(2l+3)}\right]^{\frac{1}{2}},$$

$$A(l-1m_l\pm1,lm_l)=\left[\frac{(l\mp m_l)(l\mp m_l-1)}{(2l-1)(2l+1)}\right]^{\frac{1}{2}},$$

$$A(l-1m_l,lm_l)=\left[\frac{(l-m_l)(l+m_l)}{(2l-1)(2l+1)}\right]^{\frac{1}{2}}.$$

The matrix component of $T(k)$ is, by comparison with that of $P_k(\cos\omega)$ in Eq. (8[6]9), TAS,

$$(ab|T(k)|pq)=\delta(m_s{}^a,m_s{}^p)\delta(m_s{}^b,m_s{}^q)\times\delta(m_l{}^a+m_l{}^b,m_l{}^p+m_l{}^q)(2k+1)\times c^k(l^am_l{}^a,l^pm_l{}^p)c^k(l^qm_l{}^q,l^bm_l{}^b). \quad (17)$$

The formulae for $(ab|Q_1{}^k|cd)$, etc., are calculated from Eqs. (15)–(17) by ordinary methods of matrix algebra, guided by Eqs. (12) and (14). The matrix components of $H_m{}^I$ and $H_m{}^{II}$ between the states ab and cd are then calculated according to Eqs. (11) and (13). These calculations, which are very long, are omitted. The final formulae are stated in condensed notation, by means of abbreviations which are described in the following paragraphs.

Certain factors in the matrix elements of $\mathbf{u}\cdot\mathbf{Su}\cdot\mathbf{S}'$ are connected with the matrix components of $\mathbf{u}$ by the relations

$$B(l\pm2m_l+x+y,lm_l)=A(l\pm2m_l+x+y,l\pm1m_l+x)\times A(l\pm1m_l+x,lm_l),$$

$$B(lm_l+x+y,lm_l)=-(-)^xA(lm_l+x+y,l+1m_l+x)\times A(l+1m_l+x,lm_l)-(-)^yA(lm_l+x+y,l-1m_l+x)\times A(l-1m_l+x,lm_l),$$

in which x and y may have the values $+1$, 0, and -1 in any combination, except that they

cannot be zero simultaneously in the second equation. Standard combinations of interaction integrals for which numerical tables may be constructed are

$$\left.\begin{aligned}
&\lambda^k(l'm_l', lm_l+f)\\
&\quad=(2k+1)^{\frac{1}{2}}[lA(l+1m_l+f, lm_l)\\
&\qquad\times c^k(l'm_l', l+1m_l+f)-(-)^l(l+1)\\
&\qquad\times A(l-1m_l+f, lm_l)\\
&\qquad\qquad\times c^k(l'm_l', l-1m_l+f)],\\
&\alpha^k(l'm_l', lm_l+f)\\
&\quad=(2k+1)^{\frac{1}{2}}[A(l+1m_l+f, lm_l)\\
&\qquad\times c^k(l'm_l', l+1m_l+f)+(-)^l\\
&\qquad\times A(l-1m_l+f, lm_l)\\
&\qquad\qquad\times c^k(l'm_l', l-1m_l+f)],
\end{aligned}\right\}\quad(18)$$

in which f may take the values ±1 or 0. Likewise,

$$\left.\begin{aligned}
&\beta^k(l'm_l', lm_l+f)\\
&\quad=(2k+1)[B(l+2m_l+f, lm_l)\\
&\qquad\times c^k(l'm_l', l+2m_l+f)\\
&\qquad-(-)^lB(lm_l+f, lm_l)c^k(l'm_l', lm_l+f)\\
&\qquad+(-)^lB(l-2m_l+f, lm_l)\\
&\qquad\qquad\times c^k(l'm_l', l-2m_l+f)],
\end{aligned}\right\}\quad(19)$$

in which f may take the values ±2, ±1 or 0.

Further abbreviations are of the types

$$\left.\begin{aligned}
&C^k(ac+f, bd)\\
&\quad=(2k+1)c^k(l^am_l^a, l^cm_l^c+f)c^k(l^bm_l^b, l^dm_l^d),\\
&\Lambda^k(ac+f, bd+g)\\
&\quad=\lambda^k(l^am_l^a, l^cm_l^c+f)\alpha^k(l^bm_l^b, l^dm_l^d+g),\\
&A^k(ac+f, bd+g)\\
&\quad=\alpha^k(l^am_l^a, l^cm_l^c+f)\alpha^k(l^bm_l^b, l^dm_l^d+g),\\
&B^k(ac+f, bd)\\
&\quad=\beta^k(l^am_l^a, l^cm_l^c+f)c^k(l^bm_l^b, l^dm_l^d).
\end{aligned}\right\}\quad(20)$$

The matrix component of H_m^I between states ab and cd is, in this condensed notation, with $\Delta m=m_l^a-m_l^c$,

$$\begin{aligned}
&(ab|H_m^I|cd)=2(-)^{\Delta m}\sum_k[\{\delta(m_s^a, m_s^c\mp1)\\
&\quad\times\delta(m_s^b, m_s^d)+2\delta(m_s^a, m_s^c)\delta(m_s^b, m_s^d\mp1)\}\\
&\quad\times\delta(m_l^a+m_l^b, m_l^c+m_l^d\pm1)\{2[(l^c\mp m_l^c)\\
&\quad\times(l^c\pm m_l^c+1)]^{\frac{1}{2}}C^k(ac\pm1, bd)\xi^k(ab, cd)\\
&\quad-[\Lambda^k(ac\pm1, bd)+\Lambda^k(ac, bd\pm1)]\rho^k(ab, cd)\\
&\quad+[A^k(ac\pm1, bd)+A^k(ac, bd\pm1)]\Delta^k(ab, cd)\}\\
&\quad+\delta(m_s^a, m_s^c)\delta(m_s^b, m_s^d)\delta(m_l^a+m_l^b, m_l^c+m_l^d)\\
&\quad\times(m_s^c+2m_s^d)\{-4m_l^cC^k(ac, bd)\xi^k(ab, cd)\\
&\quad+[\Lambda^k(ac+1, bd-1)-\Lambda^k(ac-1, bd+1)]\\
&\quad\times\rho^k(ab, cd)-[A^k(ac+1, bd-1)\\
&\qquad-A^k(ac-1, bd+1)]\Delta^k(ab, cd)\}].\quad(21)
\end{aligned}$$

The corresponding matrix component of H_m^{II} is

$$\begin{aligned}
&(ab|H_m^{II}|cd)=2(-)^{\Delta m}\sum_k[\delta(m_s^a, m_s^c\mp1)\\
&\quad\times\delta(m_s^b, m_s^d\mp1)\delta(m_l^a+m_l^b, m_l^c+m_l^d\pm2)\\
&\quad\times\{-B^k(ac\pm2, bd)\sigma^k(ab, cd)\\
&\quad-2A^k(ac\pm1, bd\pm1)\eta^k(ab, cd)\}\\
&\quad+\{\delta(m_s^a, m_s^c\mp1)\delta(m_s^b, m_s^d)\cdot m_s^d\\
&\quad+\delta(m_s^a, m_s^c)\delta(m_s^b, m_s^d\mp1)\cdot m_s^c\}\\
&\quad\times\delta(m_l^a+m_l^b, m_l^c+m_l^d\pm1)\\
&\quad\times\{\mp2B^k(ac\pm1, bd)\sigma^k(ab, cd)\\
&\quad\pm2[A^k(ac\pm1, bd)-A^k(ac, bd\pm1)]\eta^k(ab, cd)\}\\
&\quad+\delta(m_s^a, m_s^c\mp1)\delta(m_s^b, m_s^d\pm1)\\
&\quad\times\delta(m_l^a+m_l^b, m_l^c+m_l^d)\{B^k(ac, bd)\\
&\quad\times\sigma^k(ab, cd)+[A^k(ac\pm1, bd\mp1)\\
&\quad+A^k(ac\mp1, bd\pm1)]\eta^k(ab, cd)\\
&\quad+2C^k(ac, bd)\xi^k(ab, cd)\}+\delta(m_s^a, m_s^c)\\
&\quad\delta(m_s^b, m_s^d)\delta(m_l^a+m_l^b, m_l^c+m_l^d)\cdot m_s^cm_s^d\\
&\quad\times\{-4[B^k(ac, bd)+C^k(ac, bd)]\sigma^k(ab, cd)\\
&\quad+8A^k(ac, bd)\eta^k(ab, cd)\\
&\qquad+4C^k(ac, bd)\xi^k(ab, cd)\}].\quad(22)
\end{aligned}$$

The parameter k must satisfy the same conditions (Eqs. (8·10), TAS) as in the theory of electrostatic interaction. These conditions restrict the choice of values of l^a and l^b, and limit the range of k to a few values.

TABLE I.

$\lambda^k(l'm_l', lm_l+f)$ for $l'+l$ even

				$k=1$			$k=3$			$k=5$	
$l'l$	m_l'	m_l	$f=\pm1$	0	∓1	±1	0	∓1	±1	0	∓1
ss	0	0	0	0	0						
ds	±2	0	0	0	0	0	0	0			
	±1	0	0	0	0	0	0	0			
	0	0	0	0	0	0	0	0			
				$K=3/5$			$K=4/35$				
sd	0	±2	0	0	−12	−30	+5	−2			
	0	±1	0	+3	+6	+20	−8	+6			
	0	0	−2	−4	−2	−12	+9	−12			
				$K=3/25$			$K=3/175$				
pp	±1	±1	−8	+1	+18	+4	−3	+4			
	±1	0	+3	−16	0	−6	+8	−20			
	±1	∓1	+18	0	0	+4	−10	+60			
	0	±1	0	−1	+32	+20	−8	+6			
	0	0	−2	−4	−2	−16	+12	−16			
				$K=3/49$			$K=1/63$			$K=20/4851$	
dd	±2	±2	−72	+4	+128	+48	−16	−12	−6	+5	−6
	±2	±1	+16	−50	0	−64	+75	+30	+20	−24	+42
	±2	0	+12	0	0	+18	−180	−30	−36	+63	−168
	±2	∓1	0	0	0	+30	+245	0	+42	−112	+504
	±2	∓2	0	0	0	−500	0	0	−28	+126	−1260
	±1	±2	0	−8	+100	+120	−12	−100	−42	+24	−20
	±1	±1	−32	−1	+18	−48	+49	+192	+96	−80	+96
	±1	0	+54	−48	0	−6	−72	−180	−120	+144	−252
	±1	∓1	+18	0	0	+192	+30	+80	+96	−168	+448
	±1	∓2	0	0	0	−480	+20	0	−42	+112	−504
	0	±2	0	0	+12	+120	0	−288	−168	+63	−36
	0	±1	0	−27	+96	0	+18	+294	+252	−144	+120
	0	0	−2	−4	−2	−108	−36	−432	−216	+180	−216

$\lambda^k(l'm_l', lm_l+f)$ for $l'+l$ odd

				$k=0$			$k=2$			$k=4$	
$l'l$	m_l'	m_l	$f=\pm1$	0	∓1	±1	0	∓1	±1	0	∓1
ps	±1	0	0	0	0	0	0	0			
	0	0	0	0	0	0	0	0			
				$K=4/3$			$K=1/15$				
sp	0	±1	0	0	+2	+12	−3	+2			
	0	0	0	−1	0	−6	+4	−6			
				$K=1/15$			$K=1/147$			$K=1/245$	
dp	±2	±1	+12	0	0	−48	+18	+288	+4	−5	+10
	±2	0	0	0	0	+36	−324	0	−10	20	−70
	±2	∓1	0	0	0	+288	0	0	+10	−35	+280
	±1	±1	0	+3	0	−72	+3	+450	+20	−16	+20
	±1	0	+6	0	0	+6	−144	−36	−32	+40	−80
	±1	∓1	0	0	0	+450	−18	0	+20	−40	+140
	0	±1	0	0	+2	−48	−3	+512	+60	−30	+24
	0	0	0	+4	0	−6	−100	−6	−60	+48	−60
				$K=3/5$			$K=3/49$			$K=4/245$	
pd	±1	±2	0	0	+12	+72	−8	−12	−10	+5	−4
	±1	±1	0	−3	0	−32	+27	+18	+20	−16	+20
	±1	0	+2	0	0	+2	−48	−12	−24	+30	−60
	±1	∓1	0	0	0	+18	+50	0	+20	−40	+140
	±1	∓2	0	0	0	−128	0	0	−10	+35	−280
	0	±2	0	0	0	0	+4	−100	−70	+20	−10
	0	±1	0	0	+6	+16	+1	+96	+80	−40	+32
	0	0	0	−4	0	−54	−4	−54	−60	+48	−60

TABLE II.

$\alpha^k(l'm_l', lm_l+f)$ for $l'+l$ even

$l'l$	m_l'	m_l	$f=\pm1$	$k=1$ 0	∓1	±1	$k=3$ 0	∓1	±1	$k=5$ 0	∓1
				$K=1/3$							
ss	0	0	−2	+1	−2						
				$K=1/15$			$K=1/35$				
ds	±2	0	+12	0	0	−2	+5	−30			
	±1	0	+6	+3	0	−6	+8	−20			
	0	0	+2	+4	+2	−12	+9	−12			
				$K=3/25$			$K=3/175$				
pp	±1	±1	−8	+1	−8	+4	−3	+4			
	±1	0	+2	+1	0	−6	+8	−20			
	±1	∓1	−8	0	0	+4	−10	+60			
	0	0	−2	+9	−2	−16	+12	−16			
				$K=1/147$			$K=1/63$			$K=5/4851$	
dd	±2	±2	−162	+9	−162	+12	−4	+12	−6	+5	−6
	±2	±1	+36	+18	0	−16	+3	−30	+20	−24	+42
	±2	0	−48	0	0	+18	0	+30	−36	+63	−168
	±2	∓1	0	0	0	−30	−5	0	+42	−112	+504
	±2	∓2	0	0	0	+80	0	0	−28	+126	−1260
	±1	±1	−72	+81	−72	−12	−1	−12	+96	−80	+96
	±1	0	+6	+3	0	+6	+18	0	−120	+144	−252
	±1	∓1	−72	0	0	−12	−30	+20	+96	−168	+448
	0	0	−50	+121	−50	0	+36	0	−216	+180	−216

$\alpha^k(l'm_l', lm_l+f)$ for $l'+l$ odd

$l'l$	m_l'	m_l	$f=\pm1$	$k=0$ 0	∓1	±1	$k=2$ 0	∓1	±1	$k=4$ 0	∓1
				$K=1/3$			$K=1/15$				
ps	±1	0	+2	0	0	−2	+3	−12			
	0	0	0	+1	0	−6	+4	−6			
				$K=1/15$			$K=1/147$			$K=1/245$	
dp	±2	±1	+12	0	0	−48	+18	−162	+4	−5	+10
	±2	0	0	0	0	+36	+9	0	−10	+20	−70
	±2	∓1	0	0	0	−162	0	0	+10	−35	+280
	±1	±1	0	+3	0	−72	+3	−72	+20	−16	+20
	±1	0	+6	0	0	+6	+81	−36	−32	+40	−80
	±1	∓1	0	0	0	−72	−18	0	+20	−40	+140
	0	±1	0	0	+2	−48	−3	−50	+60	−30	+24
	0	0	0	+4	0	−6	+121	−6	−60	+48	−60

The matrix components connecting the antisymmetric states A and B are calculated from Eq. (2). The matrix components required to complete Eq. (2) are obtained by exchanging electron parameters in Eqs. (21) and (22). To prepare Eq. (2) for use in calculation of a given interaction, a complete list of the C^k, Λ^k, A^k, and B^k is made. These factors are computed according to Eqs. (20), using tables of numerical values of the c^k, λ^k, α^k, and β^k.

Tables of the three latter parameters have been computed for all combinations of s, p, and d electron states, using values of the c^k from various sources.[4] Values of λ^k are given in Table I, in three columns labeled $f=+1$, 0, and -1 under each value of k. Each number has the form $(Kx)^{\frac{1}{2}}$ preceded by a plus or a minus sign. Only the sign and the value of x are listed. The value of K, which depends only on l', l, and k, is given at the head of each section.

Values of the α^k are given in Table II. The combinations sp, sd, and pd are omitted, since they can be derived from ps, etc., by the formula

$$\alpha^k(lm_l, l'm_l'-f)=(-1)^{m_l-m_l'}\alpha^k(l'm_l', lm_l+f).$$

[4] Table 1[6], TAS and also G. H. Shortley and B. Fried, Phys. Rev. **54**, 739 (1938).

TABLE III.

$\beta^k(l'm_l', lm_l+f)$ for $l'+l$ even

$l'l$	m_l'	m_l	$f=\pm2$	$k=0$ ±1	0	∓1	∓2	±2	$k=2$ ±1	0	∓1	∓2	±2	$k=4$ ±1	0	∓1	∓2	±2	$k=6$ ±1	0	∓1	∓2
			$K=2/3$					$K=2/9$														
ss	0	0	0	0	−1	0	0	+12	−3	+2	−3	+12										
			$K=2/15$					$K=10/441$					$K=6/245$									
ds	±2	0	+4	0	0	0	0	−48	+18	−162	0	0	+4	−5	+10	−35	+280					
	±1	0	0	+1	0	0	0	−72	+3	−72	−18	0	+20	−16	+20	−40	+140					
	0	0	0	0	+2	0	0	−48	−3	−50	−3	−48	+60	−30	+24	−30	+60					
			$K=2/25$					$K=2/49$					$K=36/225$					$K=10/17787$				
pp	±1	±1	0	0	−8	0	0	+108	−12	+32	−12	+108	−10	+5	−4	+5	−10	+56	−35	+30	−35	+56
	±1	0	0	+1	0	0	0	−24	+1	−24	−6	0	+10	−8	+10	−20	+70	−140	+120	−140	+224	−504
	±1	∓1	−8	0	0	0	0	+32	−12	+108	0	0	−4	+5	−10	+35	−280	+180	−210	+336	−756	+2520
	0	0	0	0	−2	0	0	+12	−27	−2	−27	+12	+40	−20	+16	−20	+40	−140	+224	−504	+1680	−9240
			$K=2/441$					$K=50/441$					$K=6/5929$					+56	−35	+420	−2310	+27720
dd	±2	±2	0	0	−162	0	0	+48	−3	+18	−3	+48	−960	+270	−486	+270	−960	$K=10/17787$				
	±2	±1	0	+18	0	0	0	−12	0	−12	−5	0	+1080	−294	+1080	−375	+3360	−896	+560	−480	+560	−896
	±2	0	−48	0	0	0	0	+12	0	+18	0	0	−1024	+245	−1690	+35	−4480	+840	−720	+840	−1344	+3024
	±2	∓1	0	0	0	0	0	−12	−3	0	0	0	+1080	−375	+3360	+420	0	−480	+560	−896	+2016	−6720
	±2	∓2	0	0	0	0	0	+48	0	0	0	0	−960	+840	−10500	0	0	+2016	−1260	+1080	−1260	+2016
	±1	±1	0	0	−72	0	0	+12	−12	0	−12	+12	+1500	−30	+1176	−30	+1500					
	±1	0	0	+3	0	0	0	0	+3	0	0	0	−980	−4	−980	−490	−140					
	±1	∓1	−72	0	0	0	0	0	−12	+12	0	0	+1176	−30	+1500	+1890	−1680					
	0	0	0	0	−50	0	0	+12	−3	+2	−3	+12	−240	+480	−600	−480	−240					

$\beta^k(l'm_l', lm_l+f)$ for $l'+l$ odd

$l'l$	m_l'	m_l	$f=\pm2$	$k=1$ ±1	0	∓1	∓2	±2	$k=3$ ±1	0	∓1	∓2	±2	$k=5$ ±1	0	∓1	∓2
			$K=6/25$					$K=2/25$									
ps	±1	0	−8	+1	−8	0	0	+4	+3	+4	−10	+60					
	0	0	0	−1	−2	−1	0	+20	−8	+54	−8	+20					
			$K=6/245$					$K=2/45$					$K=2/441$				
dp	±2	±1	−108	+6	−108	0	0	+24	−8	+24	−15	+160	−12	+10	−12	+21	−56
	±2	0	+12	+6	0	0	0	−16	+3	−30	−5	0	+20	−24	+42	−112	+504
	±2	∓1	−108	0	0	0	0	+24	−15	+160	0	0	−12	+21	−56	+252	+2520
	±1	±1	0	−12	−24	−12	0	+60	−6	+32	−6	+60	−84	+48	−40	+48	−84
	±1	0	−24	+27	−24	0	0	−12	−1	−12	−30	+20	+96	−80	+96	−168	+448
	±1	∓1	−24	−12	0	0	0	+32	−6	+60	+10	0	−40	+48	−84	+224	−1008
	0	±1	0	0	−32	−1	−32	+60	0	+36	−3	+36	−336	+126	−72	+60	−72
	0	0	0	−1	−2	−1	0	0	−18	−6	−18	0	+252	−144	+120	−144	+252

Values of the β^k are given in Table III, in five columns labeled $f=+2$, etc., under each value of k. The combinations sp, sd, and pd can be calculated by a formula like that for the α^k.

When numerical values of the C^k, etc., are put into Eq. (2), the matrix components are obtained as polynomials in the radial integrals. These are reduced with the aid of Eqs. (10) to dependence on the elementary radial integrals ${}^3R^k$ and ${}^3D^k$. These integrals are independent if there are no relations among the four sets of electron parameters. This case occurs only in interactions between states in two different configurations.

Interaction integrals between electron states in the same configuration involve sets of parameters in which n^al^a and n^bl^b are identical with n^cl^c and n^dl^d, respectively. For such states it is convenient to write $M^k(ab)$ and $N^k(ab)$ in place of ${}^3R^k(ab, ab)$ and ${}^3R^k(ba, ab)$. It can be shown, by integrating the second of Eqs. (9) by parts, that

$$ {}^3D^k(ab, ab)=\tfrac{1}{2}(k+2)M^{k-1}(ab)+\tfrac{1}{2}(k+1)M^{k+1}(ab), $$

$$ {}^3D^k(ba, ab)=\tfrac{1}{2}(k+2)N^{k-1}(ab)+\tfrac{1}{2}(k+1)N^{k+1}(ab). $$

The matrix elements of mutual spin-orbit and spin-spin interaction between electron states in the same configuration reduce to polynomials in the M^k and N^k with numerical coefficients. These integrals resemble the F^k and G^k which appear in the theory of electrostatic interaction of electrons, but are much smaller in value.

Eigenfunctions of terms in LS coupling are constructed as linear combinations of those of the states A, B, etc., by the methods of Chapter VIII, TAS. Matrix components connecting these terms are calculated with the aid of Eq. (2).

The matrix components of mutual spin-orbit interaction for two-electron configurations of s, p, and d electrons are given in Table IV. The diagonal elements for ${}^3S_1$ and for all singlet terms are zero. The diagonal elements for the terms of each triplet are in accord with the Landé interval rule. Their values for terms with J equal to $L+1$, L and $L-1$ are in the ratio $-L:1:L+1$. Only the non-diagonal elements that are not zero, and the diagonal elements for triplet terms with J equal to L are listed.

The matrix components of spin-spin interaction for the same configurations are given in Table V. The diagonal elements of triplet terms with J equal to $L+1$, L and $L-1$ are in the ratio $-L/(2L+3):1:-(L+1)/(2L-1)$, as in the formula for sl triplets derived by Inglis.[1] The

TABLE IV. Matrix components of $H_m{}^l$.

ps

${}^3P_1, {}^3P_1=3M^0+2N^{-1}-N^1,$
${}^3P_1, {}^1P_1=(2)^{\frac{1}{2}}M^0.$

ds

${}^3D_2, {}^3D_2=3M_0+9N_0-6N_2,$
${}^3D_2, {}^1D_2=(6)^{\frac{1}{2}}M_0,$
where $M_0=M^0$, $N_0=N^0/5$, $N_2=N^2/5$.

pp

${}^1D_2, {}^3D_2=12(M_0-N_0),$
${}^3P_1, {}^3P_1=30(M_0+N_0),$
${}^1D_2, {}^3P_2=7(2)^{\frac{1}{2}}(M_0+N_0),$
${}^3D_1, {}^1P_1=-7(10/3)^{\frac{1}{2}}(M_0-N_0),$
${}^1P_1, {}^3S_1=5(2/3)^{\frac{1}{2}}(M_0-N_0),$
${}^3P_0, {}^1S_0=-5(2)^{\frac{1}{2}}(M_0+N_0),$
where $M_0=M^0/5$, $N_0=N_0/5$.

p²

${}^3P_1, {}^3P_1=30M_0,$
${}^1D_2, {}^3P_2=7(2)^{\frac{1}{2}}M_0,$
${}^3P_0, {}^1S_0=-5(2)^{\frac{1}{2}}M_0,$
where $M_0=M^0/5$.

dp

${}^3F_3, {}^3F_3=81M_0+6M_2+8N_{-1}-430N_1-3N_3,$
${}^3D_3, {}^3D_3=168M_0-42M_2-8N_{-1}+448N_1-42N_3,$
${}^3P_1, {}^3P_1=126M_0+126M_2+8N_{-1}+1190N_1-378N_3,$
${}^3F_3, {}^1F_3=(1/3)^{\frac{1}{2}}(62M_0+12M_2),$
${}^3F_3, {}^3D_3=(2)^{\frac{1}{2}}(24M_0+24M_2+8N_{-1}+344N_1-48N_3),$
${}^1F_3, {}^3D_3=(2/3)^{\frac{1}{2}}(107M_0+12M_2+567N_1),$
${}^3F_2, {}^3D_2=(7/5)^{\frac{1}{2}}(24M_0+24M_2+8N_{-1}+344N_1-48N_3),$
${}^3F_2, {}^1D_2=-(14/15)^{\frac{1}{2}}(107M_0+12M_2-567N_1),$
${}^3D_2, {}^1D_2=(2/3)^{\frac{1}{2}}(98M_0-42M_2),$
${}^3D_3, {}^3P_2=-(27/5)^{\frac{1}{2}}(42M_0+42M_2+4N_{-1}+322N_1+126N_3),$
${}^1D_2, {}^3P_2=(18/5)^{\frac{1}{2}}(21M_0-14M_2+49N_1),$
${}^3D_1, {}^3P_1=-(3)^{\frac{1}{2}}(42M_0+42M_2+4N_{-1}+322N_1+126N_3),$
${}^3D_1, {}^1P_1=-(6)^{\frac{1}{2}}(21M_0-14M_2-49N_1),$
${}^3P_1, {}^1P_1=(2)^{\frac{1}{2}}(42M_0+42M_2),$
where $M_0=M^0/35$, $M_2=M^2/35$, $N_{-1}=N^{-1}/5$, $N_1=N^1/245$, and $N_3=N^3/245$.

dd

${}^3G_4, {}^3G_4=15(M_0-N_0)+15(M_2-N_2),$
${}^3F_3, {}^3F_3=27(M_0+N_0)-51(M_2+N_2),$
${}^3D_2, {}^3D_2=36(M_0-N_0)-48(M_2-N_2),$
${}^3P_1, {}^3P_1=42(M_0+N_0)+504(M_2+N_2),$
${}^1G_4, {}^3F_4=(1/7)[154(M_0+N_0)+260(M_2+N_2)],$
${}^3G_3, {}^1F_3=-(1/7)^{\frac{1}{2}}[66(M_0-N_0)+116(M_2-N_2)],$
${}^1F_3, {}^3D_3=(3/7)^{\frac{1}{2}}[30(M_0-N_0)-142(M_2-N_2)],$
${}^3F_2, {}^1D_2=-(15/49)^{\frac{1}{2}}[42(M_0+N_0)-314(M_2+N_2)],$
${}^1D_2, {}^3P_2=(10/21)^{\frac{1}{2}}[21(M_0+N_0)+100(M_2+N_2)],$
${}^3D_1, {}^1P_1=-(2/7)^{\frac{1}{2}}[35(M_0-N_0)+156(M_2-N_2)],$
${}^1P_1, {}^3S_1=(2)^{\frac{1}{2}}[7(M_0-N_0)+6(M_2-N_2)],$
${}^3P_0, {}^1S_0=-(2/3)^{\frac{1}{2}}[21(M_0+N_0)+34(M_2+N_2)],$
where $M_0=M^0/7$, $M_2=M^2/49$, $N_0=N^0/7$, and $N_2=N^2/49$.

d²

${}^3F_3, {}^3F_3=27M_0-51M_2,$
${}^3P_1, {}^3P_1=42M_0+504M_2,$
${}^1G_4, {}^3F_4=(1/7)(154M_0+260M_2),$
${}^3F_2, {}^1D_2=-(15/49)^{\frac{1}{2}}(42M_0-314M_2),$
${}^1D_2, {}^3P_2=(10/21)^{\frac{1}{2}}(21M_0+100M_2),$
${}^3P_0, {}^1S_0=-(2/3)^{\frac{1}{2}}(21M_0+34M_2),$
where $M_0=M^0/7$ and $M_2=M^2/49$.

TABLE V. Matrix components of H_m^{II}.

	ps
$^3P_1, {}^3P_1$	$=-2M^0$.
	ds
$^3D_2, {}^3D_2$	$=-2M_0$.
	pp
$^3D_2, {}^3D_2$	$=-14(M_0-N_0)$,
$^3P_1, {}^3P_1$	$=10(M_0+N_0)$,
$^3D_1, {}^3S_1$	$=(320)^{\frac{1}{2}}(M_0-N_0)$.
	p^2
$^3P_1, {}^3P_1$	$=10M_0$.
	dp
$^3F_3, {}^3F_3$	$=-102M_0-12M_2+504N_1$,
$^3D_2, {}^3D_2$	$=14M_0+84M_2+882N_1$,
$^3P_1, {}^3P_1$	$=-42M_0-252M_2+294N_1$,
$^3F_3, {}^3D_3$	$=(2)^{\frac{1}{2}}(8M_0-12M_2-252N_1)$,
$^3F_2, {}^3D_2$	$=-(7/5)^{\frac{1}{2}}(16M_0-24M_2-504N_1)$,
$^3F_2, {}^3P_2$	$=(21/25)^{\frac{1}{2}}(104M_0+24M_2-1568N_1)$,
$^3D_2, {}^3P_2$	$=-(3/5)^{\frac{1}{2}}(56M_0-84M_2+196N_1)$,
$^3D_1, {}^3P_1$	$=(3)^{\frac{1}{2}}(56M_0-84M_2+196N_1)$.
	dd
$^3G_4, {}^3G_4$	$=-22(M_0-N_0)-44(M_2-N_2)$,
$^3F_3, {}^3F_3$	$=-6(M_0+N_0)+228(M_2+N_2)$,
$^3D_2, {}^3D_2$	$=6(M_0-N_0)-408(M_2-N_2)$,
$^3P_1, {}^3P_1$	$=14(M_0+N_0)+168(M_2+N_2)$,
$^3G_3, {}^3D_3$	$=(3/49)^{\frac{1}{2}}[48(M_0-N_0)+376(M_2-N_2)]$,
$^3F_2, {}^3P_2$	$=(14/25)^{\frac{1}{2}}[24(M_0+N_0)-312(M_2+N_2)]$,
$^3D_1, {}^3S_1$	$=(7)^{\frac{1}{2}}[8(M_0-N_0)+96(M_2-N_2)]$.
	d^2
$^3F_3, {}^3F_3$	$=-6M_0+228M_2$,
$^3P_1, {}^3P_1$	$=14M_0+168M_2$,
$^3F_2, {}^3P_2$	$=(14/25)^{\frac{1}{2}}(24M_0-312M_2)$.

diagonal elements for $^3S_1$ and for all singlet terms are zero. Only the non-diagonal elements that are not zero, and the diagonal elements for triplet terms with J equal to L are listed. The radial parameters are identical with those in Table IV.

It is apparent from its form that $M^0(ab)$ is smaller than the individual spin-orbit parameter of each electron, and that its relative value diminishes as the effective nuclear charge increases. The other M^k and N^k, with the exception of N^{-1}, are smaller than M^0.

The mutual spin-orbit interaction diminishes the triplet intervals in two-electron configurations, acting counter to the individual spin-orbit interactions. The spin-spin interaction distorts the triplets with respect to the Landé interval rule, even in configurations that are very near to LS coupling. These effects are likely to be most striking in the spectra of elements of small atomic number and in high level configurations in which the closed electron shells screen the nucleus most effectively. It is well known that the HeI triplets are actually inverted and greatly distorted.

The total number of radial integrals encountered in the theory of electrostatic, spin-orbit, and mutual magnetic interaction is smaller than the number of energy levels, in the configurations of p and d electrons. We may continue with some profit to treat the radial integrals as independent undetermined parameters which are to be adjusted to bring the theoretical energy levels near to the empirical values.

The formulae for the four energy levels of an sl configuration contain six radial integrals, when all types of electron interaction are included. These, regarded as independent parameters, are in excess of the number required to fit the formulae exactly to the empirical energy levels. The next step to be taken is to evaluate the integrals, all of which depend on the effective nuclear numbers Z_a and Z_b for the electrons. These two numbers are actually the parameters for the configuration.

Excitation of Molecular Vibrations by Electrons

TA-YOU WU
Department of Physics, National University of Peking, Kunming, China
(Received October 14, 1946)

The cross section for the excitation of molecular vibration by electron impact is calculated for two cases: (1) On the assumption that a molecule interacts with an electron through the oscillating electric moment arising from the vibration, the cross sections of excitation and deexcitation are of the order $y^2 \cdot 10^{-15}$ cm^2 where $y \cdot 10^{-18}$ c.g.s. unit is the matrix element of the electric moment associated with the vibrational transition. (2) For optically inactive vibration, an approximate estimate of the cross section in the case of the H_2 molecule is made by the method of distorted wave. The cross section is of the order $0.5 \cdot 10^{-18}$ cm^2 for electrons of a few volts. These results are compared with the experimental results on the probability of electron energy transfer to molecular vibrations.

FROM many experiments on the energy loss of electrons in passing through a gas, there seems to be evidence for a considerable probability for the exchange of energy between an electron and the vibrational motion of a molecule.[1-3] Thus it was found by Harries that about 1 percent of the collisions of 5.2-volt electrons with nitrogen molecules results in the excitation of one vibrational quantum, while for carbon monoxide it is 3.3 percent.[1] Ramien found that about 2 percent of the collisions of 7-volt electrons with hydrogen molecules result in the excitation of one vibrational quantum.[2] While the theoretical method for the calculation of the probability of such energy transfers is well developed, no calculation seems to have been carried out. In an early paper, Massey has treated the problem of elastic scattering of fast electrons by H_2 molecules by Born's method,[4] and in a later paper the same author has calculated the cross section of the excitation of the rotational state of a symmetrical top having a permanent electric moment $\mathfrak{M}=x \cdot 10^{-18}$ c.g.s. unit.[5] It was found that this cross section is of the order $x^2 \cdot 10^{-15}$ cm^2 for slow electrons. The result, however, is valid only when $\mathfrak{M} \ll h^2/8\pi^2 me$ or $x \ll 1$, a condition not met by most actual molecules. The purpose of the present work is to make some estimates of the probabilities of excitation of molecular vibrations by electrons.

I. EXCITATION OF OPTICALLY ACTIVE VIBRATION

To calculate the probability of energy transfer between the vibration-rotational motion of a molecule and an electron, it is necessary to know the law of interaction between them. A rigorous theory should consider the interactions between the electron and the nuclei and electrons in the molecule; but such a theory would involve very complicated, if not unmanageable, calculations. As an approximation, we shall, following Massey, replace the actual molecular field by one which is caused by the electric moment of the molecule. On this assumption, the interaction may be regarded as the sum of two parts, namely, the interaction between the electron and the permanent moment, and the interaction between the electron and the electric moment due to the vibration of the molecule. The Hamiltonian of the system: molecule+electron is, on neglecting the coupling between vibration and rotation,

$$H=H_v(X_1, X_2, \cdots)+H_r(\vartheta, \chi, \varphi)+H_e(R, \Theta, \Phi) + V(X_1, X_2, \cdots, \vartheta, \chi, \varphi, R, \Theta, \Phi),$$

where the X's are proportional to the normal coordinates of vibration, ϑ, χ, φ the Eulerian angles defining the orientation of the molecule, and R, Θ, Φ the polar coordinates of the electron. For definiteness, consider a symmetrical rotator and let χ be the angle defining rotation about the figure axis. If the molecule has a permanent moment $\mathfrak{M}$ along the figure axis and if we confine

[1] W. Harries, Zeits. f. Physik **42**, 26 (1927).
[2] Ramien, Zeits. f. Physik **70**, 353 (1931).
[3] For references to the work of Bailey and others, see Mott and Massey, *Theory of Atomic Collisions* (Oxford University Press, New York, 1933), p. 217.
[4] H. S. W. Massey, Proc. Roy. Soc. **A129**, 616 (1930).
[5] H. S. W. Massey, Proc. Camb. Phil. Soc. **28**, 99 (1932).

ourselves to the excitation of a parallel vibration X_i, i.e., a vibration whose change of electric moment A_iX_i is along the figure axis, we have

$$\left.\begin{aligned} V&=V^I+V^{II},\\ \text{where}\quad V^I&=\frac{\mathfrak{M}e}{R^2}\{\cos\vartheta\cos\Theta+\sin\vartheta\sin\Theta\cos(\varphi-\Phi)\},\\ V^{II}&=\sum_i V_i^{II}=\sum_i\frac{A_iX_ie}{R^2}\{\cos\vartheta\cos\Theta\\ &\qquad+\sin\vartheta\sin\Theta\cos(\varphi-\Phi)\}.\end{aligned}\right\}\quad(1)$$

This assumed form for the interaction V may perhaps be justifiable for large distance R but certainly becomes inadequate for close approach between the electron and the molecule.

The Schrödinger equation

$$H\Psi(X_1, X_2, \cdots, \vartheta, \chi, \varphi, R, \Theta, \Phi)=E\Psi \qquad (2)$$

can be solved by the usual method of expressing Ψ as a sum of products of the vibrational, rotational, and the electronic wave functions

$$\Psi=\sum_{v_1v_2\cdots JKM}\psi_{v_1v_2\cdots}(X_1, X_2, \cdots)\cdot\psi_{JKM}(\vartheta, \chi, \varphi)\cdot F_{v_1v_2\cdots JKM}(R, \Theta, \Phi), \qquad (3)$$

where the v's are the vibrational quantum numbers and $\psi_{v_1v_2}(X_1, X_2, \cdots)$ is the solution of

$$H_v\psi_{v_1v_2\cdots}(X_1, X_2, \cdots)=E_v\psi_{v_1v_2\cdots}, \qquad (4)$$

where E_v is the energy of vibration of the molecule. $\psi_{v_1v_2\cdots}(X_1, X_2, \cdots)$ is the product of the wave functions $\psi_{v_i}(X_i)$ of the normal vibrations. $\psi_{JKM}(\vartheta, \chi, \varphi)$ is the solution of the equation of a symmetrical top

$$H_r\psi_{JKM}(\vartheta, \chi, \varphi)=E_{JKM}\psi_{JKM} \qquad (5)$$

where

$$E_{JKM}=\frac{h^2}{8\pi^2A}\left\{J(J+1)-\left(\frac{A}{C}-1\right)K^2\right\}.$$

On substituting (3) into (2) and making use of (4) and (5), one obtains the following equations for the $F_{v_1v_2\cdots JKM}(R, \Theta, \Phi)$

$$\left[\nabla^2+\frac{8\pi^2m}{h^2}(E-E_v-E_{JKM})\right]F_{v_1v_2\cdots JKM}(R, \Theta, \Phi)=\sum_{v_1'v_2'\cdots J'K'M'}\frac{8\pi^2m}{h^2}V(v_1v_2\cdots JKM; v_1'v_2'\cdots J'K'M')\cdot F_{v_1'v_2'\cdots J'K'M'}(R, \Theta, \Phi) \qquad (6)$$

where

$$V(v_1'v_2'\cdots, J'K'M'; v_1v_2\cdots, JKM)=\int\overset{*}{\psi}_{v_1'v_2'\cdots}\overset{*}{\psi}_{J'K'M}(V^I+V^{II})\psi_{v_1v_2\cdots}\times\psi_{JKM}dX_1\cdots dX_nd\cos\vartheta d\chi d\varphi.$$

Now on account of the properties of the functions $\psi_{v_1v_2\cdots}(X_1, X_2, \cdots)$ and $\psi_{JKM}(\vartheta, \chi, \varphi)$, the matrix element $V^I(v_1'v_2'\cdots, J'K'M'; v_1v_2\cdots, JKM)$ vanishes unless $v_1'=v_1$, $v_2'=v_2$, $\cdots v_n'=v_n$, $J'-J=0, \pm1$, $K'=K$, $M'-M=0, \pm1$. The matrix element $V^{II}(v_1'v_2'\cdots, J'K'M'; v_1v_2\cdots, JKM)$ vanishes unless one, and only one, of the v_1', v_2', $\cdots v_n'$, say v_i', differs from v_i by ±1, and $J'-J=0, \pm1$, $K'-K=0$, $M'-M=0, \pm1$. In the following, we shall denote by v_i the vibrational state $v_1=0$, $v_2=0$, $\cdots v_{i-1}=0$, $v_i=v_i$, $v_{i+1}=0$, $\cdots$, $v_n=0$, and write

$$V(1_i, J'K'M'; 0_i, JKM)=V(0, 0, \cdots, 1_i, 0, \cdots, J'K'M'; 0, 0, \cdots 0_i, \cdots 0, JKM),$$

$$k_{v_iJKM}^2=(h^2/8\pi^2m)(E-E_{v_i}-E_{JKM}).$$

The system of Eqs. (6) becomes

$$[\nabla^2+k_{0_i000}^2]F_{0_i000}=\frac{8\pi^2m}{h^2}[V^I(0_i000; 0_i100)F_{0_i100}+V^I(0_i000; 0_i101)F_{0_i101}+V^I(0_i000; 0_i10-1)F_{0_i10-1}+\sum_j\{V_i^{II}(0_i000; 1_j100)F_{1_j100}+V_i^{II}(0_i000; 1_j101)F_{1_j101}+V_j^{II}(0_i000; 1_j10-1)F_{1_j10-1}\}],$$

$$[\nabla^2+k^2_{0_i100}]F_{0_i100}=\frac{8\pi^2m}{h^2}[V^I(0_i100;\,0_i000)F_{0_i000}+V^I(0_i100;\,0_i200)F_{0_i200}$$
$$+V^{II}(0_i100;\,0201)F_{0_i201}+V^{II}(0_i100;\,0_i20-1)F_{0_i20-1}$$
$$+\sum_j\{V_j^{II}(0_i100;\,1_j000)F_{1_j000}+V_j^{II}(0_i100;\,1_j200)F_{1_j200}$$
$$+V_j^{II}(0_i100;\,1_j201)F_{1_j201}+V_j^{II}(0_i100;\,1_j20-1)F_{1_j20-1}\}],$$
$$\cdots\cdots\cdots

expression

$$Q_{1_i100}(k)=\frac{2\pi\beta_i^2}{3}\cdot\frac{1}{k^2}\ln\frac{k+k_{1100}}{k-k_{1100}} \tag{10}$$

as a function of the initial kinetic energy $E=h^2k^2/8\pi^2m$ of the electron.

For the de-excitation or quenching process $(1_i, 100)\rightarrow(0_i, 000)$, we represent the incoming electron by a plane wave $F_{1_i100}=\exp(ikn\cdot R)$ and calculate F_{0_i000} in (7). The cross section can be shown to be

$$Q_{0_i000}(k)=\frac{2\pi\beta_i^2}{3}\cdot\frac{1}{k^2}\ln\frac{k_1+k}{k_1-k} \tag{11}$$

where $(h^2/8^2\pi^2m)(k_1^2-k^2)=\epsilon$ is the energy transferred to the electron. It is seen that $Q_{1_i100}(k)$ and $Q_{0_i000}(k)$ satisfy the relation

$$e^{-\epsilon/kT}\int_0^\infty vQ_{0_i000}(v)\cdot f(v)dv=\int_{(2\epsilon/m)^{\frac{1}{2}}}^\infty vQ_{1_i100}(v)\cdot f(v)dv,$$

as required by the principle of detailed balancing. v is the velocity of the electron and $f(v)$ is the Maxwell velocity distribution function.

For the excitation process $v_i, J, K, M\rightarrow v_i+1, J+1, K, M$, a little consideration shows that the same expression (10) holds, except for a numerical factor of the order unity. The cross section for the excitation of the vibrational state alone would be of the order $\alpha^2\beta_i^2$ times $Q_{1_i100}(k)$. This is rather a consequence of the special form (1) which we have assumed for the interaction V, and perhaps not much weight should be attached to it.

For a linear molecule, a little calculation shows that entirely similar results hold. Thus for the simultaneous excitation of a parallel active vibration and rotation $v, J, M=0, 0, 0\rightarrow 1, 1, 0$, the total cross section is given by (10) with the subscripts 1_i100 replaced by

$$v_i, J, M=1_i, 1, 0.$$

In Fig. 1, Q_{1_i100} and Q_{0_i000} are plotted as functions of the initial kinetic energy of the electron in units of $y^2\cdot10^{-15}$ cm^2 for a vibration-rotational transition for which the energy transfer is 0.1 volt, corresponding to a frequency of ~800 cm^{-1}. For a vibration with $A_iX_i(0, 1)\sim0.1\times10^{-18}$ c.g.s. unit, the cross sections are of the order 10^{-17} cm^2 for slow electrons.

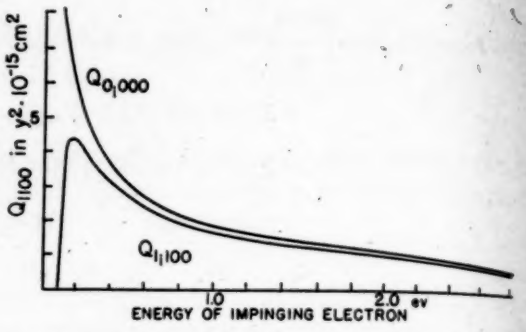

FIG. 1. Cross sections as functions of the energy of impinging electron.

A few words may be said concerning the validity of (10). For molecules having no permanent moment such as CO_2, CS_2, C_2H_2, C_3O_2, CH_4, CCl_4, etc., $V^I=0$ and the condition for the validity of (10) is $\beta_i\ll1$ or $A_iX_i(0, 1)\ll10^{-18}$. From absorption coefficient and infra-red dispersion measurements for such molecules as CO_2, estimates of the effective charge in the relation $A_iX_i(0, 1)=$effective charge$\times$change in nuclear distances lead to values which are of the order of one electronic charge.[6] As the change in nuclear distances is small compared with the interatomic distances and hence $\ll10^{-8}$ cm, it follows that $A_iX_i(1, 0)\ll10^{-18}$, although accurate values for $A_iX_i(1, 0)$ are not readily available.

For molecules with a permanent electric moment, the condition for the validity of (10) is seen from (9) to be $y\ll1$ and $x^2\sim y$. Thus (10) will be a good approximation when applied to CO for which $x=0.11$. As the gas kinetic cross section for electrons in CO is $\sim3\times10^{-16}$ cm^2, Harries'[1] observation mentioned before would lead to a value $\sim1\times10^{-17}$ for Q_{110}. On the assumption (1), this value of Q_{110} would correspond to a value 0.1×10^{-18} for the change of the electric moment due to the vibration of CO. This value is entirely reasonable, although it must be pointed out that the assumption (1) fails to account for the observed excitation of vibration of such molecules as H_2 and N_2, since for optically inactive vibrations, the above theory would predict zero cross section. In dealing with these cases, the assumed form (1) for V is obviously inadequate. Also, for most molecules,

[6] Cf. J. H. Van Vleck, *Quantum Theory of Electric and Magnetic Susceptibilities* (Oxford University Press, New York, 1931), §15.

x is of the order unity and the approximation made in obtaining (10) can no longer be justified.

II. EXCITATION OF OPTICALLY INACTIVE VIBRATION

In treating the problem without the assumption (1), it is necessary to solve the Schrödinger equation of the electron in the field of the nuclei and the electrons of the molecule. It is at once obvious that the mathematical calculations involved would be very lengthy even for the simplest of molecules, namely, hydrogen. In the following, we shall make some rough estimates in the case of hydrogen. It is reasonable to suppose that for other molecules, the essential feature is the same and results of similar order of magnitude would be obtained, although there is a great difference in mathematical complexity.

Let us denote the coordinates of the impinging electron by the subscript 1 and those of the molecular electrons by 2 and 3. Let r, p be the distances of an electron from the nuclei a and b, ρ be the nuclear separation, and ϑ, φ be the polar angles of the line of nuclei. The Hamiltonian of the system: molecule+electron is

$$H=H_e(r_2, p_2, r_3, p_3)+H_v(\rho)+H_r(\vartheta, \varphi) +H(r_1)+V(r_1, p_1, r_{12}, r_{13})$$

where H_e is the Hamiltonian of the molecular electrons in the field of the fixed nuclei; $H_v(\rho)$ is the Hamiltonian corresponding to the vibrational motion of the nuclei; $H_r(\vartheta, \varphi)$ is the Hamiltonian of the rotational motion of the molecule; $H(r_1)$ is the kinetic energy part of the impinging electron, and V is the interaction

$$V=e^2\left(-\frac{1}{r_1}-\frac{1}{\rho_1}+\frac{1}{r_{12}}+\frac{1}{r_{13}}\right). \tag{12}$$

The solution of the equation

$$(H_e+H_v+H_r)\Psi^0=E^0\Psi^0$$

may be approximated by

$$\Psi^0(r_2, p_2, r_3, p_3, \rho, \vartheta, \varphi) =\psi_n(r_2, p_2, r_3, p_3)\cdot\psi_v(\rho)\cdot\psi_{JM}(\vartheta, \varphi)$$

where $\psi_{JM}(\vartheta, \varphi)$ is the rotational wave function of a linear molecule; $\psi_v(\rho)$ the vibrational wave function; and ψ_n is the electronic wave function containing the nuclear distance ρ as a parameter. For the normal $^1\Sigma$ state, ψ_n can be taken to be that given by Wang

$$\psi_0=C^2\exp[-\tfrac{1}{2}\mu(r_2+p_3)]+\exp[-\tfrac{1}{2}\mu(r_3+p_2)],$$
$$C=(\tfrac{1}{2}\mu)^6[2\pi(1+S)]^{-1},$$
$$S=(1+\tfrac{1}{2}\mu\rho+\mu^2\rho^2/12)^2e^{-\mu\rho},$$
$$\mu=2Z/a_0, \quad Z=1.166.$$

To solve the equation

$$(H_e+H_v+H_r+H(r_1)+V)\Psi=E\Psi,$$

we proceed by the usual method of expressing Ψ as a sum of products

$$\Psi=\sum_{nvJM}\psi_n(r_2, p_2, r_3, p_3) \cdot\psi_v(\rho)\cdot\psi_{JM}(\vartheta, \varphi)\cdot F_{nvJM}(r_1), \tag{13}$$

the sum being taken over all the electronic, vibrational, and rotational states n, v, JM. On writing

$$k^2_{nvJM}=(8\pi^2m/h^2)(E-E_n-E_v-E_{JM}), \tag{14}$$

the equations for the $F_{nvJM}(r_1)$ are

$$[\nabla^2+k^2_{nvJM}]F_{nvJM}(r_1)=(8\pi^2m/h^2) \sum_{n'v'J'M'}V(n'v'J'M'; nvJM)(r_1)\cdot F_{n'v'J'M'} \tag{15}$$

where

$$V(n', v', J'M'; n, v, JM)=\int\psi_{n'}^*\psi_{v'}^*\psi_{J'M'}^* \times V\psi_n\psi_v\psi_{JM}dr_2dr_3d\rho d\cos\vartheta d\varphi.$$

The equation for F_{0000} is, for example,

$$[\nabla^2+k^2_{0000}]F_{0000}(r_1)=(8\pi^2m/h^2) \times[V(0000; 0000)(r_1)\cdot F_{0000}(r_1) +V(0000; 0010)(r_1)F_{0010}(r_1)+\cdots +V(0000; 0100)(r_1)F_{0100}(r_1) +V(0000; 1000)(r_1)F_{1000}(r_1)+\cdots] \tag{16}$$

where the F_{0010}, F_{0100}, etc., are given by similar equations. The possibility of solving this system

of equations by successive approximation depends on the smallness of certain matrix elements of V compared with others. Consider first

$$V_1=\int\psi_0^*(r_2p_2r_3p_3)\,V\psi_0(r_2p_2r_3p_3)dr_2dr_3$$

$$=-\frac{e^2}{1+S}\left\{\frac{e^{-\mu r_1}}{r_1}\left(1+\frac{\mu r_1}{2}\right)+\frac{e^{-\mu p_1}}{p_1}\left(1+\frac{\mu p_1}{2}\right)\right\}$$

$$-\frac{16\pi e^2C^2\sqrt{S}}{\mu^3}\int\left(\frac{1}{r_1}+\frac{1}{p_1}-\frac{2}{r_{12}}\right)$$

$$\times e^{-\mu(r_2+p_2)/2}dr_2. \quad (17)$$

Evaluation of the integral on the right leads to a very lengthy function in r_1 and p_1. Reference to Massey's work shows that the contribution of this term to the elastic scattering cross section is small in the limiting cases of fast electrons and of zero scattering angle.[4] For the purpose of making a rough estimate only, we shall neglect this term in the following.

For matrix elements of V with respect to the normal and an excited electronic state, general considerations lead one to expect

$$V(0, v, JM; n, v, JM)$$

$$\ll V(0, v, JM; 0, v, JM). \quad (18)$$

To calculate the matrix elements of V with respect to the rotational states

$$V_2=V(0, J'M'; 0, JM)$$

$$=\int\psi^*_{J'M'}(\vartheta, \varphi)\,V_1\psi_{JM}(\vartheta, \varphi)d\cos\vartheta d\varphi, \quad (19)$$

let us take the direction of the impinging electron as the polar axis of the angles ϑ and φ so that

$$r_1^2=r^2+(\tfrac{1}{2}\rho)^2+r\rho\cos\vartheta,$$
$$p_1^2=r^2+(\tfrac{1}{2}\rho)^2-r\rho\cos\vartheta, \quad (20)$$

where r is the distance of the colliding electron from the center of the molecule. Since V_1 does not depend on φ, and since the transformation of ϑ into $\pi-\vartheta$ leaves V_1 unchanged, it follows that

$$V_2(0, J'M'; 0, JM)=0 \text{ unless } M'=M$$

and

$$J'-1=0,\ \pm2,\ \pm4,\ \cdots. \quad (21)$$

Integration over ϑ in (19), when V_2 does not vanish, will be very complicated on account of the dependence of r_1 and p_1 on ϑ in (20); but again as an approximation, we shall replace this averaging of V_1 over all orientations of the molecule by taking a central field

$$V_2(0, 00; 0, 00)=-\frac{2e^2}{1+S}\frac{e^{-\mu r}}{r}\left(1+\frac{\mu r}{2}\right). \quad (22)$$

Finally, consider the matrix element

$$V(n', v', J'M'; n, v, J, M)$$

appearing in (15). On writing $\rho=\rho_0+\xi$ where $\xi/\rho_0\ll1$, one has

$$V_2(\rho)=V_2(\rho_0)+\left(\frac{\partial V_2}{\partial\rho}\right)_{\rho_0}\xi+\cdots$$

so that

$$V(0, 1, 00; 0, 0, 00)$$

$$=\rho_0\left(\frac{\partial V_2}{\partial\rho}\right)_{\rho_0}\cdot\int\psi_1^*(\xi)\frac{\xi}{\rho_0}\psi_0(\xi)d\xi$$

$$=\rho_0\left(\frac{\partial V_2}{\partial\rho}\right)_{\rho_0}\cdot\frac{1}{\rho_0}\left(\frac{h}{4\pi^2M\nu}\right)^{\frac{1}{2}}.$$

Now for hydrogen, $\rho_0=0.75\times10^{-8}$ cm, $\nu=4270$ cm^{-1} so that

$$\rho_0\left(\frac{\partial V_2}{\partial\rho}\right)_{\rho_0}=0.42\,V(0, 0, 00; 0, 0, 00),$$

$$\frac{1}{\rho_0}\left(\frac{h}{4\pi^2M\nu}\right)^{\frac{1}{2}}=1/9$$

and

$$V(0, 1, 00; 0, 0, 00)\simeq0.05\,V(0, 0, 00; 0, 0, 00). \quad (23)$$

In general,

$$V(n, v', JM; n, v, LM)$$
$$\ll V(n, v, JM; n, v, JM), \quad v'\neq v. \quad (24)$$

On considerations of (18), (21) and (24), we need only consider terms containing F_{0000}, F_{0020}, F_{0042}, etc., in (16). The term

$$V(0, 0, 00; 0, 0, 00)F_{0000}$$

represents the distortion of the electron wave by the molecular field, while the terms in F_{0020}, F_{0040}, etc., represent the effect of the inelastically

scattered waves on the elastically scattered wave. As a further approximation, we shall neglect the latter effect and (16) becomes

$$[\nabla^2+k_{0000}^2]F_{0000}(r)=(8\pi^2m/h^2)\times V(0,0,00;0,0,00)(r)F_{0000}(r). \quad (25)$$

The equation for $F_{0100}(r)$ is

$$[\nabla^2+k_{0100}^2]F_{0100}(r)=(8\pi^2m/h^2)\times[V(0,1,00;0,0,00)F_{0000}(r)+V(0,1,00;0,1,00)F_{0,1,00}(r)+\cdots] \quad (26)$$

in which we have neglected again terms containing $V(0,1,00;0,1,J0)$ where $J=2,4,6,\cdots$. The method of solving these equations is well known.[7] Thus

$$F_{0000}(r)=\sum_{n=0}^{\infty}(2n+1)i^ne^{i\eta_n}L_n(r)P_n(\cos\vartheta) \quad (27)$$

where $L_n(r)$ is that solution of

$$\frac{1}{r^2}\frac{d}{dr}\left(r^2\frac{dLn}{dr}\right)+\left[k_{0000}^2-\frac{8\pi^2m}{h^2}\times V(0,0,00;0,0,000)(r)-\frac{n(n+1)}{r^2}\right]L_n=0 \quad (28)$$

which is finite at the origin, and η_n is determined by $V(0,0,00;0,0,00)$ and k^2 and is given approximately by

$$\eta_n=-\frac{4\pi^3m}{h^2}\int_0^{\infty}V(0,0,00;0,0,00)(r)\times\left(\frac{2kr}{\pi}\right)^{\frac{1}{2}}L_n(r)J_{n+\frac{1}{2}}(kr)rdr \quad (29)$$

$$\simeq-\frac{4\pi^3m}{h^2}\int_0^{\infty}V(0,0,00;0,0,00)(r)\times[J_{n+\frac{1}{2}}(kr)]^2rdr$$

which is valid if η_n is small. Calculation gives

$$\eta_0=\frac{4\pi^2me^2}{h^2(1+S)k}\left\{\ln\left[1+\left(\frac{2k}{\mu}\right)^2\right]+\frac{1}{1+(\mu/2k)^2}\right\}, \quad (30)$$

and for electron energy of 2.5, 5, 10 volts,

$$\eta_0=0.43,\ 0.53,\ 0.65,$$

respectively. For these low energies, η_1 is negligibly small.

The solution of (26), which can be put, on account of (23) and the expansion of V_2 about ρ_0 given before, in the form

$$[\nabla^2+k_{0100}^2-(8\pi^2m/h^2)V(0,0,00;0,0,00)]F_{0100}(r)=(8\pi^2m/h^2)0.05\,V(0,0,00;0,0,00)F_{0000}(r), \quad (31)$$

has the asymptotic form

$$F_{0100}(r)\sim\frac{0.05\times2\pi m}{h^2}\cdot\frac{e^{ik_{0100}r}}{r}\int\mathfrak{F}(r',\pi-\Theta)\cdot V(0,0,00;0,0,00)(r')F_{0000}(r')dr' \quad (32)$$

where

$$\mathfrak{F}(r,\vartheta)=\sum_{l=0}^{\infty}(2l+1)i^le^{i\zeta_l}\mathfrak{L}_l(r)P_l(\cos\vartheta) \quad (33)$$

is the solution of the homogeneous equation obtained from (31) by equating the left-hand side to zero, and

$$\cos\Theta=\cos\vartheta\cos\vartheta'+\sin\vartheta\sin\vartheta'\cos(\varphi-\varphi').$$

On carrying out the integration in (32), one obtains

$$F_{0100}(r)\sim\frac{e^{ik_{0100}r}}{r}\left[\frac{0.05\times2\pi m}{h^2}4\pi\sum_{n=r}^{\infty}(-1)^n(2n+1)\times e^{i(\eta_n+\zeta_n)}P_n(\cos\vartheta)\int_0^{\infty}V(0,0,00;0,0,00)(r')\times L_n(r')\mathfrak{L}_n(r')r'^2dr'\right].$$

As the η_n are small according to (29), the contribution to the cross section from these harmonics is small so that the differential cross section for the excitation of the vibrational state by one quantum is

$$\left|\frac{0.05\times8\pi^2m}{h^2}\int_0^{\infty}V(0,0,00;0,0,00)(r)\times L_0(r)\mathfrak{L}_0(r)r^2dr\right|^2.$$

Now for electrons of about 10 volts and vibra-

[7] Mott and Massey, reference 3, Chaps. II and VI.

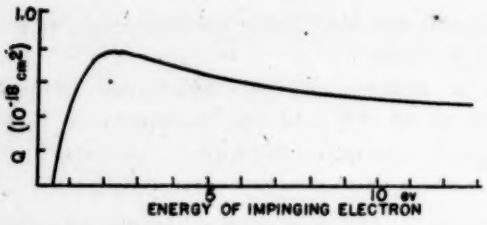

FIG. 2. Total cross section as a function of the energy of impinging electron.

tional quantum $h\nu \simeq 0.5$ volt, $k^2 \equiv k_{0000}^2 \simeq k_{0100}^2$ so that $L_0(r)\,\mathfrak{L}_0(r)$ can be replaced approximately by $|L_0(r)|^2$. By (29),

$$-\frac{8\pi^2 mk}{h^2}\int_0^\infty V(0,0,00;0,0,00)(r)L_0(r)\,\mathfrak{L}_0(r)r^2dr$$
$$\simeq -\frac{4\pi^2 m}{h^2}\int_0^\infty V(0,0,00;0,0,00)\times|J_1(kr)|^2 rdr=\eta_0(k).$$

The total cross section is then

$$Q_{0100}(k)=4\pi\left(\frac{0.05}{k}\right)^2\frac{k_{0100}}{k}\eta_0^2(k). \quad (34)$$

In Fig. 2, Q_{0100} is plotted against the energy of the impinging electron.

According to the calculated cross section, since the gas-kinetic cross section for electrons in H_2 is about 10^{-16} cm^2, one would expect about $\frac{1}{2}$ of a percent of the collisions between electrons of a few volts and H_2 to be inelastic, resulting in the excitation of one vibrational quantum. This is to be compared with the value ~ 2 percent found by Ramien for 7-volt electrons.[2] Considering the many simplifying approximations made in the calculation, one may perhaps feel that the calculation does give the correct order of magnitude for the cross section of such processes.

PHYSICAL REVIEW VOLUME 71, NUMBER 2 JANUARY 15, 1947

The Relation between the Force Constant and the Interatomic Distance of a Diatomic Linkage

II. A Modified Huggins Relation

C. K. WU AND S. C. CHAO
National University of Chekiang, Tsunyi, China
(Received October 14, 1946)

1. Huggins' relation between the force constant and the interatomic distance is modified so that the constants are now characteristic of the molecular period. 2. The new relation predicts the interatomic distance from the force constants of a diatomic linkage with an accuracy slightly better than Huggins' original relation. 3. Various aspects of the new relation are discussed.

HUGGINS[1] has shown that by assuming a modified Morse potential function for a diatomic linkage in the form

$$U=e^{-a(R-R_{12})}-C'e^{-a'(R-R_e)}, \quad (1)$$

he was able to obtain a relation between the interatomic distance R_e and the force constant K_e as

$$R_e=R_{12}-\frac{2.303}{a}\log\frac{K_e}{a^2-aa'}. \quad (2)$$

He then determined the constants a and R_{12} semi-emperically, so that for certain groups of molecules a is a group constant and R_{12} an

TABLE I. Values of A, B, and a for various molecular periods.

Molecular period	A in 10^8 cm^{-1}	B	Relation K_e in dynes/cm R_e in 10^{-8} cm	a in 10^8 cm^{-1}
00	−1.78	7.11	$\log K_e=-1.78R_e+7.11$	4.10
01	−1.356	7.17	$\log K_e=-1.356R_e+7.17$	3.12
02	−1.17	7.16	$\log K_e=-1.17R_e+7.16$	2.69
11	−1.83	8.28	$\log K_e=-1.83R_e+8.28$	4.21
12	−2.00	8.97	$\log K_e=-2.00R_e+8.97$	4.61
22	−1.10	7.71	$\log K_e=-1.10R_e+7.71$	2.53

[1] M. L. Huggins, J. Chem. Phys. 3, 473 (1935); 4, 308 (1936).

TABLE II. Values of R_e and R_{12}.

Period	Molecule	ω_e (cm^{-1})	R_e exp (10^{-8} cm)	R_e calc. (10^{-8} cm)	a (10^5 cm^{-1})	a' (10^5 cm^{-1})	R_{12} (10^{-8} cm)
00	H_2	2293	1.067	1.08	4.10	0.257	1.07
		2309	1.066	1.07	4.10	2.281	1.08
		2336.5	1.065	1.07	4.10	2.331	1.08
		2184	1.081	1.10	4.10	—	—
		2372	1.059	1.06	4.10	0.448	1.08
		2197	1.120	1.10	4.10	0.497	1.09
		2664.6	0.999	1.00	4.10	0.531	1.09
		2538	1.06	1.03	4.10	1.735	1.19
		2455	1.07	1.04	4.10	1.549	1.17
		2446.5	1.06	1.04	4.10	0.485	1.09
		1357	1.313	1.33	4.10	−0.715	1.02
		4371	0.749	0.77	4.10	1.521	1.17
01	LiH	1506	1.6	1.59	2.12	0.406	1.65
	BeH	1476	1.603	1.55	2.12	−0.011	1.61
		2220	1.310	1.29	2.12	1.316	1.78
	BeH	2088	1.330	1.33	2.12	1.318	1.78
		2058	1.340	1.35	2.12	1.106	1.75
		(2450)	1.213	1.22	2.12	—	—
		(2230)	1.226	1.28	2.12	−0.294	1.58
	CH	2675(ω_1)	1.13(γ_0)	1.16	2.12	—	—
		2800(ω_1)	1.20(γ_0)	1.14	2.12	—	—
		2851(ω_1)	1.13(γ_0)	1.13	2.12	—	—
	OH	3182	1.009	1.05	2.12	3.836	img.
		3568(ω_1)	0.969	0.974	2.12	—	—
	FH	4037	0.864	0.892	2.12	1.91	1.91
02	MgH	1138.4	2.008	1.96	2.69	−0.071	1.96
		1702.2	1.649	1.66	2.69	1.507	2.35
	HgH	(1700)	1.67	1.66	2.69	1.714	2.35
		1603	1.68	1.66	2.69	1.535	2.28
01	AlH	1681	1.644	1.67	2.69	1.143	2.18
	SiH	(2012)(ω_0)	1.527(γ_0)	1.54	2.69	—	—
	HCl^+	(2608)	1.313	1.34	2.69	0.673	2.07
	HCl	2990	1.272	1.24	2.69	2.455	2.87
11	Li_2	269.7	2.93	2.26	4.21	−0.776	1.64
		253.2	3.11	2.29	4.21	−1.017	1.63
		351.6	2.67	2.14	4.21	−0.805	1.64
	BeO	1371	1.358	1.35	4.21	0.913	1.74
		1128	1.468	1.45	4.21	1.071	1.75
		1487	1.327	1.32	4.21	1.840	1.82
	CC	1832	1.251	1.21	4.21	6.152	img.
		1793	1.261	1.22	4.21	3.572	2.13
		1603	1.315	1.27	4.21	2.040	1.84
		1642	1.308	1.26	4.21	1.943	1.83
	CF	1173	1.390	1.42	4.21	1.290	1.77
		1266	1.357	1.38	4.21	1.374	1.71
	$B^{11}O$	1280	1.301	1.35	4.21	1.773	1.81
		1259	1.348	1.36	4.21	1.908	1.82
		1885	1.199	1.17	4.21	2.184	1.35
	$B^{10}O$	1940	1.199	1.16	4.21	1.143	2.18
	CN	2164	1.148	1.11	4.21	4.052	2.46
		1789	1.236	1.20	4.21	2.44	1.89
		2069	1.169	1.13	4.21	2.511	1.89
	CO	2182	1.118	1.09	4.21	9.432	img.
		1517	1.232	1.26	4.21	3.642	1.89
	N_2	1732	1.201	1.20	4.21	—	—
		1460	1.291	1.28	4.21	2.942	1.97
		2360	1.094	1.05	4.21	3.062	1.99
	NO	1038	1.412	1.42	4.21	1.374	1.77
		2376	1.06	1.03	4.21	3.802	2.23
		1906	1.146	1.13	4.21	3.292	2.04
11	O_2	710.1	1.599	1.59	4.21	2.802	1.94
		1433	1.223	1.25	4.21	3.412	2.07
		1584	1.204	1.21	4.21	2.792	1.94

TABLE II.—*Continued.*

Period	Molecule	ω_e (cm^{-1})	R_e exp (10^{-8} cm)	R_e calc. (10^{-8} cm)	a ($10^8\ cm^{-1}$)	a' ($10^8\ cm^{-1}$)	R_{12} (10^{-8} cm)
	F_2	1140	1.278	1.32	4.21	2.762	1.93
	CO^+	1277.1	1.16	1.20	4.21	5.112	img.
		1564	1.24	1.25	4.21	2.912	1.96
		2212	1.11	1.11	4.21	3.172	2.01
	N_2	2418	1.071	1.04	4.21	4.532	img.
		2206	1.113	1.08	4.21	3.442	2.08
	O_2	1876	1.14	1.13	4.21	4.092	2.53
12	AlO	8682	1.663	1.611	4.61	0.346	1.84
		977	1.614	1.613	4.61	1.635	1.91
	CP	1062	1.667	1.607	4.61	—	—
		836	1.685	1.710	4.61	0.738	1.85
		1240	1.558	1.540	4.61	1.187	1.88
	SiN_e	1034	1.576	1.602	4.61	4.412	2.50
		1152	1.568	1.565	4.61	1.295	1.89
	CS	1282	1.56	1.523	4.61	0.952	1.87
	SiO	1240	1.505	1.504	4.61	1.272	1.89
		848	1.621(r_0)	1.668	4.61	1.075	1.88
	PN	1103	1.542	1.564	4.61	—	—
		1337	1.482	1.452	4.61	—	—
	PO	1231	1.446	1.449	4.61	1.767	1.92
	SO	628.7	1.769	1.788	4.61	1.26	1.89
		1124	1.489	1.536	4.61	1.447	1.90
22	Na_2	115.6	3.663	3.41	2.53	−0.384	2.64
		123.8	3.404	3.35	2.53	−0.140	2.62
		159.2	2.070	2.16	2.53	−0.140	2.64
	S_2	727.4	1.73	1.83	2.53	2.398	3.81
	Cl_2	564.9	1.983	2.00	2.53	3.528	img.
		261.1	2.42	2.60	2.53	4.577	img.
	P_2	779.3	1.88	1.77	2.53	2.162	3.40
		470.9	2.12	2.19	2.53	1.475	2.99

additive group constant, while a' is calculated from a and $\omega_e x_e$, the anharmonicity constant. He has shown that the values of R_e calculated from (2) checked well with experimental values with an accuracy comparable with the Badger relation.[2] The grouping of molecules according to Huggins is quite arbitrary, namely, based on the number of valence electrons in the linkage. This is not quite so adaptable to polyatomic molecules since in such cases the conception of the number of valence electrons is quite vague. It is therefore the purpose of the present note to investigate whether it is possible to determine the constants in some other way so that they are characteristic of molecular periods as in the cases of other relations.

In Huggins' second paper he has shown also that the combination

$$R_{12}-\frac{2.303}{2}\log\frac{1}{a^2-aa'}$$

is approximately constant, if this is the case then relation (2) can be rewritten in the form

$$R_e=-\frac{2.303}{a}\log K_e+\left[R_{12}-\frac{2.303}{a}\log\frac{1}{a^2-aa'}\right],$$

or

$$\log K_e=-\frac{a}{2.303}R_e+\frac{a}{2.303}\left[R_{12}-\frac{2.303}{a}\log\frac{1}{a^2-aa'}\right], \quad (3a)$$

or

$$\log K_e=AR_e+B. \quad (3b)$$

Trial plots between $\log K_e$ and R_e were then made for various molecular periods (in the usual sense) and in all cases satisfactory straight lines were found with slope A and intercept B, which were tabulated in Table I together with the values of a calculated from A. Values of R_e's were then calculated from Eq. (3b) and were tabulated with experimental values R_e for comparison in Table II.

[2] R. M. Badger; J. Chem. Phys. **2**, 128 (1934); **3**, 710 (1935).

With the values of a calculated from A we can calculate a' if $\omega_e X_e$ is known according to the formula given by Huggins. Then R_{12} can also be calculated from the values of B. These values were also tabulated in Table II. For higher molecular periods the data seem too meager to justify a plot.

DISCUSSION

An examination of the table readily reveals that the accuracy of the present relation in predicting R_e from K_e is quite comparable with all other existing relations,[3] and is slightly better than Huggins original relation. For most cases the difference is well within 5 percent except for one molecule, Li_2. The constants A and B are now characteristic of molecular period and the relation could now be used without calculating a'. The values of R_{12} thus determined show only a very small variation considering that these values are calculated from a and $\omega_e x_e$ with an accumulation of error each time. The constancy of R_{12} for each one molecule is even more noticeable. Huggins has calculated theoretically the value of a for various molecules from his Eq. (20). Unfortunately many of them are imaginary; those real values also show very wide variations. So instead of taking average values he chose rather the value to give additivity of R_{12} in which case it is analogous to the crystals where the repulsion energy term is invariant. However the physical meaning of R_{12} in this potential function seems to be a little obscure since its value is larger than R_e in the present case.

Theoretically, Huggins based his relation on the invariance of the repulsion term from an analogy of ionic crystals. On the other hand it must be admitted that the interatomic distances in ionic crystals are usually larger than those of covalent molecules; we would expect, therefore that the repulsion term which is essentially a short distance energy should become more complex in the latter case. In view of the fact that the values of a and R_{12} of Huggins and those determined presently differ markedly though both are satisfactory, we probably can hardly deny the complexity of the repulsion term.

It should be emphasized that though we can derive satisfactory relations between the interatomic distance and the force constants from certain forms of potential function we cannot make the reverse statement that the potential function must be a good approximation of the true potential function. This can easily be proved. If we add a certain term say α/R^n to the potential function we shall have a term $n(n+1)\alpha/R^{n+2}$ added to their relation between K_e and R_e or the relation (3b) can now be written as

$$K_e=(a^2-aa')\exp[-a(R_e-R_{12})]-\frac{a'n\alpha}{R_e}+\frac{n(n+1)\alpha}{R_e^{n+2}}.$$

So far as the difference between the last two terms is small for a small variation of R_e, we can neglect them. But such terms will be of significance in the potential function, or when the variation of R_e is large as in the case of Li_2 which has an abnormally large R_e compared with other molecules in the same period. So we cannot expect to calculate correctly the dissociation energy from such a simple function. This is actually the case if we try to calculate D_e from K_e, a and a', and to compare with the experimental value.

[3] Wu and Yang, J. Phys. Chem. **48**, 295 (1944).

Letters to the Editor

PUBLICATION of brief reports of important discoveries in physics may be secured by addressing them to this department. The closing date for this department is, for the issue of the 1st of the month, the 8th of the preceding month and for the issue of the 15th, the 23rd of the preceding month. No proof will be sent to the authors. The Board of Editors does not hold itself responsible for the opinions expressed by the correspondents. Communications should not exceed 600 words in length.

The Gamma-Rays of Po^{210} *

S. DE BENEDETTI AND E. H. KERNER
Clinton Laboratories, Oak Ridge, Tennessee
December 16, 1946

IN connection with Chang's studies[1] on the fine structure of the α-particles of Po and with Feather's discussion[2] on this subject it might be useful to report some recent absorption experiments on the γ-rays of this element. Since the sources at our disposal were larger than those used by previous investigators we could easily obtain more accurate results. A thin-walled glass G-M counter was used to detect the radiation.

Figure 1 shows the absorption in lead of the γ-rays of Po and a similar curve for Ra in equilibrium with its products. The ordinates are expressed in counts per minute and per Curie for Po, and in counts per minute and per 10^{-5} Curie for Ra. Within the accuracy of the absorption method it appears that the γ-radiation of Po consists of a single component of half-thickness equal to 8.5 g/cm^2 Pb. The energy of the radiation can be evaluated to be 0.8 Mev. The intensity per Curie of Po is equivalent to that of the γ-rays from 7.10^{-5} Curie of Ra, when both curves are extrapolated to zero absorption.

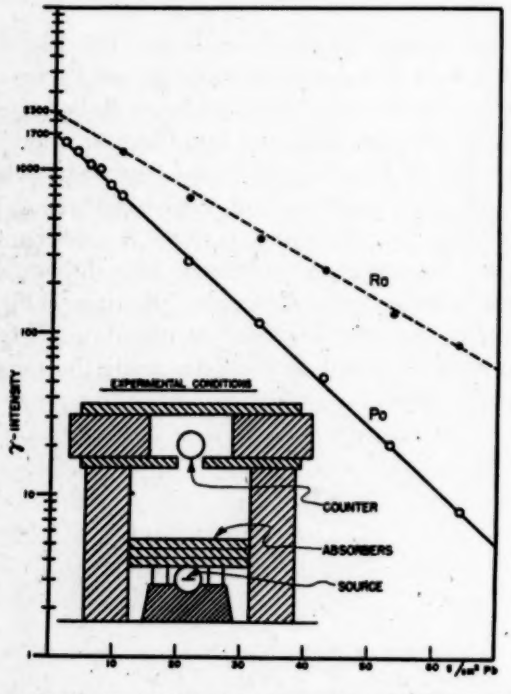

FIG. 1. Absorption in lead of the gamma-rays of polonium and of radium in equilibrium with its products. The ordinates are in counts per minute per Curie for polonium and in counts per minute per 10^{-5} Curie for radium.

The absorption experiments were repeated with many samples, always giving consistent results. The data are in general agreement with those in the literature, both for the absorption curve and for the intensity. However, no evidence of a softer γ-component, as reported by Webster[3] and by Bothe and Becker,[4] was observed.

A search for softer radiations showed no other components until, with absorbers thinner than 0.5 g/cm^2 Al, one finds a radiation whose mass absorption coefficient in Al is 18 cm^2/g and which is probably the same component observed by Curie and Joliot[5] and attributed by them to the L line of polonium.

If one assumed, as these results seem to indicate, that only one γ-component of 0.8 Mev is present, a theoretical difficulty mentioned by Feather[2] would be removed. However, Chang's results on the fine structure of α-particles would be still more difficult to explain.

* This document is based on work performed under Contract No. W-35-058-eng-71 for the Manhattan Project at Clinton Laboratories.
[1] W. Y. Chang, Phys. Rev. 69, 60 (1946).
[2] N. Feather, Phys. Rev. 70, 88 (1946).
[3] H. C. Webster, Proc. Roy. Soc. A136, 428 (1932).
[4] W. Bothe, Zeits. f. Physik 96, 607 (1935).
[5] I. Curie and F. Joliot, J. de phys. et rad. [7] 2, 20 (1931).

Gamma-Rays from Tungsten and Molybdenum

W. M. SCHWARZ*
Indiana University, Bloomington, Indiana
AND
M. L. POOL
Ohio State University, Columbus, Ohio
November 27, 1946

THE harder gamma-rays of tungsten have been investigated to date only by means of absorption techniques.[1-4] We have studied the gamma-rays from the 24-hour tungsten isotope, using a spectrometer of the usual 180-degree deflection type, measuring photoelectrons emitted from a thorium or a uranium radiator. The spectrometer had a 5-cm radius of curvature, which is small enough to provide a rather large solid angle, but at the same time provides relatively little shielding between the source and the detector. Background counts were high, and the observed peaks amounted to small differences in the counting rates recorded. The instrument was calibrated with photoelectrons produced from the annihilation radiation of copper positrons.

The peaks which were observed have been confirmed on successive runs on different samples. Observation of the decay of the peaks indicates that each of the peaks noted has the 24-hour half-life. It is not likely that any of these peaks are L peaks since the intensity was believed to be too low to show an L peak. The gamma-ray energies corresponding to the observed peaks are 480, 570, 690,

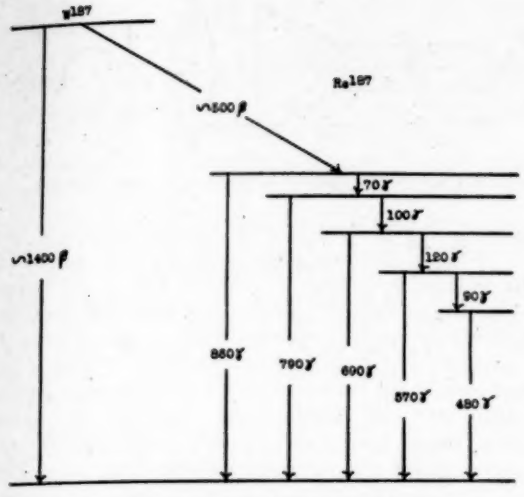

FIG. 1. Proposed energy level diagram of Re^{187}.

790, and 860 kev. An attempt was made to find a peak corresponding to a gamma-ray energy of 940 kev as previously reported,[3] but without success.

Figure 1 is a suggested energy level diagram for the resulting Re^{187} isotope. Valley[5] has reported internal conversion electrons corresponding to gamma-rays of 85, 101, and 135 kev. It is suggested that the 90, 100, and 120 kev transitions indicated in the diagram may be associated with the gamma-rays which Valley observed. Uncertainties due to width of lines can easily account for the differences in the values. The 70-kev jump has not been observed as yet, and this scheme suggests that the region roughly between 150 and 450 kev should be examined for evidence of other possible transitions between these levels.

The gamma-rays of the 67-hour molybdenum were also studied. A typical run is shown in Fig. 2. Here again the intensity of the peaks above the Compton background was not great. Three, however, seem to be confirmed—660, 705, and 730 kev—which correspond to gamma-rays of 770, 815, and 840 kev. Since Mo^{99} is in equilibrium with Ma^{99}, some or all of these gamma-rays may be associated with the masurium decay instead of with molybdenum, but work of Seaborg and Segrè[6] suggests that this is not likely.

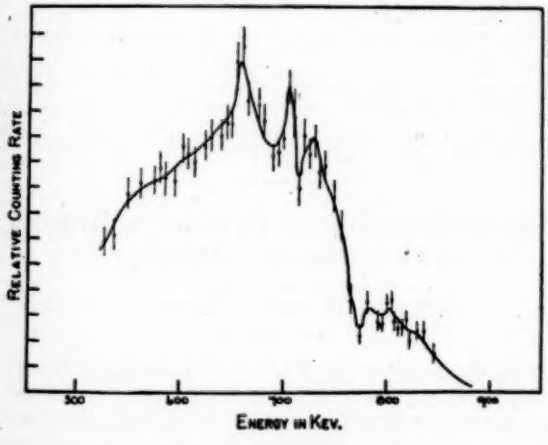

FIG. 2. Gamma-rays from 67-hour molybdenum.

* Now at Union College, Schenectady, New York.
[1] K. Fajans and W. H. Sullivan, Phys. Rev. **58**, 276L (1940).
[2] A. F. Clark, Phys. Rev. **61**, 242 (1942).
[3] C. E. Mandeville, Phys. Rev. **64**, 147 (1943).
[4] W. H. Sullivan, Phys. Rev. **68**, 277L (1945).
[5] G. E. Valley, Phys. Rev. **59**, 686A (1941).
[6] G. T. Seaborg and E. Segrè, Phys. Rev. **55**, 808 (1939).

A Proposed Detector for High Energy Electrons and Mesons*

I. A. GETTING
Massachusetts Institute of Technology, Laboratory for Nuclear Science and Engineering, and Electrical Engineering Department, Cambridge, Massachusetts
November 14, 1946

USE can be made of the visual radiation emitted by a charged particle moving at constant speed in a medium where the phase velocity of the light is smaller than the velocity of the charged particle to detect such particles. This visual radiation was first observed by Čerenkov.[1] A theoretical investigation was made by Frank and Tamm[2]; and an independent experimental quantitative verification using monoenergetic electrons was made by Collins and Reiling.[3]

If a particle of speed β impinges on a non-absorbing dielectric, then since the speed of the particle is maintained except for collision and radiative losses, the speed of the particle will remain equal to β. On the other hand the phase velocity of electromagnetic radiation is reduced to $1/n$ where n is the index of refraction of the dielectric. Frank and Tamm have shown that under these conditions the vector potential does not cancel and that coherent radiation exists directed at an angle θ with the direction of motion of the particle such that $\cos\theta = 1/\beta n$. The radiation has an energy spectrum per unit length of dielectric

$$f(\gamma)d\gamma = 4\pi^2 \frac{e^2}{C^2}\left(1-\frac{1}{\beta^2 n^2}\right)\gamma d\gamma;$$

that is, provided the radiation is not absorbed, light will be given off in that spectral region where n is substantially larger than one. For glasses and plastics like Lucite these conditions are met in the visual region; and since n is practically constant there, the number of photons per unit frequency interval emitted is independent of the frequency. It is to be noted that the Čerenkov effect depends only upon the charge and speed of the particle and not on its momentum or energy. Hence since high energy electrons

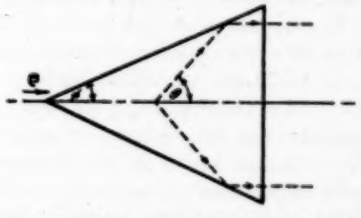

FIG. 1. Simple electron-type radiator ($n = 1.5$).

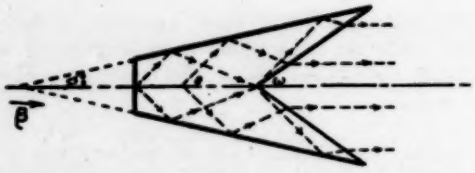

FIG. 2. Electron radiator design for optimum optical properties ($n=1.4$).

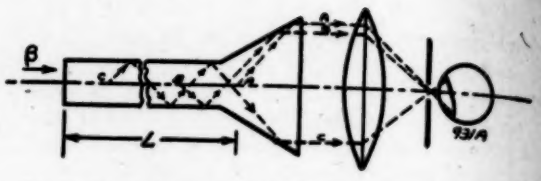

FIG. 3. Practical arrangement of electron (or meson) detector.

(greater than 100 Mev) and mesons are very penetrating, a considerable amount of light can be emitted by the passage of even one particle in a properly designed geometrical unit.

Figure 1 shows a simple cone made say of Lucite ($n_D=1.5$, $n_F-n_C=0.008$). If an electron enters along the axis from the left, all the light emitted will be reflected by the cone into a parallel beam of light if $\phi=\theta/2$. If a condensing lens with diaphragm arrangement is used as shown in Fig. 2, then light emitted at angles differing from θ will not reach the photo-multiplier. Such a unit acts therefore as a telescope. The optical system also reduces the background radiation. The loss in the original particle resulting from Čerenkov radiation is about 1 kev per cm; whereas the loss due to collisions and non-coherent radiations is of the order of 2 Mev per cm for a 100-Mev electron. One might at first expect that the recombination radiation in the dielectric would swamp out any coherent radiation. This, however, is not true, otherwise Čerenkov and Collins and Reiling would not have been able to get their photographs.

For electrons of energy sufficient to penetrate a reasonable length of dielectric, β will always be practically one. Hence for a Lucite electron detector, θ is always 48° 10′ and $\phi=24°\ 5'$. On the other hand a meson of mass 200 will have the following values of β and ϕ for 50, 100, and 200 Mev mesons: 0.73, 0.864, 0.942; 12° 2′, 19° 44′, 22° 30′. Hence an electron detector should not detect mesons unless their energy is in excess of 200 Mev (not possible in a 300-Mev synchrotron). Similarly meson detectors of given energy range sensitivity are possible. Finally, since the detector depends only upon speed, the use of a magnetic field either directly or with a cloud chamber to measure momentum should give a good measure of meson mass.

Figure 3 shows a somewhat better geometry from the standpoint of optics in that the emergent ray comes out at Brewster's angle (the electric vector is always in the radial plane). The smaller ϕ, the smaller is the color dispersion. This is not serious, however, even in the geometry of Fig. 1, where the dispersion between the F and C lines is only 0.4.

Figure 2 shows a practical geometry. The length L can be made as long as required and the cone angle is the same as in Fig. 1. An estimate of the output of the device can readily be made. One expects to get 212 photons per cm of path. Taking L as 20 cm, we should get approximately 4240 photons. If all of these arrive at the photo-multiplier and using 1.2 percent as the efficiency (obtained by using the sensitivity as quoted by the RCA tube handbook for the 931A), there should result a charge pulse at the output of the multiplier of 8.2×10^{-11} coulomb (amplification of 1,000,000). Taking the combined output capacity of the 931A (6.5 $\mu\mu$f) plus the input capacity (13.5 $\mu\mu$f) of a video amplifier as 20 $\mu\mu$f, this should give as the upper limit an output pulse of 0.4 volt. The pulse length of the original photons can be obtained from a consideration of the geometry as 8×10^{-10} sec. This will be lengthened by transit time in the multiplier tube to a total pulse length of about 10^{-9} sec.[4] Theoretically, therefore, the video amplifier should have a band pass approaching 1000 mc providing that it does not itself introduce new noise. The noise arising from the photo-multiplier is evenly distributed over the region under consideration; and some idea of the noise can be obtained from the figure of maximum dark current of the 931A as published in the RCA handbook, it being recognized that much better performance than this figure can be obtained. A dark current on the output of the 931A of 0.25μ amp corresponds to 0.16 electron in 10^{-7} sec., the resolving time of a practical 10-mc video on the output. Since the radiating particle should result in releasing 51 electrons at the first electrode, one can readily see that noise is completely negligible unless the coherency of the radiator is sufficiently reduced.

The choice of material for the radiator is dependent upon the following considerations: (1) it should consist of as low an atomic number as possible in order to have low stopping power for the primary particle; (2) it should have a high value of n to be an efficient radiator; (3) n should be large and the material transparent particularly in the ultraviolet region; (4) the material should have homogeneous optical properties; and (5) color dispersion should be small. Lucite and Plexiglass are suitable though more expensive substances like lithium fluoride would be better.

Test units are being built, and the performances of these and the results of more elaborate analysis will be published as soon as they become available.

* The research described in this letter was supported in part by Contract N5Ori-78, U. S. Navy Department.

[1] P. A. Čerenkov, Comptes Rendus Acad. Sci. USSR 8, 451 (1934); *ibid.* 14, 105 (1937); Phys. Rev. 52, 378 (1937).
[2] I. Frank and Ig. Tamm, Comptes Rendus Acad. Sci. USSR 14, 109 (1937).
[3] G. B. Collins and V. G. Reiling, Phys. Rev. 54, 499 (1938).
[4] R. D. Sard, J. App. Phys. 17, 768 (1946).

Effect of Direct-Current Potential on Initiation of Radiofrequency Discharge

ARTHUR A. VARELA
Naval Research Laboratory, Washington, D. C.
November 6, 1946

IN the course of development of radar duplexing systems at the start of the war I observed an effect which was unexpected and which to my knowledge has not been reported.

Some of the low power radar systems then being developed required a gaseous discharge switch in which a high admittance discharge would be initiated very rapidly with the lowest possible r-f potential. A very short deionization time was also desired. To encourage these characteristics I proposed to apply to the discharge tube a d.c. potential less than that required to initiate the discharge and to do this by means of a pulse network charged through an appropriate resistor from a d.c. source. It was reasoned that the presence of the d.c. field would hasten ionization with a given r-f potential by virtue of the higher peak electron velocities and that a residual potential following the discharge would hasten deionization by capture by the anode and by captor molecules. In addition the intensity of the discharge should be increased by the direct current.

By experiment it was found however that application of a d.c. potential greatly impeded the formation of the discharge. A considerably stronger r-f potential was required for initiation of the discharge. Also the admittance of the discharge was found to be lower when the bias was applied. Recovery was somewhat more rapid as had been expected.

Obviously such an effect can take place only when the alternating field is of sufficiently high frequency so that the discharge cannot form completely in part of one cycle but results from cumulative generation of ions over a number of cycles. Since ionization does not start until some critical value of potential is reached it can be regarded as occurring only through a small angle at the voltage peaks of the r-f cycle. On the other hand deionization is a continuous process. Hence, during two periods of the cycle when the voltage is above the ionization threshold the ionization rate will predominate and during the remaining periods of the cycle ions will be removed. For discharge to form there must be a net increase in the number of ions after integration over each cycle period. Now with a d.c. bias of about the same value as the r.m.s. of the alternating potential the field will exceed the ionization threshold for only one period in each cycle and the ratio of ionization time to deionization time will be considerably reduced. The increase in ionization rate due to the higher potential during the ionization period is not sufficient to offset the increase in deionization time and a higher r-f voltage is required to produce a discharge. The same effects are present during the discharge and the d.c. bias produces a reduction in intensity.

The pressure of war circumstance denied careful exploration of this effect at the time it was observed and only qualitative data were obtained. The experiments were conducted at a frequency of 120 megacycles per second with 5 microsecond pulses at a rate of 60 per second. The discharge tubes had aluminum electrodes in an atmosphere of about 5 cm of hydrogen with 20 percent argon.

Aside from obvious application in switching or modulation of high frequency currents this phenomenon appears as perhaps a useful tool for the investigation of gaseous discharge, particularly in the study of discharge formation in high frequency fields.

On the Theory of Dielectric Breakdown in the Alkali Halides

GÖETHE MALMLÖW* AND FREDERICK SEITZ
Carnegie Institute of Technology, Pittsburgh, Pennsylvania
December 16, 1946

IN 1939 Buehl and von Hippel[1] showed that the breakdown potential of KBr, when measured as a function of temperature and for direct voltage, possesses a peak in the neighborhood of 350°K. This peak appeared to be even in qualitative contradiction with the theories of dielectric breakdown developed by von Hippel,[2] Fröhlich,[3] Seeger and Teller,[4] and others, which predict a rather gradual rise of the breakdown potential with increasing temperature. Subsequently one of us[5] has shown that the temperature dependence obtained when the measurements are made with alternating potential instead of constant potential is very different from that observed by Buehl and von Hippel. In the first place, the breakdown potential is considerably lower when the measurements are made with alternating potential; in the second place, the breakdown potential appears to be nearly constant between 220°K and 300°K, the range for which measurements were made. The second of these conclusions is not yet as well verified as the first because of the fluctuations in breakdown potential which occur from specimen to specimen. In any case the newer measurements indicate that polarization effects play an important role in determining the breakdown potential for direct voltage in the alkali halides near room temperature. This conclusion is not surprising since experiments on the darkening of the alkali halides under x-ray and electron bombardment show that ionic migration is not negligible at room temperature.

If further experimental work supports the second conclusion, namely that the breakdown strength of the alkali halides is independent of temperature up to temperatures of the order of 300°K or higher, we will be forced to conclude that at least in KBr the critical factor determining the breakdown potential is not the ability of the electrons in the conduction levels to overcome the collisions with the lattice by which they dissipate the energy derived from the applied field, as first proposed by von Hippel, but is a temperature-independent quantity. It seems reasonable to suppose that this limiting factor is the disintegration by the applied field of the excitons produced by accelerated conduction electrons. As has been pointed out elsewhere[6] those conduction electrons which succeed in being accelerated to the energy range above the region of magnitude $k\Theta$ (Θ=characteristic temperature) where the lattice vibrational waves absorb their energy most efficiently, will eventually produce excitons. Moreover, this process should be far more probable than the direct production of secondary free electrons as long as the primary electrons are accelerated more or less continuously, since the production of excitons requires less energy than the production of secondary electrons. Thus, unless the excitons are spontaneously dissociated into free electrons and holes by the applied electric field, or by another agent, it will be impossible to initiate the avalanche of conduction electrons that is needed for breakdown. The newer experi-

mental observations on KBr, mentioned above, suggest that the condition determining the observed breakdown field is the requirement that this field be sufficiently strong to dissociate the excitons.

* Fellow of the American-Scandinavian Foundation.
[1] R. C. Buehl and A. von Hippel, Phys. Rev. **56**, 941 (1939).
[2] A. von Hippel, Zeits. f. Physik **75**, 145 (1932).
[3] H. Fröhlich, Proc. Roy. Soc. **A160**, 230 (1937).
[4] R. J. Seeger and E. Teller, Phys. Rev. **54**, 515 (1938).
[5] G. Malmlöw, Arkiv f. Matem., Astr. och Fysik **30B**, 1 (1943).
[6] F. Seitz, *Modern Theory of Solids* (McGraw-Hill Book Company, Inc., New York, 1940), footnote 3, p. 563.

Integral and Rational Numbers in the Nuclear Domain and Their Significance*

ENOS E. WITMER
Randal Morgan Laboratory of Physics, University of Pennsylvania, Philadelphia, Pennsylvania
September 16, 1946

THE pure number hc/e^2 is $861=\frac{1}{2}(42\times41)$ to a very high degree of precision. This, we believe, is both exactly *true* and *significant*. Also $2M_p/861$ is the binding energy of the deuteron within experimental error. This energy, or the corresponding mass, is designated a *deuterium unit*. One-twelfth of a deuterium unit is called a *prout*. Thus the mass of a proton, M_p, is exactly 5166 prouts. The mass of a neutron is 5173 prouts. Comparison with the best experimental data shows that in all probability the masses of all stable nuclei in the ground state up to and including Ne^{21} are integral numbers of prouts. This leads to the idea that the *masses of all stable nuclei in the ground state are an integral number of prouts*. The nuclear mass of O^{16} comes out to be 82,012 prouts, from which it is possible to calculate the value of a prout to eight significant figures. It is

$$1\ \text{prout}=0.000195039909\pm(26\times10^{-12})\text{MU}.$$

The masses of the proton and neutron are, respectively,

$$M_p=1.00757617\ \text{MU},\quad M_n=1.00894145\ \text{MU}.$$

A study of the binding energy per particle in prouts seems to indicate that this quantity never exceeds the integral value 48, although it comes very close to 48 in a number of cases. In fact this quantity probably lies between 47 and 48 for all stable nuclei between $Z=22$ and $Z=42$. Between $Z=42$ and $Z=84$ it drops gradually to about 42 prouts per particle.

Furthermore the evidence just given together with other evidence lends some support to the idea that each "shell" of protons in the nucleus has 42 protons.

The values of the disintegration energies in α-emission and the energies of γ-rays in γ-emission support to a considerable extent the idea that the masses of nuclei in excited states are always a rational number of prouts. This would be a natural generalization of the result just given.

Also the magnetic moments of nuclei appear to be integral multiples of $\mu_N/42\times41$, where μ_N is the nuclear magneton.

The experimental value of $\beta=M_p/m$ is compatible with the assumption that it is $(16/15)\times42\times41$. If this is so, the mass of the electron is given by

$$m=45/16\ \text{prouts}.$$

The value of

$$\gamma=e^2/GM_p^2\ \text{is in the neighborhood of}\ e^{2\times42}.$$

All this shows the great importance of the number 42.

It is suggested that all intrinsic observable nuclear quantities are rational multiples of a natural unit for that quantity. The term intrinsic nuclear quantity does not include such quantities as cross sections where interaction with an external entity is involved.

This dominance of integral and rational numbers appears to be irreconcilable with a theory of the nucleus in which the constituent particles are held together by forces which are continuous functions of continuously varying space coordinates, *even with quantization*. This seems to point to the necessity of "quantizing" the space and time coordinates. What the detailed nature of such "quantization" is remains to be seen. Now this idea fits in quite well with the importance of the number 42. For the Riemann-Christoffel tensor of space-time has 21 *different* components. It is suggested that the importance of the number 42 derives from this source, the factor 2 coming perhaps from spin.

All this leads up to the idea that nuclear structure is to be explained with the aid of a quantized space-time, in which the component, of the Riemann-Christoffel tensor are not identically zero. In the limit of macroscopic matter this must yield the Einstein equations of gravitation. In such a theory the integers and rational numbers mentioned above would appear as derived quantities.

It is hoped that our long article on this subject will appear very soon.

* See also E. E. Witmer, Proc. Nat. Acad. Sci. **32**, 283 (1946).

Determination of Nuclear Spin from the Stark Effect of Microwave Rotational Spectra

W. V. SMITH
Department of Physics, Duke University, Durham, North Carolina
December 11, 1946

DAKIN, Good, and Coles[1] have observed the quadratic Stark effect of a linear molecule (OCS) at 24,320 megacycles, obtaining a splitting of about 4 megacycles in the $J=1$ to $J=2$ transition for an electric field of 1070 volts per cm. This observation suggests a means of extending to microwave regions the method of obtaining nuclear spins from the intensity ratio of rotational spectrum lines. Such intensity ratios occur, for instance, in symmetric tops with 3 identical atoms such as $CHCl_3$, where the $K=0,\ 3,\ 6\cdots$ sublevels of each J level are strong (S), while the sublevels $K=1,\ 2,\ 4,\ 5,\ 7,\ 8\cdots$ are weak (W). The ratio S/W is given by[2]

$$S/W=1+\frac{3}{4(I^2+I)},$$

where I is the nuclear spin. At 10,000 to 25,000 megacycles, however, the different K sublevels for a given J are spread over a band of less than a megacycle, so that this effect is not very useful.

If, however, a d.c. electric field is applied to the gas, the multiplet separation is large particularly since for

symmetric tops the linear Stark effect is quite pronounced. The frequency shift $J, K, P \rightarrow J+1, K, P$, is $\nu=\nu_0+\Delta\nu$ where ν_0 is the unperturbed frequency and[3]

$$\Delta\nu=\frac{\mu E}{h}\left(\frac{2KP}{J(J+1)(J+2)}\right)$$

plus higher order terms, and is independent of frequency. Here the "external quantum number" P determines the quantization with respect to the external field E, and μ is the dipole moment. For low quantum numbers the multiplet components are separated by several megacycles for fields as low as 100 volts per cm or less. By applying the d.c. field parallel to the a.c. field, the selection rule $\Delta P=0$ applies, and no further complications arise in the spectrum.[1]

Since both quantum numbers K and P can range from $-J$ to $+J$, each component of a multiplet has several rotational terms contributing to its statistical weight G. Those multiplet components near the undisturbed frequency (low $|K|$ and $|P|$) and the extreme ends of the band (high $|K|$ and $|P|$) however contain sufficiently few terms so that useful intensity relations can be obtained. Table I shows the composition of the three lowest and two highest values of $|\Delta\nu|$ in columns 1, 2, 3, and 4. Columns 5 and 6 show specific values for the $J=3$ to $J=4$ transition of $CHCl_3$, occurring near 27,000 megacycles. A dipole moment of 1.05 e.s.u.[4] and spin I of 5/2 (questionable)[5] are assumed.

For $J=3, 6, \cdots$ it is seen that the ratio of the $|KP|=J^2$ to $|KP|=1$ lines gives S/W directly. By maintaining a fixed value of $\Delta\nu$ and varying E to bring successive lines to this frequency, it should be possible to make accurate intensity comparisons. The intensities of course will be low, the intensity ratio of the $|KP|=1$ and $|KP|=J^2$ lines to the unresolved line being $2/(2J+1)^2$ (ignoring nuclear spins), or 0.041 for the $J=3$ line under consideration.

The above method depends on the use of a uniform d.c. field which is difficult to achieve using wave-guide technique.[1] A less sensitive method, perhaps only useful for low spin numbers, and $J=1$ or 2 spectrum lines, consists in comparing the intensities at the unperturbed frequency ν_0 without field and with a field large enough to sweep out all terms for which $\Delta\nu\neq 0$. The intensity ratio is

$$\frac{3S/W+4}{3S/W+2} \text{ for } J=1 \quad \text{and} \quad \frac{5S/W+20}{5S/W+4} \text{ for } J=2.$$

TABLE I. Frequency shifts and statistical weights of Stark effect multiplets for rotational spectra of 3 homonuclear symmetric tops, with values for $J=3$ to 4 transition of $CHCl_3$ for field of 100 volts per cm.

$\lvert KP\rvert$	$\lvert K\rvert$	$\lvert P\rvert$	G	$\Delta\nu$ $CHCl_3$ (mc)	G/W $CHCl_3$
1	1	1	$2W$	1.8	2
2	1 2	2 1	$4W$	3.6	4
3	1 3	3 1	$2W+2S$	5.4	$2\left(1+\frac{38}{35}\right)$
$J(J-1)$	$J-1$ J	J $J-1$	$2W+2S$[a] or $4W$[b]	10.8	$2\left(1+\frac{38}{35}\right)$
J^2	J	J	$2S$[c] or $2W$[d]	16.2	$2\left(\frac{38}{35}\right)$

[a] J or $J-1$ divisible by 3.
[b] Neither J nor $J-1$ divisible by 3.
[c] J divisible by 3.
[d] J not divisible by 3.

[1] T. W. Dakin, W. E. Good, and D. K. Coles, Phys. Rev. 70, 560 (1946).
[2] D. M. Dennison, Rev. Mod. Phys. 3, 280 (1931).
[3] R. de L. Kronig, Proc. Nat. Acad., Wash. 12, 608 (1926).
[4] R. J. W. Le Fevre, *Dipole Moments* (Chemical Publishing Company, New York, 1938).
[5] J. B. M. Kellog and S. Millman, Rev. Mod. Phys. 18, 323 (1946).

Energy Levels in the Nucleus Mn^{56}

A. B. MARTIN
Yale University, New Haven, Connecticut
December 13, 1946

A NUMBER of investigators[1] have observed the energy levels in nuclei of low and medium mass number which are exhibited in the process of d,p reactions. The energy level spacing observed in practically all cases was of the order of 1 Mev or greater, for excitations up to about 5 Mev above the ground state. When these results are compared with the 5-kev to 100-kev level spacings predicted by theory,[2] the influence of strong selection rules is indicated.

In order to shed more light on the nature of the selection rules operating, a study has been made of the energy levels resulting from a (d,p) process in an element of medium atomic weight; i.e., a nucleus containing a sufficient number of particles to render the statistical approach of the theory at least reasonably valid. The excitation obtained extended to 4.3 Mev above ground. The results show that, while there are probably many other energy levels in the Mn^{56} nucleus, a certain type of level (that associated with the (d,p) reaction) seems to persist at an average spacing of about 0.85 Mev.

The reaction studied was:

$$Mn^{55}+H^2 \rightarrow Mn^{56}+H^1.$$

The assignment of levels is unique, since only one isotope is involved.

Deuterons having a mean energy of 3.68 Mev were obtained from the Yale cyclotron and the energy of the emitted protons was determined by absorption in air and Al foils. The proton counting system included two each proportional counters, capacity-neutralized preamplifier

TABLE I.

Proton range (cm air)	Proton energy (Mev)	Q (Mev)	Levels (Mev)	Spacing (Mev)
22.9	3.98	0.38	4.38	
				0.77
30.8	4.73	1.15	3.61	
				1.13
44.7	5.85	2.28	2.48	
				0.71
54.4	6.55	2.99	1.77	
				0.70
64.7	7.23	3.69	1.07	
				1.07
82.3	8.29	4.76	0	

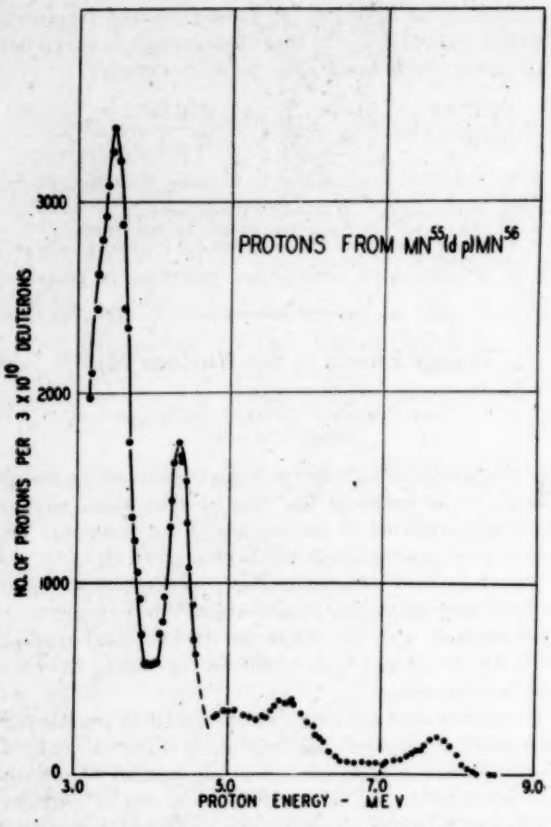

FIG. 1. Proton groups from the reaction $Mn^{55}(d, p)Mn^{56}$. The number of protons counted per unit deuteron beam is plotted against the proton energy.

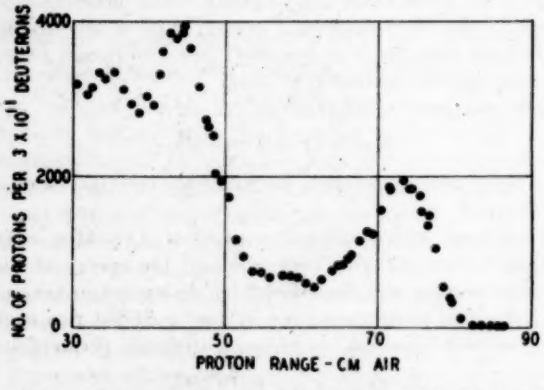

FIG. 2. Proton groups of ranges greater than 30 cm from the reaction $Mn^{55}(d, p)Mn^{56}$, plotted to an expanded scale. The number of protons counted is plotted against the proton range. (Averaged data for 11 runs.)

units and linear amplifiers, a coincidence circuit and a slightly modified Higinbotham scale-of-64 circuit. The over-all resolution of the method for the accurate determination of proton ranges is placed at 0.3 Mev.

Figure 1 shows the results obtained over the range of proton energies investigated. The total number of counts used to plot the two prominent groups between 3 and 5 Mev is to be obtained by dividing the ordinate by three.

Figure 2 shows the groups having ranges greater than 30 cm of air (4.66 Mev) on an expanded scale. A total of 21 separate runs were made over this interval, all of which are useful for analysis purposes, although only 11 were used to form the averages shown on this graph. On this curve, the total number of counts taken to determine a particular point is given by the ordinate in each case.

The Q-values shown in Table I below are calculated from the average values of the proton ranges obtained from several plots, each plot representing the averaged results from several runs.

The author wishes to thank Professor Ernest Pollard for suggesting this problem and for generous interest and advice throughout the course of the study. The design of the amplifiers and coincidence circuits used is due to Professor H. L. Schultz. This work was supported by funds from O.N.R.

[1] For example, W. L. Davidson, Jr., Phys. Rev. 56, 1062 (1939); Ernest Pollard and W. W. Watson, Phys. Rev. 58, 12 (1940); M. G. Holloway and B. L. Moore, Phys. Rev. 58, 847 (1940); E. B. M. Murrell and L. C. Smith, Proc. Roy. Soc. 173, 410 (1939).
[2] H. A. Bethe, Rev. Mod. Phys. 9, 86 (1937).

Propagation of Spherical Shock Waves in Water

R. H. COLE* AND J. S. COLES**
Woods Hole Oceanographic Institution, Woods Hole, Massachusetts.
December 4, 1946

IN a recent paper in this journal,[1] Osborne and Taylor have reported comparative measurements of shock wave pressures in water at distances of 1 ft. and 31.3 ft. from No. 6 blasting caps (containing approximately 0.3 g of explosive). Their results showed a larger decrease in initial (or peak) pressure of the steep fronted shock wave than predicted from the theory of infinitesimal, spherically diverging waves, but gave no detectable increase in duration of the wave at the larger distance. As Osborne and Taylor show, the attenuation in excess of an inverse first power decrease with distance is a natural consequence of the non-linear propagation and steep fronts of finite amplitude waves. The failure to observe a significant broadening of the decaying pressure profile behind this front as the wave spreads out is, however, puzzling, as this effect is also to be expected both from the hydrodynamical properties of the medium and from results of other experimental work.

Measurements made at the Underwater Explosives Research Laboratory[2] with high explosive charges over a large range of charge weights and distances leave no doubt that both the increased attenuation and spreading of the wave profile predicted by theory are realized to a significant extent. The shock wave pressure decays very nearly exponentially in time at a given point in space until the pressure has fallen to roughly one-third its initial value. In the initial stages, the pressure P at a given point as a function of time t can therefore be characterized by a peak pressure P_m and time constant θ in the formula $P(t)=P_m \exp(-t/\theta)$. At a distance of 20 ft. from a 300-lb. charge of TNT the peak pressure P_m has been measured with tourmaline crystal piezoelectric gauges to be 6000 lb./in.^{2}. At a distance of 500 ft., a value of 160 lb./in.^{2} is

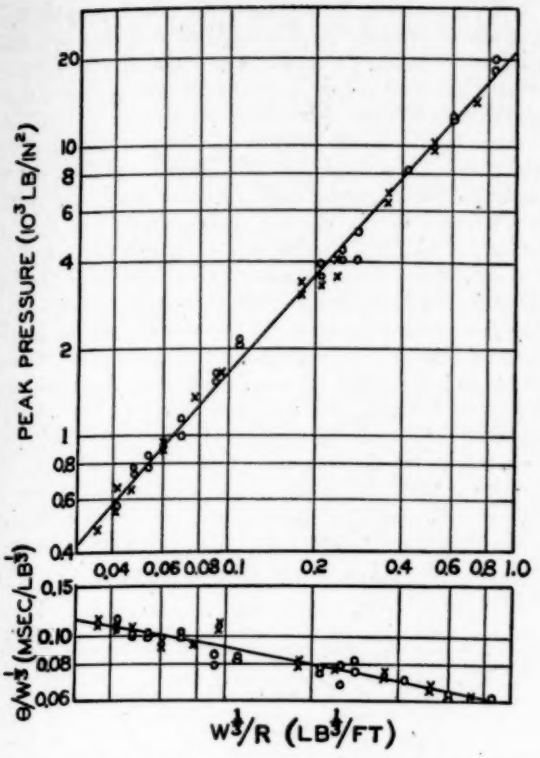

FIG. 1. Peak pressure and reduced time constant for spherical TNT charges of weight W at a distance R. Circles are for 76-lb. charges, crosses for 48-lb. charges.

obtained, or two-thirds the value of 240 lb./in.^{2} which would be realized if the decay were as the inverse first power of the distance. The time constant θ expressing the duration of the pressure is found to increase by nearly a factor of two from 0.50 m sec. at 20 ft. to 0.90 m sec. at 500 ft.

The large differences from the behavior for acoustic waves have been confirmed by so many measurements under widely different conditions that there can be little doubt of their reality. As an example, there may be cited the results of a series of measurements with spherical charges containing 48 and 76 lb. of TNT and at distances from 7 to 100 ft. The peak pressure is found to be a single valued function of the ratio $W^{1/3}/R$, where W is the weight of explosive and R the distance, as shown in the plot of peak pressure against $W^{1/3}/R$ on a double logarithmic scale in Fig. 1. The slope of the best straight line fitting these data is 1.13 and hence the peak pressure varies approximately as $R^{-1.13}$ for the pressure range of these data. The reduced time constant $\theta/W^{1/3}$ should also be a single valued function of $W^{1/3}/R$ (a result of the principle of similarity derivable from the hydrodynamical equations for shock waves), and this is shown by the lower curve of Fig. 1. Although the data have some scatter, they show very definitely the increase in duration of the shock front at greater distances (smaller values of $W^{1/3}/R$).

A very direct indication of the broadening in profile of the shock wave and dissipation at the steep front can also be seen by examination of pressure-time curves which have small bumps or discontinuities behind the front. As the distance increases, the bumps at higher pressure are found to be increasingly far in advance of those in later, lower pressure regions and also are increasingly close to the front. This progression toward, and dissipation at, the front are just what the increasing velocity of sound with pressure leads one to expect, as found for example by the approximate analysis of Osborne and Taylor for plane waves and the more detailed propagation theory of Kirkwood and Bethe[3] for spherical waves.

The failure of Osborne and Taylor to observe the broadening of the shock wave is thus surprising, as the results mentioned here and many others confirm the effect for larger charges and demonstrate the principle of similarity for scaling results to different charge weights and distances. The small quantities of explosive used by these workers do, however, make precise measurement difficult because of the very short durations of the pressure wave, the problem being much less difficult in this respect if larger charges are used.

* Now at the University of Missouri, Columbia, Missouri.
** Now at Brown University, Providence, Rhode Island.
[1] M. F. Osborne and A. H. Taylor, Phys. Rev. 70, 322 (1946).
[2] Established at the Woods Hole Oceanographic Institution, Woods Hole, Massachusetts under OSRD contract OEMsr-569 and under contract with the Bureau of Ordnance, U. S. Navy.
[3] J. G. Kirkwood and H. A. Bethe, "The pressure wave produced by an underwater explosion" I, OSRD Report 588 (available as photostat or microfilm copies from Office of the Publication Board, U. S. Department of Commerce, Washington).

Nuclear Electrostatic Generator

E. G. LINDER
RCA Laboratories, Princeton, New Jersey
October 30, 1946

ELECTROSTATIC generators in which a high voltage is produced by charging a collector by means of high energy particles from a radioactive material have been discussed in several recent articles. Among them is the letter of P. H. Miller[1] who proposed the use of polonium, and suggested that it could be produced from bismuth in a chain reacting pile. There is also the article by M. L. Pool,[2] and that by I. A. Lobanev and A. P. Beliakov.[3] The latter authors state that a nuclear generator was constructed which delivered currents of 10^{-10} to 10^{-9} ampere. The earliest publication on this topic with which the present writer is familiar, is that of H. G. J. Moseley[4] entitled "The Attainment of High Potentials by the Use of Radium," which appeared in 1913. It describes a device yielding potentials of about 150,000 volts.

Interest in this type of device would seem to be justified by its enhanced possibilities in view of the now greatly increased availability of radioactive substances. Since any of the above articles were written, the list of materials obtainable from the Manhattan Project has been published, and it is evident that many more suitable materials are now available than were tried or suggested previously. For example, there is europium 154, caesium 134, and cobalt 60. These have half-lives of several years and are priced at approximately $100 per Curie-year. Furthermore they are beta-ray emitters, and would therefore be more suitable

than an alpha-ray emitter, such as polonium. because of the larger current (of the order of 100 times) obtainable per unit area due to the smaller absorption by the emitting substance. It seems likely that in the future the production of such materials will increase, so that they promise to be obtainable in quantities and at prices which make their use as electric voltage sources worthy of consideration from a practical standpoint.

Plans for constructing such a generator were made in this laboratory last year, and work is now progressing. It is hoped to exceed Moseley's results several-fold, with the help of the new supplies of radioactive materials, modern technique of high voltage insulation, and the use of shields to reduce the deleterious effects of secondary radiations.

Generators of this type offer a means for the direct conversion of nuclear energy into electrical energy. The practical realization of such conversion would seem to depend mainly upon a supply of suitable radioactive material, and probably (at least in the case of large power generators) upon the utilization of a controllable reaction, by means of which the emission of particles could be stopped and started at will.

[1] P. H. Miller, Phys. Rev. 69, 666 (1946).
[2] M. L. Pool, J. App. Phys. 15, 716 (1944).
[3] I. A. Lobanev and A. P. Beliakov, Comptes Rendus, Acad. Sci. USSR 47, 332 (1945).
[4] H. G. J. Moseley, Proc. Roy. Soc. A88, 471 (1913).

Artificial Activities Produced in Europium and Holmium by Slow Neutron Bombardment*

M. G. Inghram and R. J. Hayden
Argonne National Laboratory, Chicago, Illinois
December 6, 1946

A NITRIC acid solution of Ho_2O_3 was irradiated with slow neutrons in an attempt to produce the 35-hour holmium activity reported in Seaborg's table.[1] An aliquot of this irradiated sample was placed on the filament source of a mass spectrograph. By operation of the spectrograph the holmium isotopes were separated according to mass and deposited on a photographic plate. After removal from the spectrograph this plate was placed face to face with another photographic plate, for convenience called a transfer plate. With the passage of time the radioactive decay particles emitted from the active isotope on the first plate gave rise to a developable image on the second plate. After development, the first plate showed the normal holmium spectrum, a strong line at mass 165 due to Ho, and a much weaker line at mass 181 due to HoO. The transfer plate showed a single weak line corresponding to mass 166 on the original plate. A decay curve of another aliquot of the irradiated sample counted for nine half-lives during the period of transfer showed that 96 percent of the activity recorded on the transfer plate decayed with a 27.5-hour half-life, and the remainder with a half-life of approximately 3 hours. Thus we may conclude that the artificial radioactive isotope of half-life 27.5 hours has a mass of 166. This is undoubtedly the same activity given in Seaborg's table as 35 hours. At present the 3-hour activity observed in the sample is ascribed to an impurity of dysprosium.

A nitric acid solution of Eu_2O_3 was irradiated with slow neutrons to produce the 9.2-hour and 5–8-year activities reported in Seaborg's table.[1] The mass of the 9.2-hour activity has been shown to be 152 by previous mass spectrographic analysis.[2] The irradiated sample was allowed to stand for two weeks in order that the 9.2-hour activity might decay. An aliquot of this sample was then run in the mass spectrograph, and a transfer plate was made. Development of the transfer plate showed two lines at masses 152 and 154. The deposit was allowed to stand for 4 months and a second transfer taken. The lines 152 and 154 appeared at the same relative strength as previously. This proved that the mass 152 line was not caused by the 9.2-hour activity of europium. Neither line 152 or 154 can be due to neodymium, illinium, samarium, or gadolinium since these elements emit copiously as NdO^+, IlO^+, SmO^+, and GdO^+ while europium emits only as Eu^+. Thus europium must have two long lived activities, one of mass 152 and one of mass 154, as well as the established 9.2 hour at mass 152. A magnetic investigation of the activities showed no detectable positron emission. Absorption curves showed at least two betas and one gamma. The energy of the gamma was 1.4 Mev.

* This report is based on work performed under Contract No. W-31-109-Eng-38 with the Manhattan Project at the Argonne National Laboratory.
[1] G. T. Seaborg, Rev. Mod. Phys. 16, 1 (1944).
[2] R. J. Hayden and M. G. Inghram, Phys. Rev. 70, 89 (1946).

The Oscillator Concept in the Theory of Solids

E. M. Corson
The Institute for Advanced Study, Princeton, New Jersey
and
I. Kaplan
The Carbide and Carbon Chemical Company, New York, New York
November 18, 1946

A RECENT problem has occasioned the question as to the role which the "bounded" linear oscillator might play in the theory of the specific heats of solids. As is well known, the Debye theory on closer comparison with experiment is in many cases more qualitatively than quantitatively correct, although the Debye specific heat function has certain of the required properties. Heretofore, all attempts to improve the status of theory (anomalies excepted) have been in the direction of obtaining more accurate frequency distributions in the manner of Born, Von Karman, Blackman, *et al.* The common ground of all these analyses has been the basic *a priori* assumption that the oscillator levels are given by $(n+\frac{1}{2})\hbar\omega$; i.e., the "ideal" or "Planck" oscillator.

We do not cavil at the "formal" use of the ideal oscillator in boson theory, but we do ask the question: How is it possible to obtain even qualitatively correct results using this model in the theory of solids? Although it is quite true that the probability amplitude is large only in and near the classical region, the quantizing condition is still the vanishing at infinity so that the amplitude is non-zero (in the strict sense) over a very large region. If, as is generally done, we take the somewhat literal picture of "material" oscillators then it would seem physically reasonable that

we treat instead a "boxed" oscillator in much the same sense as a "boxed" particle in elementary electron theory. This follows both from the point of view of our *a priori* physical knowledge as to the *finite* limits of a material atomic oscillator, and the simple fact that an oscillator in either classical or quantal theory can be termed simple harmonic *only* for *small* displacements. As to the latter, it seems rather meaningless to ascribe specific heat anomalies to anharmonicity in view of the infinite domain accessible to the Planck oscillator, which must be considered as simple harmonic *only by definition*.

The eigenvalues of a bounded oscillator in the first approximation are found to be

$$E_n = n^2h^2/32ma^2 - m\omega^2a^2/n^2\pi^2 + m\omega^2a^2/6, \qquad (1)^*$$

where the boundary conditions are the vanishing of ψ at $\pm a$, and the unperturbed problem is obviously the corresponding boxed particle. This part of the problem is rather trivial, and one may readily verify by the variation theorem that the correction term is as above; $O(a^3)$. These eigenvalues lead to rather involved thermodynamic functions, which however can be approximately evaluated either in terms of Error or Bessel functions. Both methods were used, as was the classical sum of states which is here given since it is useful for asymptotic considerations $(T\to\infty)$.†

$$Q=\left(\frac{kT}{h\omega}\right)erf(z), \quad E=\frac{kT}{2}\left\{2-z\frac{d}{dz}\ln erf(z)\right\}, \qquad (2)$$
$$z=a(m\omega^2/2kT)^{\frac{1}{2}}, \quad E_\infty=kT/2, \quad C_{v\infty}=k/2.$$

We note first of all that this result is not unexpected since the "equipartition theorem" applies only to the momentum in this case, and as might be anticipated on physical grounds (cf. Eq. (1)), the particle properties dominate at high energies (temperature); hence the above asymptotic values. However, the oscillator properties are not completely washed out, and the specific heat curve for $3N$ bounded linear oscillators shows a monotonic decrease to zero in much the manner of the Debye curve. Allowing the lattice parameter to be an arbitrary function of T (varying box, which should correspond closely to calculating $\dot{C}_v$) does not appear to make any significant difference in the conclusions obtained. The correct quantal average energy E and specific heat C_v are found to be remarkably sensitive to small variations in the lattice parameter (our a above). This might lead one to hope that further development along these lines could remove the high temperature anomaly, and hence give a theory of specific heats which introduces the lattice constants in a fundamental way.

However, it seems possible that the real issue involved is that the usual oscillator picture is entirely too literal, and that one must instead treat the elastic oscillations as an ideal "phonon" gas which is again formally described by an aggregate of ideal oscillators as in boson theory. Such a phonon gas is no less real or fictitious than the boson gas, from which it differs only in having a finite frequency spectrum (defined by the modes of the lattice), and longitudinal vibrations. All other properties such as creation, annihilation, non-conservation of numbers, Compton effect, etc., are common to both types of particles. This approach to the problem appears to eliminate most of the conceptual difficulties and leads back to the issue of proper frequency distributions, but it prohibits the interpretation of anomalies in terms of anharmonicity.

* A Morse potential adds a great many terms to the energy, but the essential dependence on the quantum number n, is the same.

† The quantal expressions are not given because they are so lengthy and involved, but they lead to the same conclusions for asymptotic T. Note also in Eqs. (2) that $E\to kT$, $C_V\to k$, as $a\to\infty$.

Centrifugal Fields*

J. W. Beams and James L. Young, III
Rouss Physical Laboratory, University of Virginia, Charlottesville, Virginia

December 5, 1946

RECENT experiments[1,2] on the production of high centrifugal fields have been extended using rotors with somewhat smaller diameters. The various sized rotors have similar spherical shapes and are made of hardened steel. They were suspended magnetically in a vacuum and spun by a rotating magnetic field using an apparatus previously described.[2] Table I shows the new results obtained with the smallest rotor so far tried together with some results previously reported for comparison. The rotational speed measurements were made just before rotor explosion.

Table I.

Diameter of rotor mm	Rotor speed r.p.s.	Peripheral speed cm/sec.	Centrifugal acceleration
1.59	211,000	1.05×10^5	1.43×10^8 g
0.795	386,000	9.65×10^4	2.40×10^8 g
0.521	633,000	1.04×10^5	4.28×10^8 g

It will be observed that each rotor exploded at a peripheral speed of approximately 10^5 cm/sec. Since the rotors were all hard steel and had similar shapes this result is in accord with theory which shows that in a spinning homogeneous elastic rotor the maximum stress produced is proportional to $(2\pi N)^2r^2=v^2$ where N is the number of revolutions per sec., r is the rotor radius, and v is the peripheral speed. In order to measure the rotor speed,[2] one-half of the steel rotor was darkened by dipping it into dilute H_2SO_4 which had been in contact with metallic antimony. Microscopic examination of some of the broken pieces shows that small patches of this coating apparently were ripped off the periphery of the 0.521-mm rotor where this coating was too thick. From the table it will be observed that this rotor attained a speed of 633,000 r.p.s. which gave a centrifugal field of 428 million times gravity.

We are much indebted to the New Departure Division of the General Motors Company for supplying us with the steel balls from which the 0.521-mm rotors were made.

* This work has been supported by the Bureau of Ordnance, U. S. Navy under Contract NOrd-7873.

[1] J. W. Beams and J. L. Young, III, Phys. Rev. **69**, 537 (1946).
[2] J. W. Beams, J. L. Young, III, and J. W. Moore, J. App. Phys. **17**, 886 (1946).

Concentration of Plutonium in Pitchblende

M. I. CORVALEN
Instituto de Física, Universidad Nacional de la Plata, Argentina
October 19, 1946

IN a recent paper[1] Marieta da Silveira succeeded in explaining anomalies in the penetrating power of γ-rays belonging to U-products by a spontaneous neutron emission attributed to ${}_{91}UX_2^{234}$, and stated important experimental evidence for the neutron radiation. According to her results the disintegration scheme of U becomes

$$ {}_{92}UI^{238} \xrightarrow{\alpha} {}_{90}UX_1^{234} \xrightarrow{\beta} {}_{91}UX_2^{234} \xrightarrow{\beta} {}_{92}UII^{234}, $$
$$ {}_{91}UX^{233} \xleftarrow{n} $$

We have investigated the question whether the neutron emission of UX_2 can explain the existence of plutonium in a uranium deposit found by Seaborg.[2]

Neutrons from UX_2 should indeed slow down in small steps by colliding with heavy atoms passing through the 38-ev resonance region of ${}_{92}U^{238}$ and producing successively ${}_{92}U^{239}$, ${}_{93}Np^{239}$ and ${}_{94}Pu^{239}$ (10^6 years).

Taking into account the lifetime of Pu and assuming that all neutrons emitted by UX_2 lead to the formation of Pu-atoms we obtain an equilibrium concentration of Pu of 4.10^{-12} percent. Less favorable absorption capture by other nuclei present would reduce the mentioned equilibrium concentration.

It is therefore not impossible that the plutonium found by Seaborg in the pitchblende is caused by the spontaneous neutron emission of UX_2.

[1] Marieta da Silveira, *Contribuição para o estudo da radiações do UX complexo Publicação* No 2. Faculdade de Ciências de Lisboa, Portugal, 1945.
[2] Glenn Seaborg, Chem. and Eng. News, p. 2190 (December 10, 1945).

Proceedings of the American Physical Society

Meeting of the New England Section at New Haven, Connecticut, October 26, 1946

THE twenty-seventh meeting of the New England Section of the American Physical Society was held at the Sloane Physics Laboratory of Yale University in New Haven, Connecticut, on Saturday, October 26, 1946. At least one hundred and fifteen members were in attendance. The programme included a symposium of six invited papers on the subject of microwaves and twelve contributed ten-minute papers. There follow the titles of the invited papers and the abstracts of the ten-minute papers.

At the business meeting the following officers were elected for 1947:

Chairman, H. Margenau, *Yale University.*
Vice Chairman, K. T. Bainbridge, *Harvard University.*
Secretary-Treasurer, G. F. Hull, Jr., *Dartmouth College.*
Programme Committee, R. D. Rusk, *Mount Holyoke College*, C. W. Miller, *Brown University.*

Invited Papers

Microwave Circuits. C. G. Montgomery, *Yale University.*

Microwave Studies of Electrical Discharges in Gases. S. C. Brown, *Massachusetts Institute of Technology.*

Absorption of Microwaves by Liquids. D. H. Whiffen, *Oxford University.*

Absorption of Microwaves by Gases. W. D. Hershberger, *RCA Laboratories.*

Molecular Line Spectra in the Microwave Region. C. H. Townes, *Bell Telephone Laboratories.*

Experiments in Gaseous Absorption at Microwave Frequencies. R. Beringer, *Yale University.*

Contributed Papers

1. The Metastable State $a^1\pi g$ of N_2 as a Factor in Active Nitrogen. Roland Meyerott, *Sloane Physics Laboratory, Yale University.* Herzberg* has suggested from spectroscopic evidence, that the $a^1\pi g$ state of N_2 (the lowest known excited singlet state) is metastable. Conclusive evidence for this is lacking, since the fine structure of bands originating or ending on this state has not been resolved. Additional support to Herzberg's conclusion can be found in the spectra of impurities in active nitrogen. Two types of transitions are possible for an N_2 molecule in the $a^1\pi g$ state on collision with an impurity molecule having the proper energy levels; either the transition $a^1\pi g \rightarrow X^1\Sigma g^+$, or $a^1\pi g \rightarrow A^3\Sigma u$. The first is forbidden (if Herzberg's conclusions are correct) since it is a g to g transition, while the second is a singlet to triplet transition. The spectra of the impurity, then, must originate in energy levels above the ground state, corresponding to the energy available in the particular N_2 transition. The CN red system and the lower vibrational levels of the CN violet systems excited in active nitrogen will be discussed as examples of enhancements due to the $a^1\pi g \rightarrow A^3\Sigma u$ transition, while the ultraviolet bands of N_2^+ will be used as an example of enhancement due to the $a^1\pi g \rightarrow X^1\Sigma g$ transition.

* G. Herzberg, Phys. Rev. 69, 362 (1946).

2. Ultraviolet Bands of Nitrogen. R. B. Setlow, Roland Meyerott, and W. W. Watson, *Sloane Physics Laboratory, Yale University.* Rotational constants for the upper $^2\Sigma$ state involved in the ultraviolet bands of N_2^+ have been measured for several vibrational levels. Thus vibrational constants are given in terms of band origins rather than band heads. The peculiar intensity distribution in these bands obtained using a discharge in nitrogen will be discussed and correlated with the previous paper by one of us. Gaydon and Penney,[1] in discussing the dissociation energy of CO^+, rest their argument, in part, on the break in the $\Delta G - v$ curve for the upper $^2\Sigma$ state of N_2^+.[2] The evidence for this break has been reexamined and is considered insufficient basis for postulating its existence. Two of the upper states of N_2 discovered by Watson and Koontz[2] have been assigned by Tschulanowsky[3] to vibrational levels 2 and 3 of Birge and Hopfield's b' state.[4] Plates taken of a discharge in nitrogen showed single headed bands at the same position as the double headed ones of Hopfield's c state. The observed frequencies of these bands correspond to those expected from transitions of the $v=1$ level of b' to the ground state.

[1] A. G. Gaydon and W. G. Penney, Proc. Roy. Soc. A183, 374 (1944).
[2] W. W. Watson and P. G. Koontz, Phys. Rev. 46, 32 (1934).
[3] W. M. Tschulanowsky, Bull. Acad. Sci. U.S.S.R. 1313 (1935).
[4] R. T. Birge and J. J. Hopfield, Astrophys. J. 68, 257 (1928).

3. Line Strengths in the FeI Spectrum in Intermediate Coupling, with Application to the Solar Curve of Growth. Winston M. Gottschalk,* *Raytheon Manufacturing Company, Waltham, Massachusetts.* Menzel has given the theory of the curve of growth of a star, the curve of growth being essentially a plot of stellar intensity against theoretical intensity. Curves of growth for the sum have been derived by several authors. One objection to the validity

of values derived from the curve of growth has been the use of line strengths based on the Russell-Saunders approximation in atomic spectra. Wright, in particular, has avoided this difficulty by using measured values of intensities in the FeI and TiI spectra. The formalism for the computation of line strengths in intermediate coupling is given in Condon and Shortley *Theory of Atomic Spectra*. This was adapted to a transition array in the FeI spectrum with reasonable success. As a check on the transformation matrices used g values were computed and agree with experimental values. The curve of growth plotted from these computed line strengths is in substantial agreement with curves of other investigators. A long range program of computing line strengths in intermediate coupling should be undertaken in order to provide the astrophysicist with useful tables of line strengths.

* This work was done at Harvard University and is part of a thesis submitted to Harvard University in partial fulfillment of the requirements for the degree of Doctor of Philosophy.

4. Perot-Fabry Interferometers as Filters (with demonstrations). H. M. O'BRYAN, *Baird Associates, Cambridge, Massachusetts.*—The Perot-Fabry interferometer has been used for measurement of spectral lines for many years and recently filters have been obtained from Germany which are based on this principle. Filters of this type made by the Evaporated Metal Films Corporation will be shown and some of their unique properties described. The filters are made by evaporation of two metallic semi-reflecting layers with an evaporated dielectric layer several wave-lengths thick. The transmission bands are approximately 150Å wide with a maximum of about 30 percent at normal incidence. The order of interference varies from 2 to 10 wave-lengths. At oblique incidence the transmission band shifts toward shorter wave-lengths and splits into two bands of different polarization. These filters make it possible to demonstrate before a large audience some aspects of interference and are also useful in many experiments in spectroscopy and optics.

5. Physical Interpretation of Electromagnetic Radiation from an Antenna. RONOLD W. P. KING, *Cruft Laboratory, Harvard University.* The physical interpretation of electromagnetic radiation from an antenna has been confused by two common errors. These are the assumptions (1) that the axial distribution of current in a cylindrical antenna is sinusoidal and (2) that the Poynting vector is a true measure of the direction and magnitude of "energy flow" at every point in space. Conclusions which follow the making of both errors, of each error separately, and of neither error are considered and discussed in terms of their physical and practical significance in the theory of antennas. The importance of careful presentation of electromagnetic principles in the classroom is pointed out.

6. Optical Theory of the Corner Reflector, ROY C. SPENCER,* *AAF, Air Materiel Command, Watson Laboratories, Cambridge Field Station, Cambridge, Massachusetts.* A corner made from three glass mirrors enables one to observe the regions of the incident plane wave which undergo single, double, or triple reflection. All three are analyzed. Only the triple reflection is at all times exactly reversed causing a maximum signal at the transmitter. The equivalent scattering cross section σ of the corner is $4\pi(A/\lambda)^2$ where A is the actual cross section of the triply reflected beam. A has a maximum value A_0 along the symmetric axis of $a^2/\sqrt{3}$ for triangular corners and $\sqrt{3}a^2$ for square corners where a is the edge. A chart gives σ for various values of a and λ. The variation of A with direction of the line of sight is illustrated by means of cardboard models. The equations for A are derived and the results shown in charts. For the triangular corner, A/A_0 approximates a paraboloid of revolution $(1-.00076\delta^2)$ for $\delta<26°$ where δ is the deviation in degrees from the symmetric axis. For the square corner A/A_0 approximates a cone $(1-.0274\delta)$ for $\delta<26°$ which makes it unsuitable as a standard target. The analysis of the effect of errors in perpendicularity of adjacent sides, as treated by G. A. Van Lear, Jr., has been extended and applied to both triangular and square corners.

* Formerly, Radiation Laboratory, Massachusetts Institute of Technology, Cambridge, Massachusetts. This paper is based on work done for OSRD under Contract OEMse-262 with M.I.T.

7. Large Angle Scattering of Gamma-Radiation. E. C. POLLARD AND B. B. BENSON, *Yale University.* Observations of the scattering of gamma-radiation from Mg^{24} (from the beta-decay of Na^{24}) by lead, copper, aluminum, and magnesium at an average angle of 135° have been made. In order to determine the proportion of Compton scattering and annihilation radiation, absorbers up to 2.2 cm thickness have been placed around the counter used to detect the gamma-rays. In the case of copper and aluminum the results indicate that the great majority of scattered radiation is attributed to Compton recoil and annihilation. Some additional effect seems definitely to be present in the case of lead scattering. Comparison of the scattering from aluminum and magnesium should show the presence of resonant absorption and re-emission from Mg^{24}. There is some evidence that there is an excess of scattering by Mg^{24} at high counter absorption. An estimate of the cross section gives a probable value of 2×10^{-27} cm^2 with an upper limit of 5×10^{-27} cm^2. This corresponds to a line width of the order of 1/100 ev which would be a reasonable fit to a quadruple transition.

8. The Determination of Small Time Intervals between Related Nuclear Events. H. L. SCHULTZ, *Yale University.* The method to be described makes use of techniques for the accurate measurement of very short time intervals between electrical pulses. It can be applied in the determination of short lived activities where related nuclear events occur (e.g., the case of ThC′ or RaC′ where a β-particle leads to the formation of the element which subsequently emits an α-particle). The method is applicable also to the determination of time of flight of charged particles. The equipment consists of two proportional counters with independent wide band amplifiers each feeding into a coincidence circuit of high resolving power. The number of coincidences is measured as a function of time delay introduced electrically in one of the channels. Preliminary measurements show that for simultaneous excitation of

both amplifiers by a pulse signal generator a variation in electrical delay of approximately 10^{-9} sec. can be detected. However, in actual nuclear applications the precision is reduced because of the statistical nature of the ionization process and because of the fact that pulse shape will depend upon the direction of entry of the ionizing particle into the counter. For the case of α-particles traversing two counters placed in line under highly collimated conditions, a time of flight in the region of 10^{-8} sec. can be detected.

9. Reversible Binary Counter and Shaft Position Indicator.* H. P. STABLER, *Williams College.* A binary counter has been developed that responds to subtracting pulses as well as to adding pulses. The two types of pulses are distinguished by different input channels, by polarity, or by size, and the reversible action is accomplished by suitable carry-over provisions between the counter stages. Each stage employs four 6AK5's. Resolving times of 10^{-8} sec. and less are readily obtainable. In conjunction with a photoelectric actuated pulse generator and a reading circuit, the counter has been used to indicate the angular position of a rotating shaft. The pulse generator produces adding pulses for clockwise rotation of the shaft and subtracting pulses for counterclockwise rotation. The reading circuit "scans" the several counter stages and gives the counter reading in the form of a microsecond pulse binary wave form number. While the system has been designed to provide one of the input parameters to a digital electronic computer, the methods employed can be used for other situations involving two directional motion and differential counting.

* This paper is based on work done at the Radiation Laboratory, Massachusetts Institute of Technology, for the Office of Scientific Research and Development under contract OEMsr-262.

10. A Proposed Focusing Cosmic-Ray Telescope. W. T. HARRIS, *United States Time Corporation, Waterbury, Connecticut.* A magnetic lens which will focus charged particles entering its aperture parallel to the axis can be constructed in the form of a toroidal winding. For an air or iron core toroid, the cross section of the winding is parabolic. If partial iron filling is used, trapezoidal or rectangular cross sections may be employed to produce sharp focusing. The focal length is proportional to the particle momentum, and hence a telescope of this type is also a spectrograph. By using coincidence counters and anticoincidence guard counters for observations, a collimating tube effect can be obtained, permitting full use of the properties of the telescope lens without a background due to particles which do not pass through the lens. There are some advantages to an installation in a deep shaft in the earth having two lenses. With such a device charged and uncharged components can be studied separately.

11. Free Ring Discharge in a Metallic Torus. CHARLES G. SMITH, *Raytheon Manufacturing Company,* Waltham, Massachusetts.* The limits of intensity of excitation of a gas at pressures below .001 mm can apparently be extended if a toroidal discharge is arranged so that unwanted magnetic fields are controlled. One field, that linking the torus supplying the current driving e.m.f., is confined in a closed iron core upon which the primary winding is uniformly distributed. This field links without invading the discharge region. The second field, that of the gaseous current, usually reacts upon the discharge forcing it against the outer walls of the torus. By employing a metallic torus (conducting except for a radial insulating cut to prevent short circuiting the driving e.m.f.) a new distribution of the second field results causing the current to be held away from the walls. The resulting discharge should be free of material bounds. Mercury vapor at about .0004 mm pressure within a cast aluminum torus was energized by 890-cycle e.m.f. at 8 volts. Current in the vapor (600 amperes) was more than that in a comparable glass torus. However, glass side arms glowed brilliantly indicating appreciable electron bombardment of the toroidal boundary after all. The observations nevertheless encourage further effort.

* Experiments were done at Harvard University.

12. Interpretation of the Microwave Absorption of HDO at 1.3 Centimeters. GILBERT W. KING AND R. M. HAINER, *Arthur D. Little, Inc., Cambridge, Massachusetts.* The pure rotational absorption spectrum of HDO differs from those of H_2O or D_2O because the permanent dipole moment has components along both the axes of intermediate and least moments of inertia. The selection rules for the latter component are quite different from those of the former, which obtain alone in H_2O and D_2O. They permit transitions between neighboring rotational levels which are split from the doubly degenerate levels of the prolate symmetric rotor. This splitting is a function of the K_{-1}-index of the level, and covers (for a rigid rotor) the whole range from a few to less than 10^{-5} cm^{-1}. Thus absorption lines of HDO will occur throughout the microwave and radio regions. HDO is of further interest in that its rotational term values are not known. A completely resolved vibrational band of HDO at 1.1μ has been analyzed by Herzberg[1] and effective moments of inertia of the ground state determined. With these, one can calculate the position of lines in the microwave region with sufficient accuracy to guide experimental investigation, from the theory of the rigid rotor, because, although deviations from this theory due to centrifugal distortion and the like are high, as in H_2O and D_2O, these corrections cancel to a large extent in the transitions considered since they are between neighboring levels of the same J and K_{-1} values. The absolute intensity of absorption can be calculated quite accurately because the dipole moment and line width will be the same as the known values of H_2O. At our suggestion, Townes[2] has investigated the region of 0.7 to 0.8 cm^{-1}, and found a line at 0.7441 cm^{-1}, with absorption coefficient of $30\pm14\times10^{-6}$ cm^{-1}. The transition $5_{33}-5_{32}$ is predicted at 0.79 cm^{-1} with absorption coefficient of 26×10^{-6} cm^{-1}. There are other lines which would have more nearly the observed absorption, were they to appear at .74 cm^{-1}; but the required change in position we believe is outside the possible corrections that could be added in the calculations of the energy levels based on the rigid rotor.

[1] L. Herzberg, Zeits. f. Physik **107**, 549 (1937).
[2] C. H. Townes and F. R. Merritt, Phys. Rev. **70**, 558 (1946).

Proceedings of the American Physical Society

MINUTES OF THE

MEETING AT MINNEAPOLIS, MINNESOTA, NOVEMBER 29–30, 1946

THE 275th meeting of the American Physical Society was held at Minneapolis, in the Physics Building of the University of Minnesota, on Friday and Saturday, November 29 and 30, 1946. With about two hundred registrants, and some two hundred and seventy-five people in attendance at the most populous session, this meeting assumed the congenial character of those of the pre-war days: no simultaneous sessions and no overcrowding. There were three invited papers, by S. A. Goudsmit, H. D. Hagstrum, and D. W. Kerst, respectively; contributed papers numbered thirty-five. The arrangements for the meeting were very well handled by J. W. Buchta and Mrs. J. T. Tate.

The dinner was held in the Coffman Memorial Union on the Friday evening, with an attendance of 196. E. U. Condon gave an analysis of the various proposals for a National Science Foundation which came before Congress in 1946, and J. T. Tate received from Columbia University a medal signalizing his eminent contributions to the war effort. Impressive movies of the events at Bikini were exhibited.

The Council met on Saturday afternoon and evening. It elected to Fellowship the eight candidates and to Membership the one hundred and eighty-six candidates whose names appear below. The Council also nominated to the Governing Board of the American Institute of Physics J. T. Tate and E. U. Condon for three-year terms and A. J. Dempster for a two-year term. Including L. A. DuBridge and G. B. Pegram who continue in office, the Governing Board will after next February comprise five representatives of the American Physical Society.

The Society has lost through death the following Fellows and Members: J. R. Carr (Zurich), H. L. Cooke (F, Princeton), Dunham Jackson (F, Minnesota), Enoch Karrer (F, New Orleans), G. N. Lewis (F, University of California, Berkeley), P. K. McGall (Orange, N. J.), P. S. Turner (Washington, D. C.), J. E. Walter (Princeton), J. M. Willson (Rolla, Mo.).

Elected to Fellowship: C. R. Burrows, R. F. Christy, J. M. Davies, D. J. Hughes, Urner Liddel, J. A. Simpson, A. M. Weinberg, and G. J. Young.

Elected to Membership: N. Z. Alcock, Robert R. Allen, R. O. Anderson, George B. Arfken, Jr., Emerson D. Bailey, Carl Ernest Behrens, Felix M. Beiduk, Locklin Savage Bell, Philip Joseph Bendt, Verne Harrington Berry, Paul L. Betz, Karl W. Bewig, Garrett Birkhoff, John S. Blair, Ingram Bloch, Ralph Herbert Blumenthal, Lawrence A. Bornstein, Ralph Bray, Laurie Mark Brown, Gordon Lee Brownell, Donald C. Brunton, Anne Mary Buchy, Lawrence Whitney Burgess, Henry J. Butler, Julius H. Cahn, Hartman B. Canon, H. B. G. Casimir, Louis Chandler, Robert L. Chapman, Francis H. Clauser, Martin J. Cohen, Marius Cohn, Richard Louis Conklin, Thomas Coor, Jr., James Edward Corry, Jr., George Edward Crouch, Jr., Cassius W. Curtis, G. C. Dewey, Jean E. Dickey, Kenneth Edwin Dorcas, John J. Downing, Sidney David Drell, Ralph William Dressel, Stuart B. Dunham, William Walter Durding, Shirley L. Eberlin, Bengt Edlin, Daniel M. Ekstein, James Emmett Erickson, Gustave A. Essig, Harold Feeny, Fred G. Fender, John H. Fergus, Kenneth R. Ferguson, Bernard A. Fleishman, Sidney Frankel, Rachel G. Franklin, Hans Frauenfelder, Henry Charles Froula, Jr., Everett Gladding Fuller, Simeon V. Galginaitis, Richard Lawrence Geiger, Stanley Geschwind, Marvin L. Goldberger, Howard D. Goldgraber, James N. Grant, Victor Graziano, John H. Greig, John W. Gryder, Robert C. Gunton, Charles B. Haenny, Erwin Louis Hahn, Crockett Hall, Jr., Herbert J. Hall, Robert H. Hardoen, David Harker, Jack Heller, Donald L. Herr, Joseph Hirsch, Paul O. Hoffmann, John Hovorka, Horia Hulubei, Frank B. Isakson, Mary Caroline Jansen, Walter C. Johnson, Abraham Karen, Jesse R. Karp, David R. Kasanof, Robert H. Kasriel, Samuel C. Kelly, Charles T. Keniston, Madeline C. Kessler, Simon C. Kirsch, E. D. Klema, George Kolodny, Alexander Kossiakoff, Bernard Kramer, Henry Lawrence Kraybill, K. S. Krishnan, Charles B. Kunz, Louis Landweber, Jean Langevin, Elmer C. Larsen, Philip G. Law, Richard W. Lee, Lucille Leibowitz, Meyer Leifer, Alfred Leitner, Franklyn Kussel Levin, Leo Charles Levitt, George G. Libowitz, William A. Lindeke, Harry J. Lipkin, Stuart Phinney Lloyd, Idos W. Lohmann, Albert London, William Low, Franklin E. Lowance, James E. LuValle, Lloyd Godfrey Mann, Pierre Marmier, Marvin D. Martin, Joe T. Massey, Everett Lee McCleary, Robert E. McConnell, Harry Joseph McCready, Jr., William G. McMillan, Jr., Franz Metzger, John William Mihelich, Julian Malcolm Miller, Jatinder Nath Nanda, David B. Nicodemus, Sol Nudelman, Irving P. Orens, Jehuda Ovadia, Harry Palevsky, Robert G. Parr, Philip Parzen, T. P. Pepper, I. Perlman, Rolland Perry, Helen Peterson, Jack M. Peterson, James Alfred Phillips,

Herbert Priestley, Richard D. Radford, Robert Basil Randels, George Rappaport, Jerome M. Rehr, J. Gordon Retallack, Charles A. Reynolds, Joseph M. Reynolds, Richard Ayer Rhodes II, John E. Richardson, Kenneth Clay Ripley, Robert Sumner Rochlin, George Wayne Rodeback, Philip Rosen, Stanley Rowlands, James Reynolds Sagurton, Vance L. Sailor, Oscar Sala, Jacob Schroeder, Ernest Sharo, John R. Sites, Philip Bartlett Smith, Harold Stein, Jack Steinberger, Peter A. Stewart, William H. Sullivan, Karl Dale Swartzel, Ernest A. Taft, Paul Tamarkin, Stephen Tamor, William C. Taylor, D. Ter Haar, Frederick W. Van Name, Jr., Jerry M. Waite, Joseph Henry Wegstein, Leslie Swales Wilcoxson, John E. Willard, Bruce Donald Witwer, Joseph Laurence Wolfson, Donald Calhoun Worth, Marvin Eugene Wyman, and Marshall C. Yovits.

The names of the invited speakers and titles of their papers, and the abstracts of the contributed papers, are printed hereinafter.

KARL K. DARROW, *Secretary*
American Physical Society
Columbia University
New York 27, New York

Invited Papers

Why Germany had No Atomic Bomb. S. A. GOUDSMIT, *Northwestern University.*
Molecular Ionization and Dissociation Induced by Electron Impact. H. D. HAGSTRUM, *Bell Telephone Laboratories.*
The Design of the Large Illinois Betatron. D. W. KERST, *University of Illinois.*

ABSTRACTS OF CONTRIBUTED PAPERS

A1. Rotational Structure of InCl Bands at 2670A. J. G. WINANS AND H. M. FROSLIE, *University of Wisconsin.*—InCl bands near 2670 were photographed with dispersion 0.6 A/mm with absorption cells containing $InCl_3$ and excess of indium metal. The isotope effect showed carrier InCl not HgIn.[1] Observations and vibrational analysis of Miescher and Wehrli[2] were verified. System is probably $^1\Pi_1 \rightarrow {}^1\Sigma_0{}^+$. Bands with $v'=1$ show no rotational structure. Assuming dissociation products In $^2P_{1/2}$+Cl $^2P_{1/2}$ and predissociating limit In $^2P_{1/2}$+Cl $^2P_{3/2}$ fixes D_0'' between 4.62 and 4.65 volts. The 00 Q branch extends to $m>100$. For Q, $\nu = 37{,}410.599 - 0.00696\ m(m+1) - 1.39\times10^{-7}m^2\ (m+1)^2$. For P, $\nu = 37{,}410.599 + 0.214\ m - 0.00696m^2$. The unresolved R branch has head at 37,412.251 cm^{-1}. These give $B_0' = 0.1037$, $B_0'' = 0.1107$. Analysis of band 0–2 gives $B_0'' = 0.1032$, $B_2'' = 0.1093$ cm^{-1}. These give $r_0'' = 2.38$A.

[1] J. G. Winans, Francis Davis, and Victor Leitzke, Phys. Rev. **57**, 1079 (1940).
[2] E. Miescher and M. Wehrli, Helv. Phys. Acta **7**, 298 (1934).

A2. An Experimental Relation Between ω_e and Reduced Mass for Diatomic Molecules. R. L. PURBRICK, *University of Wisconsin.*—An equation of the form

$$\omega_e = a + c\mu^b$$

has been applied to the molecules of the first column of the periodic system. With constants $a=0$, $b=-0.734$, and $c=878.6$, the equation predicts ω_e for both molecules having identical nuclei and those formed from non-identical alkali atoms. The equation shows that the force constant, K, is approximately the same for these molecules. Indications are that similar equations may be developed for other columns of the periodic system, but with different constants.

A3. The Analysis of Molecular Spectra and the Calculation of Thermodynamic Quantities. ENOS E. WITMER, *Thermodynamics Research Laboratory, University of Pennsylvania.*—It is generally agreed that zero-pressure values of enthalpy, reduced entropy, and specific heat for gases can be calculated from spectroscopic data more accurately than they can be inferred from calorimetric measurements extrapolated to zero pressure. The University of Pennsylvania Thermodynamics Research Laboratory, operated under contract with the Navy Department, Bureau of Ships, has undertaken a comprehensive program of calculations aimed at obtaining definitive information regarding gases and gas mixtures of technical importance. In this connection it has been deemed advisable to improve existing machinery for the analysis of the spectra of polyatomic molecules. To that end, a very accurate and fine-grained table for computing quickly and accurately the energy levels of the asymmetric rotator is being prepared. The paper will discuss this table in relation to others previously published.

A4. Decay of Phosphorescence in Cu-Activated ZnS. HUBERT M. JAMES, *Purdue University, West Lafayette, Indiana.*—Phosphorescent fine-grained Cu-activated ZnS gives rapidly decaying flash radiation with intensity $I \cong I_0/(1+At)^2$, followed by more persistent radiation with intensity $I = C/(t+t_0)$ through a range of 10^4 in I. Here t is time elapsed after excitation and $t_0 \cong 2\times10^{-4}$ sec. These and other observations can be explained quantitatively if the trapping states in the crystal are surface states such as those discussed by Tamm. The conduction band is pictured as consisting of two parts, the main part corresponding to states in which the excited electrons move throughout the body of the crystal, and the lower to states in which they are trapped on the surface. The density of levels in the trap will be much smaller than that in the main band; both densities are assumed uniform. Thermal equilibrium is assumed between electrons in all these states. It is essential to apply the Fermi-Dirac statistics in discussing this equilibrium, since the trapping states may be almost filled. Only electrons in body states can reach holes and radiate; I is proportional to the product of this number and the number of holes. The theory satisfactorily describes the entire course of the intensity decay, and yields reasonable estimates of the characteristics of the trapping band.

A5. Minimum Sparking Potentials of Barium, Magnesium, and Aluminum in Argon. HAROLD JACOBS AND ARMAND P. LAROCQUE, *Sylvania Electric Products, Inc.*—Minimum sparking potentials of barium, magnesium, and aluminum in argon are found to be $93\pm\frac{1}{2}V$, $123\pm1V$, and $155\pm1V$, respectively. Utilizing the data in measuring the minimum sparking potentials, the ratios of electrons emitted from the cathode per bombarding positive ion (γ_m) are determined and found to be $0.149\pm.001$ for barium, $0.089\pm.033$ for magnesium, and $0.045\pm.002$ for aluminum. A relationship is found such that, at a given field per unit pressure, a lower work function indicates a lower sparking potential and a higher γ_m indicates a lower sparking potential, for the case of the three metals studied. A graphical method is proposed for predicting the minimum sparking potentials for metals, whose sparking potential values have not been determined, based upon the values of γ_m or the work function ϕ.

A6. Photoelectron Emission from Liquid Ammonia Solutions of the Alkali Metals. GORDON K. TEAL, *Bell Telephone Laboratories*.—The photoelectron emission of liquid ammonia solutions of sodium, potassium, and cesium was studied. Spectral sensitivity measurements on concentrated solutions of sodium and of cesium at -78°C reveal maximum responses at $\lambda=5200$A. Copper-colored (concentrated) and intensely blue (dilute) solutions of potassium both gave maxima at $\lambda=4800$A, the magnitude of the response being greater for the more concentrated solution. Sodium solutions are relatively insensitive in comparison to solutions of potassium and cesium. The long wavelength limits for all solutions studied are greater than 7000A and less than 9000A. The results are in agreement with the view that the valence electrons from the alkali metals are not closely associated with the alkali metal atoms but exist in energy states characteristic of the solvent and are bound with approximately the same energy for concentrated and moderately dilute solutions of all the alkali metals.

A7. A Measurement of the Self-Diffusion Coefficient of Uranium Hexafluoride.* EDWARD P. NEY AND FONTAINE C. ARMISTEAD,** *Rouss Physical Laboratory, University of Virginia*.—A method has been developed and successfully used for the measurement of ρD (ρ = density; D = diffusion-coefficient) for an isotopic mixture. The D thus measured should be a close approximation to the true self-diffusion coefficient. Two vessels were filled with UF_6 vapor of different isotopic concentrations but equal pressure. To start the experiment, the material in the two vessels was allowed to diffuse through a connecting pipe. The isotopic ratio in one vessel was measured as a function of the time with a mass spectrometer into which a very small sample was continuously being drawn. The isotopic ratio measured by the mass spectrometer is an exponential function of the time. The relaxation time together with the dimensions of the apparatus give the self-diffusion coefficient. Knowledge of the pressure allows calculation of ρD. The value of ρD at 30°C is 234 micro poise ±5 percent. Classically ρD is associated with the viscosity through the equation $\rho D = e\eta$, where e is a pure number whose value is determined by the force law interaction of the molecules. Therefore, knowing the ratio of ρD to the viscosity, one can determine the force law interaction.

* This paper is based on work performed under Contract OEMsr-393 with the Office of Scientific Research and Development at the University of Virginia in 1942–1943.
** Now at Clinton Laboratories, Oak Ridge, Tennessee.

A8. Bridge Type Electrical Computers. WILLIAM KRASNY ERGEN, *Minneapolis-Honeywell Regulator Company, Minneapolis, Minnesota*.[1]—The prototype of the computers in question is a Wheatstone bridge, with the resistances in two opposite legs proportional to two magnitudes, a and b respectively, and the resistance in a third leg proportional to c. The fourth leg is adjusted to balance the bridge, either manually or by a servo mechanism. The resistance of the fourth leg is then proportional to ab/c. This bridge can be generalized by replacing the resistors in each leg by a series connection of resistors, each of which is proportional to a variable. Such a bridge solves quadratic equations, but only if the equation is of rank 4 and signature zero. By connecting several resistances in parallel into each leg of the bridge, one can solve higher order equations. A bridge used for the solution of a quartic equation will be shown. The equation was the equation of a straight line in bipolar coordinates and was used to guide an airplane on a straight line when the distances of the plane from two fixed ground stations were known by Shoran.

[1] Now at RCA Victor Division, Radio Corporation of America, Camden, New Jersey.

A9. Single Magnetic Poles and Cosmic Radiation. FELIX EHRENHAFT, *New York, New York*.—Photomicrographs will be shown of iron particles of light wave-length magnitude moving in helical paths in constant homogeneous magnetic fields (e.g., 3000 gauss), describing more than 40 regularly spaced equidistant turns per second (e.g., diameter 10^{-3} cm and pitch 2.5 times 10^{-3} cm) and bursts of clusters occurring in such fields each part of the cluster describing separately its own helical path after the burst. After many different experiments, movements of matter in homogeneous magnetic fields, reversal of movements with reversal of fields, and helical paths have been confirmed by Tauzin[1] and Rault who could find no other explanation[2] than single magnetic poles.[3] Single magnetic charges can be replaced neither by Ampere's circuit electric currents nor by spin of electrons. The admitted failure[4] in explaining the structure of elementary particles in cosmic radiation originates in the unfounded assumption that charged particles bear only electronic charges and in the non-recognition of magnetic charges. Electrically charged and uncharged particles can also bear magnetic charges. By taking into account that magnetism flows and penetrates matter the understanding of the phenomena of cosmic radiation will be facilitated.

[1] P. Tauzin; P. Tauzin and L. Rault, Soc. franc. de physique, Nov. 16 (1945); May 17 (1946); Comptes rendus 222, 1037 (1946).
[2] A. Cotton, Ann. de physique 20, 557 (1945).
[3] F. Ehrenhaft, J. Frank. Inst. 233, 236 (1942); Science 101, 676 (1945); Comptes rendus 222, 1100, 1345 (1946).
[4] W. Heitler, Bull. Am. Phys. Soc. 21, No. 5, 14 (September 19, 1946).

B1. The Electrical Charge on Precipitation at Various Altitudes and its Relation to Thunderstorms. Ross Gunn, *Army-Navy Atmospheric Electricity Project, Naval Research Laboratory, Washington, D. C.*—The free electrical charges on individual precipitation particles were measured at various altitudes up to 26,000 feet by an induction method that avoids touching them. In a weak cold front exhibiting no thunderstorm activity, and having the freezing level at 11,000 feet, positive charges averaging 0.033 e.s.u. were observed from 10,000 to 26,000 feet. Negative charges averaging 0.04 e.s.u. were measured from the surface up to 20,000 feet. Positive charges were not observed below 10,000 feet and negative ones were not detected above 20,000 feet. Between these levels a mixture existed. The free charge on a large number of the particles was so great that the electric field at their surface was an appreciable fraction of the breakdown field for air, showing that powerful electrifying agencies exist even under rather quiet frontal conditions. Electric field measurements on the airplane show that the particle charges are largely neutralized by nearby charges, presumably on the air or on the tiny cloud droplets. It is shown that the removal of this neutralizing charge will immediately produce thunderstorm electric fields and potentials. A time plot of the electric field on the surface of a flying airplane during the interval of a lightning strike is given.

B2. Biological Effects of Low Frequency Vibrations. H. B. Wahlin and B. R. Russell.—Vibrating string type generators operating in the range 1000 to 2500 cycles per second and at 60 cycles per second have been used for a series of preliminary studies. The string is a spring-brass or piano wire under tension held fast at two points a few centimeters apart; it is driven electromagnetically at the frequency of its own fundamental vibration, a magnetron type permanent magnet supplying the magnetic flux. A wire plunger fastened to the center of the vibrating section transmits the motion to a few cubic centimeters of liquid in a test tube. Experiments so far indicate rather slow breakdown of most biological cells; even the comparatively fragile red blood cells withstand ten minutes of vibration before 50 percent disappear; certain protozoa are 90 percent destroyed within two minutes, however. With the large amplitudes available at 60 c.p.s., such a vibrator serves as a tissue dispersing instrument which separates the cells without extensive rupture. Experiments on dispersion of liver and pituitary gland tissue and effects on sarcoma tissue and spermatozoa are in progress. Extension of the useful frequency range from 200 to 4000 c.p.s. is planned.

B3. The Ionization and Dissociation of Formic Acid Monomer by Electron Impact. Thomas Mariner* and Walker Bleakney, *Princeton University.*—In HCOOH vapor 65-volt electrons in a mass spectrometer produced $HCOOH^+$, one negative and twelve positive fragment ions. Unique reactions could not be found to account for the production of the negative ion and six of the positive ions. However, the first appearance potentials of $COOH^+$, CO_2^+, HCO^+, CO^+, H_2O^+, and H_2^+ require that they originate in reactions involving the least dissociation energy for the production of the corresponding radicals. CO_2^+ has a second appearance potential for which the responsible reaction is also deducible. Excess energy in all the assignable reactions is less than 1.0 volt. The low appearance potentials of $COOH^+$ and HCO^+ require that the trivalency of O^+ be utilized in the ionic structure, as was found for some of the ions produced from methyl and ethyl alcohol.[1] Ionization potentials at 11.0 ± 0.1 and 11.6 ± 0.2 volts were found for HCOOH. The upper one is consistent with the value of 11.29 volts reported in analyses of the band spectrum.[2] The possible explanation of the lower value in terms of a transform of HCOOH will be discussed.

* Now at the Stamford Research Laboratories, American Cyanamid Company, Stamford, Connecticut.

[1] Cummings and Bleakney, Phys. Rev. **58**, 787 (1940).

[2] Price and Evans, Proc. Roy. Soc. **A162**, 110 (1937).

B4. Peak Contour and Half-Life of Metastable Ions Appearing in Mass Spectra. J. A. Hipple, *Westinghouse Research Laboratories, East Pittsburgh, Pennsylvania.*—The diffuse peaks appearing in the mass spectra of hydrocarbons have recently been attributed to the spontaneous dissociation of metastable ions during transit through the instrument. Several workers in the field have objected to this interpretation on the basis that the appearance of diffuse peaks in the 180° instrument is unexplained—the peaks having roughly the same appearance as in the sectored-field instrument such as that employing a deflection of 90°. It will be shown that these peaks should be similar in both types of instrument. By varying the ion-draw-out voltage from 0.18 to 10.0 volts, and thus varying the time spent in the ion source, the half-life has been measured for the $C_4H_{10}^+$ ion in the metastable state responsible for the diffuse peak at the apparent mass 31.9 in *n*-butane. This dissociation process is $C_4H_{10}^+ \rightarrow C_3H_7^+ + [CH_3]$. The experimental points lie very closely to a straight line on a semi-log plot from 1.4 to 6×10^{-6} second. The half-life for this metastable state is 2×10^{-6} second.

C1. Reconstruction of a 400-kv d.c. High Potential Source. Samuel K. Allison, Leticia del Rosario, Joan Hinton, and Howard Wilcox, *Institute for Nuclear Studies, University of Chicago.*—The voltage quadrupling circuit, which was used before the war for studies in the transmutation of the light elements and as a *d-d* source during the war, is being largely reconstructed. The high resistance, of approximately 6.8×10^9 ohms, which was used to measure the high voltage, has been completely reassembled in a new helical structure which provides a separation of the individual resistors, good contacts, and corona prevention. The condensers in the voltage quadrupling circuit have been replaced by new ones of several times the previous capacity, and the new units have been distributed in rough agreement with a circuit analysis which minimizes the ripple and voltage lowering. The rectifiers used previously, which required continuous pumping, have been replaced with permanently evacuated units designed to operate under 250 kv inverse peak voltage. Surge resistors have been installed as structural elements in the high voltage circuit.

C2. Correction of G. M. Counter Data for High Counting Rates. III. DONALD N. GIDEON AND J. D. KURBATOV, *Ohio State University.*—The experimental work of correction of G. M. counter data has been extended to gamma radiation. The energies of the gamma sources used were mainly in the range 1–2 Mev. Similar to the studies of corrections for beta radiation, a series of samples of known true counting rates and identical geometry were prepared having up to 200,000 counts/minute. An arrangement of the large window G. M. tube with Neher-Harper and decade-counting circuits was used. The resolving time τ, calculated from the experimental data by means of an expression previously derived,* has been found to decrease for gamma- as well as for beta-rays with increasing density of radiations. Log τ for gamma-rays plotted against log of true counting rate is a straight line, with a smaller change in τ for gamma- than for beta-rays. A similar plot of τ for beta-rays is a curve which exhibits no simple relation between τ and true counting rate. The correction factor calculated for gamma-rays is smaller than that for beta-rays in the range below about 20,000 counts/min. for this counting arrangement and approaches similar values for higher counting rates.

* J. D. Kurbatov and H. B. Mann, Phys. Rev. 68, 40 (1945).

C3. Radiations from Radioactive Lanthanum (140).[1] ALLAN C. G. MITCHELL, LAWRENCE M. LANGER, AND LEON J. BROWN, *Indiana University.*—Radioactive lanthanum, La^{140}, which occurs as a product in uranium fission, has been investigated. La^{140} grows from a Ba^{140} parent of 300-hour half-life. In order to measure the energy of the gamma-rays from a separated La^{140} source, the range of Compton electrons, ejected from an aluminum radiator, was measured by coincidence counters. The most energetic gamma-ray was thus found to have an energy of 2.0 ± 0.10 Mev. By placing the source between two gamma-ray counters, gamma-gamma coincidences were found. It is estimated that there are two gamma-ray quanta per disintegration. An absorption curve of the gamma-rays showed a gamma-ray of 2.0 Mev and one of approximately 300 kv. The beta-ray end-point was found to be 1.96 Mev. Beta-gamma coincidences were found. The number of beta-gamma coincidences per recorded beta-ray was independent of the energy of the beta-rays indicating a simple beta-ray spectrum. Experiments performed on a separated Ba^{140} source showed that the intensity of the gamma-rays grew from the barium with the expected period. In these experiments the barium source was placed in a coincidence apparatus set to measure Compton electrons from gamma-rays of energy greater than 500 kv. Both the coincidence rate and the singles rate grew in a manner to be expected if the La^{140} daughter emits the gamma-rays, and the Ba^{140} parent emits no high energy gamma-ray.

[1] Work done under auspices of Manhattan District.

C4. $d-H^3$ Reaction in Cb and Ag. D. N. KUNDU AND M. L. POOL, *Ohio State University.*—With heavy nuclei, $d-H^3$ reactions had been reported in Ag and Cu, but the possibility of spurious $n-2n$ reactions with neutrons from $d+d$ reactions, neutrons produced within the target material, chamber background neutrons was not completely ruled out. In the following, a number of thin foils of spectrochemically tested Cb of the same area and thickness, and shielded on all sides except the front, were bombarded with 10 Mev deuterons for various lengths of time. The foils were of such a thickness (0.005″) that the deuterons were completely stopped by the first foil; the other foils were subjected to neutron reactions only, if any. The Cb^{92} (10.1 D) activity was found, with and without chemistry, in good strength in the first foil; there was no measurable activity of this half-life in the other foils. The decay curves (10.1 D), β^- (1.38 Mev), γ (1.0 Mev), and ZrK_α x-rays (0.78A) decaying with 10.1 D checked well with Cb^{92}. With the deuteron energy used, the $d-(p, 2n)$ and $d-(d, n)$ reactions being less probable, the reaction is mostly $Cb^{93}(d, H^3)Cb^{92}$. With Ag target the same method gave Ag^{106} (24.5 min.) due to $d-H^3$ reaction.

C5. Yield of Photo-Neutrons from U^{235} Fission Products in Heavy Water. S. BERNSTEIN, W. M. PRESTON, G. WOLFE, R. E. SLATTERY, *Clinton Laboratories.*—The photo-disintegration of the deuteron has been used to study the hard gamma-rays emitted by fission products of U^{235}. The neutrons created in the process were used as the indicator of the presence of hard γ-rays. The fission products were placed at the center of a 10″ radius sphere of heavy water. Conclusions about the periods and yields of the hard γ-rays were made from the total number of photo-neutrons being captured in a large tank of oil surrounding the sphere of heavy water. Seven half-lives were found: 2.5 sec., 41 sec., 2.4 min., 7.7 min., 27 min., 1.6 hours, 4.4 hours, and 53 hours. The shortest one and longest one of these are least reliable. Eighty-five percent of the photo-neutrons appear in the two shortest half-lives, the 2.5-sec. component being three times as intense as the 30-sec. component. The total saturated activity of the photo-neutrons for an infinite amount of heavy water was calculated from the 10″ radius sphere measurements to be about 16.5 percent of the saturated delayed neutron activity. It is calculated that there must be of the order of one to two photons of energy above 2.2 Mev emitted per fission by fission products with half-lives greater than one second.

C6. The Total Scattering Cross Sections of Deuterium and Oxygen for Fast Neutrons. RICHARD G. NUCKOLLS,* CARL L. BAILEY, WILLIAM E. BENNETT,* THOR BERGSTRAHL,** HUGH T. RICHARDS,*** AND JOHN H. WILLIAMS, *University of Minnesota.*—The transmissions of H_2O and D_2O for neutrons of discrete energies between 0.35 and 6.0 Mev have been measured. These neutrons were produced by Li (p, n), C (d, n), and D (d, n) reactions with monoenergetic ions accelerated by the Minnesota pressure electrostatic generator. Previous experimental values**** of the (n, p) scattering cross section in the same energy region by the same technique were used to calculate $\sigma_s(D)$ and $\sigma_s(O)$ from the observed transmissions of H_2O and D_2O. $\sigma_s(D)$ is a monotonic function of neutron energy in this region. $\sigma_s(O)$ shows evidence for resonance phenomena.

* Now at Illinois Institute of Technology.
** Now at Naval Research Laboratory.
*** Now at University of Wisconsin.
**** Phys. Rev. (to be published).

C7. Resonance Scattering of Neutrons by Mn. N. H. BARBRE* AND M. GOLDHABER, *University of Illinois.*—It was previously shown that Mn has a neutron resonance level where resonance scattering predominates compared with resonance capture.[1] Continuing this work, we have measured the energy dependence of the scattering cross section of Mn in a "back scattering" arrangement. Detectors responding to resonance neutrons of different energy (25 to ~100 ev) have been used, and a gradual increase of the effective scattering cross section of Mn with increasing neutron energy of the detector has been found in this energy region. Absolute cross sections were obtained by comparison with carbon for which a scattering cross section of 4.8×10^{-24} cm² was assumed. The effective Mn scattering cross section is found to rise from 6×10^{-24} cm² at 25 ev to 120×10^{-24} at ~100 ev, while the scattering cross section of Ni, measured in a similar way, remains constant. Tentatively, and subject to a more final neutron energy scale, it is concluded that the resonance level of Mn has a resonance energy E_0~100 ev, a neutron width Γ_n~10 ev, and a radiation width Γ_γ~0.1 ev.

* Now at Western Kentucky State College.
[1] M. Goldhaber and A. A. Yalow, Phys. Rev. **69**, 47(A) (1946).

C8. Calculation of Angular Distributions in Resonance Reactions. G. BREIT AND B. T. DARLING, *University of Wisconsin.*—The treatment of angular distribution of disintegration products in nuclear resonance reactions can be shortened by applying the following two theorems: (I) A statistical mixture without correlation and with equal probabilities of states having definite projections of two uncoupled spins along an axis is[1] also a statistical mixture in the same sense of states corresponding to compounded spins with definite projections along the same axis. (II) When two angular momenta l, s are compounded to form a resultant j, the probability of the projection of l along an axis fixed in space having a certain value m, when summed over all states corresponding to the same j, is $(2j+1)/(2l+1)$. By means of these theorems and the symbolic ξ, η method, one can avoid much of the explicit calculation of normalized wave functions corresponding to the composition of angular momenta. The financial support of the ONR of the Navy Department is gratefully acknowledged.

[1] J. von Neumann, *Mathematische Grundlagen der Quantenmechanik* (1932), p. 183.

C9. Range Distribution of U^{235} Fission Fragments in Photographic Emulsion. H. T. RICHARDS* AND LYDA SPECK, *Los Alamos Laboratory.*—Eastman's fine grain emulsion 548–0 has been found suitable for recording fission fragments while remaining completely insensitive to alpha-particles. The high background grain count of this emulsion was removed by Liebermann and Barschall's technique[1] and the plates then impregnated with uranyl salts. One set of plates was used as a control and the other exposed to slow neutrons. The plates were then developed and examined under dark field illumination. No tracks were observed on the control plates. Four hundred tracks on the exposed plates were measured, and the range distribution is in agreement with ionization chamber measurements of total energy distribution reported by other workers. No large angle scatterings were observed for the portion of the range to which the emulsion is sensitive. No ternary fissions were observed. The measured range distribution showed a sharp maximum at 23 microns and extended from 11 to 33 microns.

* Now at the University of Wisconsin.
[1] L. N. Liebermann and H. H. Barschall, Rev. Sci. Inst. **14**, 89 (1943).

C10. The 93 kev-γ-Line of UX_1. H. L. BRADT* AND P. SCHERRER, *Federal Institute of Technology, Zürich.*—In the β-spectrum of UX_1 there occur L-, M-, and N-conversion lines of a 93 kev-γ-radiation. The fact that the wave-length as measured by Meitner is just the wave-length of the $K\alpha_2$ x-rays of the daughter product UX_2 suggested to Meitner that the observed β-lines are nothing but conversion lines of the $UX_2-K\alpha_2$ x-radiation. However, there seemed to be no acceptable reason for an excitation of this K-radiation. Our investigation of the β-spectrum and the γ-radiation of UX, using a magnetic spectrometer and counters of calibrated efficiencies, leads to the result that the lines occuring in the β-spectrum are, with high probability, like the similar RdTh lines (*Surugue* and *Tsien-San-Tsiang*[1]), conversion lines of a nuclear γ-radiation. The L_1-conversion coefficient of this 93 kev-γ-radiation has been determined from the intensity of the L_1-conversion line (0.05_1 electrons/β-decay) and the intensity of the unconverted γ-radiation (0.15 quanta/β-decay) as $N_e/N_\gamma=0.34$, in agreement with the theoretical value for quadrupole radiation, calculated by Fisk. The upper limit of the UX_1-β-spectrum has been determined as (0.205 ± 0.01) Mev. 80 percent of all β-transitions lead to UX_2 in its normal state, while 20 percent lead to the excited 0.093 Mev level.

* Now at Purdue University.
[1] J. Surugue and Tsien-San-Tsiang, Comptes rendus **213**, 172 (1941)

D1. Ge—Ge Contacts.* S. BENZER, *Department of Physics, Purdue University.*—When contacted with each other, germanium crystals of various impurity content produce rectification and a rectification series** exists. Such a contact between two pieces of the same (homogeneous) crystal should produce a linear current-voltage characteristic, caused only by spreading resistance, if no appreciable surface layers exist. However, the characteristic observed for both polarities is more of the order of the back resistance observed when either piece of the crystal is contacted with a metal; in both directions, the negative resistance at high voltages appears, which is typical of the back characteristics of metal-Ge contacts using these alloys. Therefore, surface layers other than the natural blocking layer (caused by the contact potential difference between the two contacting elements, which should be zero in this experiment) must be taken into account for high voltage crystals and may help to explain their properties.

* This work has been carried out under contract No. W-36-039-sc-32020 between the Purdue Research Foundation and the Signal Corps.
** W. Brattain, Phys. Rev. **69**, 682(A) (1946).

D2. Photo- and Thermo-Effects in p-Type Germanium Rectifiers. RALPH BRAY AND K. LARK-HOROVITZ, *Physics Department, Purdue University.**—In contact rectifiers

(metal *p*-type germanium) the rectification efficiency depends on the metal and the resistivity and surface treatment of the germanium. Photo-conductive effects, *depending in magnitude on the particular germanium sample and the metal*, leave the "forward" resistance relatively unaffected, yet may so greatly reduce the "back" resistance as to apparently reverse the rectification. Photo-voltaic effects are observed usually in the back direction. Sometimes both polarities are observed indicating probably local changes in sign of contact potential. The photo-effects approach maximum sensitivity in the near infra-red (about 1.3μ). Quanta of this energy may lift electrons from the full band to the conducting band. The light affects only the immediate vicinity of the contact. At elevated temperatures, electrons are excited from the full to the conducting band and again apparent reversal of rectification occurs (as in the photo-effect above). The thermal effect however is independent of the metal. The lower the resistivity of the sample, the higher is the temperature required to produce the effect.

* This work has been carried out under Contract No. W-36-039-sc-32020, (Signal Corps) between the Purdue Research Foundation and the Signal Corps.

D3. Measurements of Hall Effect and Resistivity of Germanium and Silicon from 10° to 600°K. G. L. PEARSON AND W. SHOCKLEY, *Bell Telephone Laboratories*.—Hall effect and resistivity measurements of the type made at Purdue[1] have been extended over wider temperature and impurity range. Two samples of germanium, one *P*- and the other *N*-type at room temperature, were measured[2] from 600°K to 10°K. For the *P*-type germanium the log Hall coefficient is linear in $1/T$°K below 90°K, giving an activation energy 0.007 ev (a hydrogen-like wave function with a dielectric constant of 25 for which the binding energy is 0.02 ev predicts an activation energy of 0.01 ev). For the *N*-type sample a similar straight plot with approximately the same activation energy is obtained between 17 and 90°K. Silicon containing 0.03 atomic percent boron has essentially constant resistivity and Hall coefficient below 100°K. The interpretation of this result is that a free electron gas is formed by the overlapping impurity wave functions with a degeneracy temperature of about 275°K.

[1] K. Lark-Horovitz, A. E. Middleton, E. P. Miller, and I. Wallerstein, Phys. Rev. **69**, 258 (1946).
[2] We are indebted to Dr. E. U. Condon and members of the Low Temperature Laboratory at the Bureau of Standards whose cooperation made the low temperature measurements possible.

D4. Boltzmann's Superposition Principle and the Viscous Behavior of Grain Boundaries in Metals.* T'ING-SUI KÊ, *Institute for the Study of Metals, University of Chicago*.—The mechanical behavior of grain boundaries in metals has been a subject of constant controversy. The present research is designed to examine thoroughly the mechanical behavior of grain boundaries in metals in a quantitative manner. A simple torsional apparatus has been devised for measuring four types of anelastic effects at very low stress levels, namely: internal friction at low frequencies; variation of dynamic rigidity with temperature; creep under constant stress; and stress relaxation at constant strain. All four types of anelastic effects have been studied in 99.991 percent polycrystalline aluminum as well as in single crystal aluminum; the behavior in the two cases is very different. The four types of anelastic effects observed in polycrystalline aluminum satisfy the interrelations derived by Zener from Boltzmann's superposition principle within experimental error. These measurements corroborate quantitatively the concept that the grain boundaries behave as if they were viscous with a coefficient of viscosity decreasing with increasing temperature. The heat of activation associated with the viscous slip along the grain boundaries has been found to be 34,500 calories per mole, corresponding to a rapidly decreasing grain boundary viscosity with increasing temperature. Similar anelastic effects have been also observed in polycrystalline magnesium, indicating that the viscous behavior of grain boundaries is probably common to all metals.

* This research has been supported by ORI (Contract No. N6ori-20-IV) since May 1, 1946.

D5. Determination of the Lattice Spacing of Silver Bromide for Varying x-Ray Exposures. J. C. M. BRENTANO AND L. VAN CLIEF SPENCER, *Northwestern University*.—A recent theory of the latent photographic image by M. L. Huggins[1] postulates domains within the silver bromide crystal in which AgBr assumes a B3 structure. Experiments by B. Hess[2] indicate that with increasing exposure of photographic emulsions to x-rays, changes in the AgBr spacing of about 2×10^{-3}A occur. These could partly be interpreted in terms of this theory. Using an x-ray goniometer with high resolution and microdensitometric evaluation, we determined the lattice constant of pure AgBr crystals for increasing x-ray exposures. No change of spacing within the limits of error 2×10^{-4}A was observed. Our interpretation varies from that of Hess in that, for exposures to x-ray, the rising density range does not represent a gradual modification of the grains and that the transition from the range of increasing densities to that of solarization constitutes essentially a shift of statistical balance. We thus attach more significance to a comparison of spacing for maximum density with that for solarization than to a comparison of spacings within the rising density range of within the solarization range.

[1] M. L. Huggins, J. Chem. Phys. **11**, 412 (1943).
[2] B. Hess, Physik. Zeits. **44**, 245 (1944).

D6. Further Experiments on the Elastic Single Scattering of Electrons by Nuclei. W. W. BUECHNER, E. A. BURRILL, A. SPERDUTO, R. J. VAN DE GRAAFF, AND H. FESHBACH, *Massachusetts Institute of Technology*.—The apparatus used in making the observations previously reported[1] has been reassembled and the measurements extended to a lower atomic number by using beryllium as a scattering material. For angles up to 60° and for electron energies of 2.1, 2.2, and 2.3 Mev, the ratio of the observed scattering to that predicted by the Mott formula is 0.99 with a standard deviation of 0.04. Measurements have also been repeated on aluminum in this angular and energy range and the ratio of observed scattering to that predicted is found to be 1.00 with a standard deviation of 0.05. The earlier result for aluminum at 2.27 Mev which was reported

as anomalous and to be repeated has thus been found to be in error. Some preliminary measurements have also been made on carbon indicating agreement with theory. The present results, together with those reported earlier,[1] show that in this angular and energy range the elastic single scattering of electrons is in good agreement with theory for various nuclei ranging in atomic number from 4 to 79 (beryllium to gold).

[1] Van de Graaff, Buechner, and Feshbach, Phys. Rev. 69, 452 (1946).

D7. The Relativistic Clock Paradox. E. L. HILL, *Department of Physics, University of Minnesota.*—A new solution has been obtained of the problem of relativity theory in which time intervals as measured by two relatively accelerated clocks are compared. This solution is based on the group of conformal transformations in four dimensions, which is known to express the kinematics of uniformly accelerated motions. It does not imply that the accelerations are produced by gravitational fields. The calculation has been carried only to second-order terms in the relative velocity and acceleration of the two clocks. It is found that there exists a doubly infinite family of solutions, the readings of the clocks being adjusted at first passage and their rates compared when they are at relative rest. For all solutions the readings are again the same when the clocks are in coincidence. The existence of multiple solutions shows that new conditions must be imposed to make the problem unique, but their physical meaning is not apparent.

D8. The Hydrodynamical Equations in Quantum Mechanics. M. DRESDEN, *University of Kansas.*—In the classical theory the hydrodynamical equations are obtained by an averaging process from the Boltzmann equation. The difficulty encountered in carrying over this program in the quantum theory is that it is quantum-mechanically impossible to define a probability density in phase space. Wigner,[1] however, has constructed a function—in terms of the wave function of the system—which is in a "certain sense" analogous to that probability density. Utilizing that function the quantum analog of the Boltzmann equation was found. It contains apart from the classical terms an infinite series of terms depending on h. The hydrodynamical equations which follow possess the same formal structure as the classical equations. The quantities occurring in them are, of course, different from those in the classical theory. They are defined—in terms of the distribution function—which in turn depends upon the wave function. One can prove that the quantum-mechanical analog of the hydrodynamical current density is actually equal to the quantum-mechanical mean value of the Landau operator[2] for that quantity.

[1] E. Wigner, Phys. Rev. 40, 749 (1932).
[2] L. Landau, J. Phys. 5, 71 (1941).

D9. The Abundance of He^3 in Helium. L. T. ALDRICH AND ALFRED O. NIER, *University of Minnesota.*—Alvarez and Cornog[1] have reported the existence of He^3 in atmospheric and well helium. The abundances given were 10^{-7} and 10^{-8} mole fractions respectively. With a high resolution 60° mass spectrometer a mass spectrum analysis of helium has been made. A spectroscopically pure sample obtained from the Air Reduction Sales Company through regular commercial channels indicated a small peak in the mass three position. This peak was proportional to the mass four peak for variations of pressure and electron energy. The peak was completely resolved from HD which was added to the sample in various concentrations to insure that the peak observed was not due to a hydrogen impurity. If, as seems likely, the peak is due to He^3, the concentration was approximately one part in 9×10^5. Other samples are being investigated.

[1] Phys. Rev. 56, 613 (1939); 56, 379 (1939).

T1. Note on a Discrepancy in Gyromagnetic Measurements and the Question of a Possible Variation of the Torsional Modulus of German Silver with Frequency. S. J. BARNETT AND D. S. WEBBER, *University of California and California Institute of Technology.*—A four or five percent deficit of the gyromagnetic ratios for certain ferromagnetic substances obtained some years ago by Sucksmith and Bates from the mean ratio obtained in much more elaborate investigations by one of us might be explained if the dynamic torsional modulus of German silver wire, Md, were smaller, and four or five percent smaller, than the static modulus, Ms. The calibrating operations of Sucksmith and Bates were carried out partly with rapid oscillations, partly with steady deflections, the two moduli being (implicitly) assumed equal. We have not worked with the true static modulus, but have determined the ratio of Md for frequencies ranging from 17 to 50 per second, comparable with those used by the authors mentioned, to Md for periods ranging from 4 seconds to 28 seconds—doubtless quite comparable with or greater than the times required for steady twists in the work referred to. We have detected no change within the high frequency range, or within the low frequency range; but the modulus has been found to diminish by about 1 percent from the low frequency range to the high frequency range—a diminuition interesting in itself, though sufficient to account for but little of the discrepancy mentioned.

T2. Electrophotophoresis and Electric Charges Smaller than the Electronic Charge. FELIX EHRENHAFT, *New York, New York.*—The phenomenon of electrophotophoresis as described long ago by the author[1] was recently confirmed by Tauzin.[2] Electrophotophoresis is a movement under the simultaneous action of light and homogeneous electric fields of particles proven to be otherwise electrically uncharged. The particles move in or against the direction of the field and reverse with its reversal. When irradiated by light, they carry an excess of positive or negative charge. Individual testbodies can lose or regain their electric charge suddenly or gradually, partly or entirely. Photomicrographs indicate that particles describe helical paths with regularly spaced turns in electric fields. Schedling calculated such electric charges e carried by single spherical bodies of Te of determined density and mobility B using their measured[3] electrophotophoretic velocity v in viscous medium in constant homogeneous fields E using the relationship $v=eEB$. Electric charges smaller than 10^{-10} e.s.u.

result thereby, and changes of charge take place seemingly continuously as described previously by the author in the case of radioactive testbodies of spherical shape and known density.[4] Here is a new proof of smaller than the electronic charge.[5]

[1] F. Ehrenhaft, J. Frank. Inst. 235, 237 (1942).
[2] P. Tauzin, Revue scientifique (June–Dec. 1945), p. 276.
[3] P. Selner, Zeits. f. Physik 71, 658 (1931).
[4] F. Ehrenhaft and D. Konstantinowsky, Ann. d. Physik 63, 797 (1920); J. Frank. Inst. 230, 384 (1940).
[5] F. Ehrenhaft, Physik. Zeits. 39, 673 (1938); Phil. Sci. 8 (July, 1941).

T3. On Creep and Relaxation. B. GROSS, *National Institute of Technology, Rio de Janeiro, Brazil.*—When the principle of superposition is valid, the rate of creep $\varphi(t)$ and that of relaxation $\bar{\varphi}(t)$ are connected by $L[\bar{\varphi}]+L[\bar{\varphi}]L[\varphi]=L[\varphi]$, where L means the Laplace transform. φ and $\bar{\varphi}$ can be represented as Laplace transforms of primitive functions ρ (distribution function for creep) and $\bar{\rho}$ (distribution function for relaxation); thus $\varphi=L[\rho]$ and $\bar{\varphi}=L[\bar{\rho}]$. These expressions are substituted into the first equation, the iterated Laplace transforms giving Stieltje's integral equation; this is inverted by a formula due to Borel. There results a general relation, suitable for numerical computation, for the conversion of one distribution into another:

$$\bar{\rho}dp=\rho dp\Big/\left[1+\int_0^\infty \frac{\rho ds}{s-p}\right]^2+\pi^2\rho^2.$$

The integral is a principal value. The distribution function of relaxation times corresponding to a given rage of relaxation is given by

$$\pi\bar{\rho}=L[Im\bar{\varphi}(-t)], \quad \text{where} \quad \bar{\varphi}(-t)=\bar{\varphi}(t \exp. -i\pi),$$

provided $\bar{\varphi}$ satisfies certain conditions.

S1. Abnormal Isotope Abundances Produced by Neutron Absorption in Cadmium. A. J. DEMPSTER, *Argonne National Laboratory.**—Mass spectra of samples of cadmium will be shown that had been given a prolonged exposure to slow neutrons. The isotope at mass 113 is reduced to approximately one-eighth its normal abundance and the isotope at mass 114 is increased. The change is confined to the surface of the sample as the interior is completely shielded from the neutrons. No change in the abundances of the other isotopes could be detected. These mass spectra confirm the direct measurements reported by Moyer, Peters, and Schmidt[1] of neutron absorption by samples enriched in various isotopes, which indicated that the cadmium isotope at mass 113 is the main absorber of slow neutrons.

* To be called for after paper C9 if time permits.
[1] Phys. Rev. 69, 666 (1946).

S2. Some Neutron Induced Activities in the Rare Earths. MARK G. INGHRAM AND RICHARD J. HAYDEN, *Argonne National Laboratory.**—Nitric acid solutions of samarium, europium, holmium, and ytterbium were subjected to neutron bombardment in the Argonne pile. Half-life and absorption data were obtained with standard counting equipment. Masses of certain activities were obtained by use of the mass spectrograph.[1] Using these techniques, the 46-hr. Sm activity was shown to result from an isotope of mass 153, the 9.2-hr Eu activity from an isotope of mass 152, and the 27-hr holmium previously given as 35 hr[2] from a mass of 166. The long-lived activity in europium was shown to result from two isotopes, the previously reported 154 and a new, long-lived 152 isomeric with the 9.2-hr europium. A new 99-hr activity found in ytterbium was found to be caused by an isotope of mass 175. Present evidence points to a mass of 177 for the short lived activity resulting from neutron bombardment of ytterbium.

* To be called for after paper C9 if time permits.
[1] R. J. Hayden and M. G. Inghram, Phys. Rev. 69, 89 (1946).
[2] G. T. Seaborg, Rev. Mod. Phys. 16, 1 (1944).

S3. A Nomogram to Facilitate the Determination of the Resolving Time of Counter Equipment. L. JACKSON LASLETT, *Iowa State College.**—The nature and the determination of the resolving-time parameters required for the coincidence correction of counter equipment has been discussed by Kohman.[1] In cases in which the counting rate is moderate, a simple, first-order correction may suffice. The resolving-time parameter, τ, may then be conveniently determined by counting two uncalibrated sources together (S counts/min.) and separately (C_1, C_2)—preferably in the order C_1, S, C_2. The value of τ may then be taken as given by $(S^2-C_1^2-C_2^2)\tau=D$, in which $D=(C_1+C_2)-(S+B)$, with B representing the background counting rate. A nomogram has been prepared to facilitate the solution of the above equation for τ. This nomogram may also be used, once τ has been determined, to obtain directly the correction which must be applied to any moderate, observed counting rate. It is believed that a nomogram can be particularly useful if determinations of resolving time and counter corrections are to be made as a matter of routine by technicians.

* To be called for after paper D9 if time permits.
[1] T. P. Kohman, Phys. Rev. 65, 63 (A) (1944).

S4. The Escape Probability of Protons and Neutrons from Bombarded Bismuth. J. M. CORK, *University of Michigan.**—The bombardment of bismuth with deuterons has been extended to higher energies. In this bombardment the single bismuth isotope of mass 209 may be transformed into polonium^{210} (RaF) or bismuth^{210} (RaE) by d,n and d,p reactions, respectively. The latter is a beta-emitter of half-life 5 days which on decay converts into the alpha-emitting RaF. Thus, by noting the build-up of the alpha activity after bombardment, the yield of each product can be determined and hence the relative probability of the two competing d,p and d,n processes. Previous measurements up to 9 Mev indicated that the above ratio dropped from above 10 to a value of about 5, a result not unexpected in consideration of the Oppenheimer-Phillips process. At higher energies the d,n process might have been expected to become more probable, but up to 14.5 Mev the ratio d,p to d,n continues at about the same value as at 9 Mev.

* To be called for after paper D9 if time permits.